ABSTRACT

Title of Thesis:	INVESTIGATION OF SWIRL ASSISTED COLORLESS DISTRIBUTED COMBUSTION (CDC) FOR GAS TURBINE APPLICATION
	Joseph Samuel Feser, Master of Science, 2019
Thesis Directed By:	Dr. Ashwani K. Gupta Distinguished University Professor Department of Mechanical Engineering

Colorless Distributed Combustion (CDC) is a novel method to enhance flame stability and thermal field uniformity, increase combustion efficiency and reduce pollutants emission, including noise. The focus of this thesis is to investigate swirl-assisted distributed combustion at high thermal intensity for gas turbine application. This thesis investigates the impact of fuel enrichment on CDC conditions by using naphthalene as a fuel additive in ethanol to increase the heating value without compromising ultra-low emissions, in addition to investigating how CDC fuel flexibility can mitigate instability associate with hydrogen enriched alternate fuels. To better predict and implement CDC design in future gas turbine combustors a distributed combustion index (DCI) will be developed to determine the impact of heat release intensity, equivalence ratio, preheat temperature and entrainment gas on distributed conditions. Lastly, the impact of flowfield interaction on achieving CDC condition will be examined for enhanced understanding of mixing required for CDC.

INVESTIGATION OF SWIRL ASSISTED COLORLESS DISTRIBUTED COMBUSTION (CDC) FOR GAS TURBINE APPLICATION

by

Joseph Samuel Feser

Thesis submitted to the Faculty of the Graduate School of the
University of Maryland, College Park, in partial fulfillment
of the requirements for the degree of
Master of Science
2019

Advisory Committee:
Professor Ashwani Gupta, Chair
Professor Bao Yang
Associate Professor Gary Pertmer

Acknowledgments

The work contained herein was the result of my time at the University of Maryland Combustion Laboratory. I extremely grateful for my advisor Dr. Gupta for not only giving me the opportunity to pursue work on such an interesting topic but also for his patience along the way. I would like to express my gratitude for the vast resources provided to support me during my graduate studies.

I would also like to thank my fellow lab members at the combustion lab both past and present for all their support and making the lab an enjoyable workplace. I would like to thank Dr. Khalil for showing me the lab and all the training provided. I would like to thank the visiting researchers I have worked closely with, namely, Dr. Ghada and Dr. Serhat for their assistance, knowledge and insight without which this would not be possible. I would especially like to thank Kiran for his valuable insights and thought-provoking discussions. I would like to thank my undergrad and high school interns: Herman, Sabrina, Edward and Lydia for their help with experiments as well as making my time in the lab interesting and enjoyable.

I would like to thank my family for their continued support along this journey. In addition, I would like to thank my friend both in and out of the lab for supporting me along the way as well.

I would like to express my gratitude to the Office of Naval Research (ONR) who has provided the financial support, which made this research possible.

Table of Contents

Acknowledgments ii

Table of Contents iii

List of Tables v

List of Figures vi

Chapter 1: Introduction 1

1.1 Background and Objective 1
1.2 Gas Turbine Design Considerations 3
1.2.1 Stable Combustion 4
1.2.2 Wide Stability Limits 4
1.2.3 Low Pollutant Emission 5
1.2.4 High Thermal Intensity 6
1.2.5 Low Pressure Drop 7
1.2.6 Desired Pattern Factor 7
1.2.7 Fuel Flexibility 7
1.3 Pollutant Formation 8
1.3.1 NO_x Formation 8
1.3.2 CO and UHC Formation 11
1.3.3 Soot Formation 11
1.4 NO_x Abatement Strategies 12
1.4.1 Injection of Diluents 12
1.4.2 Exhaust Clean-up 13
1.4.3 Limiting Formation 13

Chapter 2: Literature Review 15

2.1 High Temperature Air Combustion (HiTAC) 15
2.2 Flameless Oxidation (FLOX) 20
2.3 Moderate or Intense Low Oxygen Dilution (MILD) 21
2.4 Colorless Distributed Combustion (CDC) 22

Chapter 3: CDC Fuel Enrichment 25

3.1 Naphthalene Fuel Addition to Ethanol 25
3.1.1 Materials and Methods 26
3.1.2 OH* Chemiluminescence 29
3.1.3 Pollutants Emission 31
3.2 Hydrogen Enriched Fuel 36
3.2.1 Materials and Methods 39

3.2.2 OH* Chemiluminescence 42
3.2.3 Pollutants Emission 46
3.3 Summary 51

Chapter 4: Distributed Combustion Index 54

4.1 Materials and Methods 54
4.2 Heat Release Intensity 57
4.3 Equivalence Ratio 64
4.4 Preheat Temperature 69
4.5 Realistic Combustor Conditions and Developing a DCI 74
4.6 Summary 76

Chapter 5: Flowfield Impact on CDC 78

5.1 Materials and Methods 78
5.2 OH* Chemiluminescence 82
5.3 Non-reacting Flowfield using PIV 84
5.4 Pollutants Emission 88
5.5 Summary 91

Chapter 6: Conclusions and Recommendations for Future Work 93

6.1 Summary and Conclusions 93
6.3 Recommendations for Future Work 94

Appendix A: List of Papers 96

A1: Published Journal Papers 96
A2: Journal Papers Under Review 96
A3: Conference Papers 96

Bibliography 98

List of Tables

Table 1.1 Parameters of typical land based and aviation gas turbine combustors 3

Table 3.1 Experimental parameters at a fuel flow rate of 10 mL/min and fuel inlet temperature of 500 K 29

Table 3.2 Calculated heat content of the naphthalene-ethanol mixture at various naphthalene concentrations 32

Table 3.3 Composition of select hydrogen enriched gases (volume %), calorific value, and volumetric flow rate for constant heat release intensity of 5.7 MW/m^3-atm 41

Table 3.4 Hydrogen enriched fuels experimental parameters 42

Table 4.1 Distributed combustion index experimental parameters 52

Table 5.1 PIV Parameters 73

Table 5.2 Effect of flowfield experimental parameters 74

List of Figures

Figure 1.1 Principle of gas turbine operation 1

Figure 1.2 Pollutant emission trade-off 2

Figure 1.3 Mechanisms of NO_x formation 9

Figure 2.1 Concept of HiTAC 16

Figure 2.2 Temporal temperature history for conventional combustion (a), convention combustion with a recuperator (b) and HiTAC (c) 17

Figure 2.3 Global photographs with combustion air preheat of 1373K and varying O2 concentration (N2 dilution) 19

Figure 2.4 Temperature distribution of conventional (A) and FLOX (B) combustion 21

Figure 2.5 Combustion regimes 23

Figure 2.6 Global images for various CDC combustors 24

Figure 2.7 Oxygen concentration for CDC transition for various fuel types 24

Figure 3.1 Schematic of the experimental test combustor facility 27

Figure 3.2 Schematic of the experimental setup 27

Figure 3.3 OH* Chemiluminescence intensity signals for $\Phi = 0.9$ at different concentrations of Naphthalene in Ethanol 31

Figure 3.4 OH* Chemiluminescence intensity signals for $\Phi = 0.7$ at different concentrations of Naphthalene in Ethanol 31

Figure 3.5 NO emissions for $\Phi = 0.9$ at different concentrations of Naphthalene in Ethanol 33

Figure 3.6 CO emissions for $\Phi = 0.9$ at different concentrations of Naphthalene in Ethanol 33

Figure 3.7 NO emissions for $\Phi = 0.7$ at different concentrations of Naphthalene in Ethanol 34

Figure 3.8 CO emissions for $\Phi = 0.7$ at different concentrations of Naphthalene in Ethanol 35

Figure 3.9 A schematic diagram of the combustion test facility 40

Figure 3.10 OH* chemiluminescence signatures for $\phi = 0.9$ at different oxygen concentration using N2 dilution (at a scale of 0–1) 43

Figure 3.11 OH* chemiluminescence signatures for $\phi = 0.9$ at different oxygen concentration using N2 dilution (at a low intensity scale of 0–0.25) 43

Figure 3.12 OH* chemiluminescence for $\phi = 0.9$ at different oxygen concentration using CO2 dilution (at a scale of 0–1) 45

Figure 3.13 OH* chemiluminescence for $\phi = 0.9$ at different oxygen concentration under CO2 dilution (at low intensity scale of 0–0.25) 45

Figure 3.14 OH* chemiluminescence at various equivalence ratios (at a scale of 0–1) 46

Figure 3.15 NO emission for $\phi = 0.9$ at different oxygen concentration using N2 dilution 47

Figure 3.16 NO emission for $\phi = 0.9$ at different oxygen concentration using CO2 dilution 48

Figure 3.17 NO emission at different equivalence ratios 49

Figure 3.18 CO emission for $\phi = 0.9$ at different oxygen concentration using N2 dilution 50

Figure 3.19 CO emission for $\phi = 0.9$ at different oxygen concentration using CO2 dilution 50

Figure 4.1 Schematic of the combustion test facility 55

Figure 4.2 OH* chemiluminescence signature using N2 dilution at various heat release intensities 59

Figure 4.3 OH* chemiluminescence using CO2 dilution under various heat release intensities 59

Figure 4.4 NO emission at different HRI using N2 dilution 60

Figure 4.5 NO emission for different HRI using CO2 dilution 61

Figure 4.6 CO emission for different HRI using N2 dilution 63

Figure 4.7 CO emission for different HRI using CO2 dilution 63

Figure 4.8 OH* chemiluminescence using N2 dilution at various equivalence ratios 64

Figure 4.9 OH* chemiluminescence using CO2 dilution at various equivalence ratios 65

Figure 4.10 NO emission for different equivalence ratio using N2 dilution 66

Figure 4.11 NO emission for different equivalence ratio using CO2 dilution 66

Figure 4.12 CO emission for different equivalence ratio using N2 dilution 68

Figure 4.13 CO emission for different equivalence ratio using CO2 dilution 68

Figure 4.14 OH* chemiluminescence using N2 dilution under various oxidizer preheat temperatures 70

Figure 4.15 OH* chemiluminescence using CO2 dilution under various oxidizer preheat temperatures 70

Figure 4.16 NO emission for different oxidizer preheat temperatures using N2 dilution 71

Figure 4.17. NO emission for different oxidizer preheat temperatures using CO2 dilution 71

Figure 4.18 CO emission for different mixture temperature using N2 dilution 73

Figure 4.19 CO emission for different mixture temperature using CO2 dilution 73

Figure 4.20 Oxygen concentration at transition to CDC for different mixture temperatures 75

Figure 5.1 A schematic diagram of the experimental facility including flow controllers and laser diagnostics 79

Figure 5.2 OH* chemiluminescence signatures using either N2 or CO2 dilution, Φ=0.9 83

Figure 5.3 OH* chemiluminescence signatures at various equivalence ratios 83

Figure 5.4 Radial mean (left of frame) and rms (right of frame) velocity for: (A) normal air combustion, Φ=0.9; (B) normal air combustion, Φ=0.65; C) CDC with N2 dilution, O2 conc.=15%; and (D) CDC with CO2 dilution, O2 conc.=17% 86

Figure 5.5 Axial mean (left of frame) and rms (right of frame) velocity for: (A) normal air combustion, Φ=0.9; (B) normal air combustion, Φ=0.65; (C) CDC w/ N2 dilution, O2 conc.=15%; and (D) CDC w/ CO2 dilution, O2 conc.=17% 86

Figure 5.6 Kolmogorov length (left of frame) and Reynold's stress (right of frame) for: (A) normal air combustion, Φ=0.9; (B) normal air combustion, Φ=0.65; (C) CDC w/ N2 dilution, O2 conc.=15%; and CDC w/ CO2 dilution, O2 conc.=17% 88

Figure 5.7 NO emission corrected to 15% O2 conc. at various oxygen concentrations 89

Figure 5.8 CO emission corrected to 15% O2 conc. at various oxygen concentrations 89

Figure 5.9 NO and CO emissions corrected to 15% O2 conc. at various equivalence ratios 90

Chapter 1: Introduction

1.1 Background and Objective

The focus of this thesis is on investigation of Colorless Distributed Combustion (CDC) for gas turbine combustors. Gas turbine operation follows the Brayton cycle shown in Fig. 1.1. In an ideal Brayton cycle, air first enters a compressor where it is compressed isentropically. The compressed air then enters a combustor, where fuel is added and subsequentially combusted in order to add heat to the system under a constant pressure process. The high temperature and pressure gases exiting the combustor are used to run a turbine where the work is extracted as the gas expands isentropically. The primary purpose of the combustor is to significantly increase the temperature of the gases entering the turbine in order to maximize the work output of the turbine. Combustors for gas turbine use are operated at an elevated pressure and temperature. Generally, the operational conditions at the inlet of the combustor are 15-16 atm and 700K.

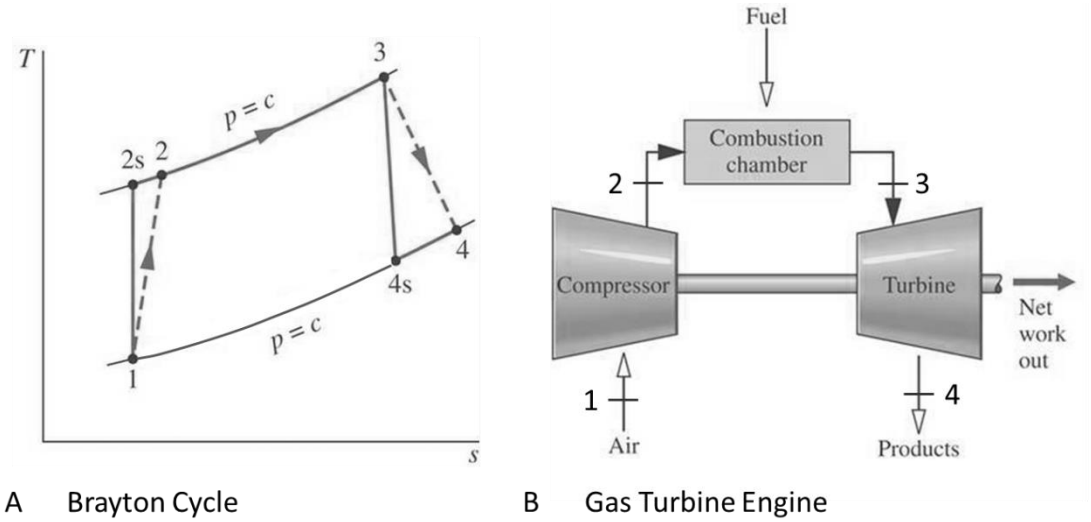

A Brayton Cycle B Gas Turbine Engine

Fig. 1.1. Principle of gas turbine operation

Gas turbines can be used for both land-based and aviation purposes and can run on either gaseous or liquid fuels. Land based gas turbines are used primarily for electricity generation and are commonly run off of natural gas. Liquid fuels such as Jet-A, JP-8, JP-10 and other petroleum based liquid fuels are typically used in aviation gas turbines due to high energy density by both weight and volume. According to the Energy Information Administration (EIA), as of 2019 the United States produces the greatest share of electricity from natural gas. Natural gas accounts for 34% of the U.S. electricity production, followed by coal at 28%, nuclear at 19% and renewables making contributing 18%. The EIA predicts by 2050 that the share of electricity production with natural gas will rise to 39% alongside an increase in renewables to 31%, while coal and nuclear electricity share are expected to drop to 17% and 12% respectively. This is largely due to an increase in natural gas powerplants being built as natural gas prices continue to decline. Additionally, coal and nuclear powerplants are not being built at the same rate due to increased regulation and concerns over excessive carbon emission and safety respectively, meanwhile a push toward renewables by 2050 will lead to a greater share of electric generation [1]. Although renewable energy will make up almost one-third of the electricity portfolio of the U.S. by 2050, the long-term viability of gas turbines remains as nearly two-fifths of the electricity produces by 2050 will be from natural gas plants. In addition, there are not yet any viable solutions to replacing gas turbines for aircraft, due to a lack of high energy density power sources which are also lightweight. Parameters for typical land based and aviation gas turbine combustors are found in Table 1.1.

Table 1.1 Parameters of typical land based and aviation gas turbine combustors

	Land Based	Aviation
Length	60”	10”
Residence Time	20 ms	2-3 ms
Thermal Intensity	15 MW/m^3-atm	150MW/m^3-atm
Fuel	Natural Gas	Petroleum Based Liquid Fuel
Pressure	15 atm	10 atm (cruise), 40 atm (takeoff)
Fuel Introduction	Lean Premixed	Liquid Fuel Atomization

The focus of this thesis is the investigation of an advanced combustion technology, Colorless Distributed Combustion (CDC), for high intensity land based gas turbine applications. Investigation of a CDC combustor employing direct injection of both fuel and air without the need for any flame stabilizer such as swirlers or bluff bodies. Benefits of CDC include ultra-low pollutant emission, low noise emission, enhanced combustion stability, low pressure drop, and increased thermal field uniformity. Thermal intensity corresponding to land-based gas turbines is of interest here with interest on a variety of fuels.

1.2 Gas Turbine Design Considerations

Basic design considerations [2] for a gas turbine combustor are given as follows and will be discussed briefly in the following sub-sections.

- Stable Combustion
- Wide Stability Limits

- Low Pollutant Emission
- High Thermal Intensity
- Low Pressure Drop
- Desired Pattern Factor
- Fuel Flexibility

1.2.1 Stable Combustion

It is critical to have stable combustion in a gas turbine combustor. Not only to maintain a flame but also to prevent burnout and damage the combustor walls and turbine blades. Land based gas turbines are often ran in an ultra-lean premixed mode in order to reduce hot spots and minimize NO_x emissions. However, combustion instabilities are of concern in these ultra-lean premixed combustors as the near lean operational limits are approached [3]. As combustion approaches the lean operational limit instabilities can occur where large pressure oscillations occur due to unsteady combustion. Combustion instability is undesirable as the pressure fluctuations can lead to stress induced fatigue to the combustor, thermal stresses can be enhanced, and flame instabilities such as flashback or blow off may occur. It is therefore desirable to design a combustor with limited pressure fluctuations, with the industrially accepted value for the pressure fluctuations of 1.5% root mean square (rms).

1.2.2 Wide Stability Limits

Having a wide operational limit is desirable for a gas turbine for part load conditions. For land-based turbines, this is desirable for balancing supply power generation with variable load adjustment. Land based turbines typically can operate at

50-100% of their load without influencing the emission profile [4]. Aviation gas turbines have additional need for wide operational limits as the power requirements for take-off, cruise, and taxi have a factor of 2-3 times between them.

1.2.3 Low Pollutant Emission

The development and design of gas turbine combustors has been driven by the desire for ultra-low pollutant emissions. In order to maximize power output of a gas turbine and reduce fuel costs, it is imperative that the combustion process be as complete as possible in order to extract the maximum energy out of the fuel. Therefore a high combustion efficiency (~100%) is desired, wherein ultra-low unburnt hydrocarbon (UHC) emissions are kept to a minimum level. It is also important to limit soot formation which can not only harm the environment but also damage equipment if left to build up over time. NO_x which is a contributor to smog and acid rain is regulated by the EPA and is set to limits of 9ppm at 15% O_2 concentration for land-based gas turbines over 10MW [6]. Figure 1.2 details the typical emission trade-off for UHC/CO, soot, and NO_x emissions. From Fig. 1.2, it can be seen that there are optimal points for each emission type, and that a delicate balance is typically required to keep all emission types low.

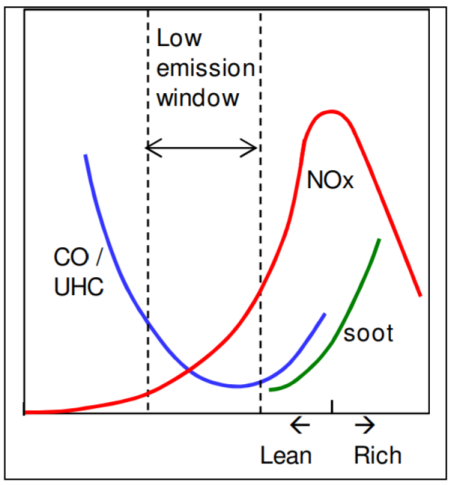

Fig. 1.2. Pollutant emission trade-off

1.2.4 High Thermal Intensity

Thermal intensity is the amount of energy released per unit volume of the combustor, normalized per unit atmosphere of combustor operation [6]. The higher the thermal intensity the smaller the combustor size for the same thermal load. It is desirable to have high thermal intensity in order to reduce combustor size and weight requirements. This is desired to not only cut down on material costs, but especially in aviation gas turbines keep the engine as lightweight as possible. Although thermal intensity is desired to be high especially in the aviation industry, where space and weight are a premium, it is important to consider the heightened thermal stresses and material properties of the combustor in order to have maintain reliability. Land based gas turbines operate in the 5-50 MW/m^3-atm range, while aviation gas turbines generally operate with a thermal intensity of 100-200 MW/m^3-atm.

1.2.5 Low Pressure Drop

It is undesirable to have significant pressure drop across the combustor, as keeping the pressure as high as possible increases the amount of power which can be extracted from the turbine. Pressure drop over a combustor typically lies within 4-8% [2]. The overall pressure drop measured in the cold flow condition is:

$$Overall\ pressure\ drop = \frac{p_{in} - p_{out}}{p_{in}} \quad \text{(Eq. 1.1)}$$

Additionally, the combustion pressure drop for a constant area duct is given by equation 1.2 and is generally 0.5-1% of the total inlet pressure [2].

$$Combustion\ pressure\ drop = \Delta p_{comb.} = p_{dynamic\ in} * \left(\frac{T_{out}}{T_{in}}\right) \quad \text{(Eq. 1.2)}$$

1.2.6 Desired Pattern Factor

It is important to maintain an even temperature profile across the combustor outlet in order to maximize the reliability and lifetime of the turbine blades by minimizing thermal stresses induced from high thermal gradients across them [2]. The pattern factor is a measure of this unevenness in the temperature profile and in given by:

$$Pattern\ factor = \frac{T_{\max out} - T_{avg\ out}}{T_{avg\ out} - T_{avg\ in}} \quad \text{(Eq. 1.3)}$$

It is thus important to design a combustor with a uniform temperature field to keep the pattern factor low.

1.2.7 Fuel Flexibility

It is also desirable to have a gas turbine combustor which has a wide range of fuel flexibility. For land-based gas turbines, the typical fuel is natural gas; however, it

is desirable to be able to burn liquid and biofuels. Although natural gas is abundant at this time, by increasing the amount of fuels which can be efficiently and effectively used energy security is enhanced. In addition it may be desirable to use syngas and low-calorific value fuels (namely those with high hydrogen, CO, and diluent content) as an alternative fuel source depending on the location of the plant, as proximity to fuel sources is also a major economic consideration. For the aviation industry, energy security is even more important as the kerosene/petroleum based liquid fuels have depleting fuel sources and can have high fluctuations in costs due to political factors.

1.3 Pollutant Formation

As discussed in section 1.2.3, it is desirable to keep pollutant emissions low in gas turbine combustion. Particularly, there is concern over NO_x formation, CO and UHC, as well as soot. Increasingly stringent emission standards, desire for combustion efficiency of 100% and impact on health and the environment lead to the need to keep pollutant emissions low.

1.3.1 NO_x Formation

Concern over NO_x due to photochemical smog and acid rain concerns has led to strict NO_x emissions standards for gas turbines from the EPA [5]. NO_x is primarily the combination of nitric oxide (NO) and nitrogen dioxide (NO_2). NO is the primary component of NO_x, at upwards of 90%. There is concern over multiple reaction mechanisms for NO_x formation for gas turbine combustors depending on operating conditions. A list of major NO_x reaction mechanisms is given in Fig. 1.3.

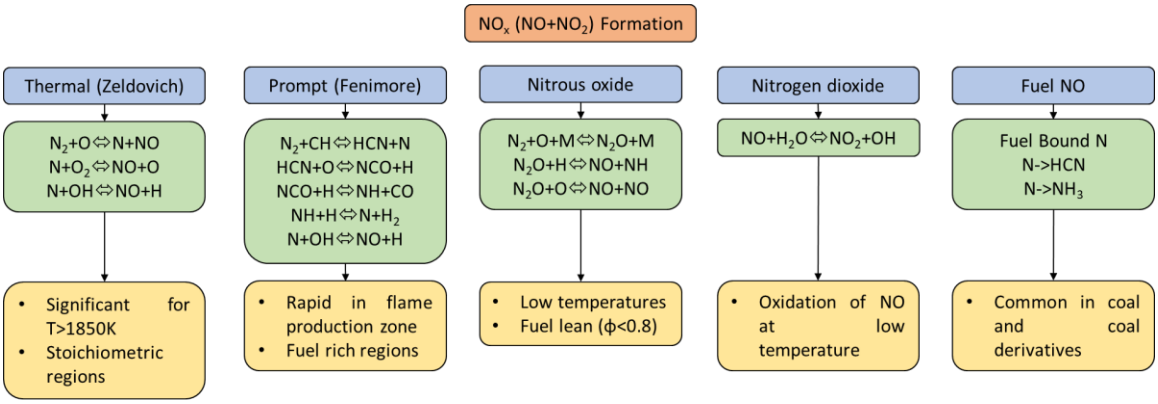

Fig. 1.3. Mechanisms of NO_x formation [2]

First, the thermal, or Zeldovich, mechanism is the dominant NO_x reaction mechanism at high temperatures and near stoichiometric regions within the flame. The Zeldovich mechanism is given by the following equations:

$$N_2+O \Leftrightarrow N+NO \quad \text{(Eq. 1.4)}$$

$$N+O_2 \Leftrightarrow NO+O \quad \text{(Eq. 1.5)}$$

$$N+OH \Leftrightarrow NO+H \quad \text{(Eq. 1.6)}$$

The Zeldovich mechanism is dependent on breaking atmospheric nitrogen down into elemental nitrogen and NO by reacting with an O atom. Due to high activation energy required to break down the N_2, this mechanism is limited to high temperature conditions, hence thermal mechanism. Generally, this reaction will not occur unless temperatures exceed 1850K. Thus, NO formation due to this mechanism occurs in hot spot regions of near stochiometric conditions, where the flame temperature is hottest.

The prompt, or Fenimore, NO mechanism is dependent of hydrocarbon chemistry. Fernimore NO is associated with the interaction of CH radicals and nitrogen to form HCN which further reactions occur until NO is formed as follows:

$$N_2+CH \Leftrightarrow HCN+N \quad \text{(Eq. 1.7)}$$

$$HCN+O \Leftrightarrow NCO+H \quad \text{(Eq. 1.8)}$$

$$NCO+H \Leftrightarrow NH+CO \quad \text{(Eq. 1.9)}$$

$$NH+H \Leftrightarrow N+H_2 \quad \text{(Eq. 1.10)}$$

$$N+OH \Leftrightarrow NO+H \quad \text{(Eq. 1.11)}$$

The Fernimore reaction mechanism occurs very rapidly (prompt) and can additionally result in producing elemental nitrogen to be used in the Zeldovich mechanism. The Fernimore reaction mechanism is used when equivalence ratios fall below 1.2 [4]. Due the dependence on hydrocarbon chemistry above an equivalence ratio of 1.2, this reaction scheme becomes more complex; however, due to gas turbines typically being operated under lean conditions this is not of concern.

The nitrous oxide, N_2O mechanism becomes more predominate under fuel lean conditions and low temperature conditions. A third body can be used to aid formation of N_2O by reacting O with N_2, which can further be oxidized until NO is formed [4]. This mechanism is more favored at low temperatures and equivalence ratios due to the reduction of temperature not driving the more dominate Zeldovich mechanism and a greater chance for a third body interaction due to higher N_2 concentration, if combustion occurs in air, which will be more likely to be inert at the lower temperature. The N_2O mechanism is given as follows:

$$N_2+O+M \Leftrightarrow N_2O+M \quad \text{(Eq. 1.12)}$$

$$N_2O+H \Leftrightarrow NO+NH \quad \text{(Eq. 1.13)}$$

$$N_2O+O \Leftrightarrow NO+NO \quad \text{(Eq. 1.14)}$$

Nitrogen dioxide formation can occur when hater is present and reacts with NO, given by equation 1.15. The oxidation of NO to NO_2 in this way can occur at low temperatures where H_2O is still reactive.

$$NO + H_2O \Leftrightarrow NO_2 + OH \quad \text{(Eq. 1.15)}$$

Fuel NO is not generally a concern for most gas turbine combustion, as natural gas and other gaseous fuels primarily used for gas turbine combustion do not contain much if any fuel-bound nitrogen. This can be a concern in the aviation industry if the liquid fuel used has significant fuel bound nitrogen. Fuel NO is mush more common with the burning of coal and coal derivatives as nitrogen impurities are found here. This may also be a concern if ammonia was to be used as a fuel source, which has been considered as a possible alternative fuel [8].

1.3.2 CO and UHC Formation

Carbon monoxide has two major pathways of formation. First, oxidation of carbon atoms present in the fuel is desired, as complete combustion dictates all carbon atoms present should go to CO_2. However, the oxidation of CO to CO_2 takes significant time and thus is dependent of the residence time of the combustor. Additionally, if there is not enough oxygen to react with the CO then carbon dioxide emission goes up as well. Lack of oxygen occurs more prevalently in rich flames, and thus higher CO is present under rich conditions. Second, dissociation of CO_2 into CO can occur under higher temperatures (>1600K). It has been found that UHC production occurs due to similar factors as CO emissions [2].

1.3.3 Soot Formation

Soot formation occurs in fuel rich regions and in regions of poor mixing, where there is not enough oxygen to oxidize the carbon present in the fuel [2]. Gas turbines are generally run under lean conditions, but soot can further be mitigated by either

premixing the fuel and air or by increasing mixing to reduce rich zones present in the combustor.

1.4 NO_x Abatement Strategies

Due to NO_x being a significant concern, it has been a prerogative for gas turbine combustor design to mitigate NO_x and reduce this and other pollutants. This section will go over some NO_x abatement strategies used in industry today.

1.4.1 Injection of Diluents

Diluents are added into either directly into the reaction region or are premixed with the fuel and air prior to combustor injection. These diluents have no calorific value and if combustion efficiency is high, they should be considered inert for all practical purposes. Several methods of diluent injection exist one of which being steam injection. Steam injection works by injecting steam directly into the reaction zone to cool the reaction zone and limit thermal NO_x. The used of water can unfortunately lead to corrosion. Additionally, the system to inject this steam is costly and requires additional maintenance. Reduced temperatures may also lead to limiting full conversion and oxidation of CO and UHC [2].

Another diluent injection method is exhaust-gas recirculation, wherein a portion of the exhaust products is returned to the combustor inlet. This not only dilutes the incoming mixture, but also contributes to preheating the mixture which prevents temperatures from being too low that they promote UHC and CO production. Fouling can be a concern, however if a clean fuel is not used [2].

1.4.2 Exhaust Clean-up

Instead of trying to reduce the temperature of the reaction zone, NO_x can be produced freely and then cleaned up post combustion. Typically, the exhaust will be passed through a catalyst which contains ammonia as the reducing agent which will oxidize the NO_x and produce N_2 and H_2O. This may also lead to some oxidization of some CO and UHC as well and is deemed very effective in reducing NO_x removal at up to 90% effectiveness [2]. Unfortunately, the added cost of the catalyst as well as a way to replenish the ammonia is concerning can make this method of NO_x abatement unattractive.

1.4.3 Limiting Formation

Several techniques have been developed to control the combustion process in a way that is favorable for NO_x abatement. One such method is lean premixed (pre-vaporized combustion) [9]. As the Zeldovich mechanism is the primary contributor to NO_x it is important to limit the peak temperatures in the combustion chamber. By premixing the fuel and air rich and near stoichiometric zones can be reduced (peak temperatures occur approximately at φ=1.1). If liquid fuels are used, they are pre-vaporized to prevent droplet size effects from affecting the combustion chemistry. Additionally, temperature is further reduced by keeping the combustion lean. Although NO_x can be greatly reduced, challenges in combustion stability may arise due to due to operation near the lean flammability limit.

Premixing the fuel and air may present challenges, especially when flame speed in high which can result in flashback. Additionally, premixing may not always be possible with combustor and gas turbine size constraints. When a non-premixed mode

is required, lean direct injection allows for similar NO_x emissions and lean premixed combustion [10]. In lean direct injection, fuel is injected into air and mixed rapidly to so that burning can occur nearly the same as if premixing was employed. In order to enhance mixing, multiple fuel injectors, swirlers, and other turbulence enhancers can be used helpful in both mixing and flame stabilization. There can be residence time concerns over lean direct injection due to additional mixing time requirements.

Another method for reducing NO_x is to use a catalytic combustor. By using a catalyst to reduce the activation energy of reaction combustion can be maintained at lower temperatures. A catalytic combustor is typically a multi-stage combustor with a catalytic section ran under very lean conditions and temperatures less than 1270K and a thermal reactor in which temperatures exceeding 1270K are reached [11]. The catalytic reactor keeps NO_x emissions low, while the thermal reactor allows for further oxidation of CO and UHC and raises the temperature of the products to appropriate temperatures prior to the turbine.

The rich-burn, quick quench, lean-burn (RQL) technique takes advantage of the emissions curves in Fig. 1.2. Combustion using RQL starts under a rich burn where NO_x remains low while CO and UHC levels are high. By rapidly quenching the system thermal NO_x is avoided when transitioning to a lean-burn stage, wherein the UHC and CO can subsequently be oxidized resulting in low emissions [7]. Although this system promises low emissions, combustor size is large, the quenching process must be done precisely, and the hardware implementation can be complex.

Chapter 2: Literature Review

This chapter will review the various techniques developed and investigated by different researchers with focus on combustion with ultra-low pollutant emissions. Focus here is on technologies which are used to employ a distributed combustion reaction zone for enhanced mixing and reduced pollutant emissions will be examined. Several techniques with this goal have demonstrated success in achieving this goal, namely: High Temperature Air Combustion (HiTAC), Flameless Oxidation (FLOX), Moderate or Intense Low-oxygen Dilution (MILD), and Colorless Distributed Combustion which is the focus of this thesis.

2.1 High Temperature Air Combustion (HiTAC)

The focus of this thesis, colorless distributed combustion (CDC), is based on the concepts and principles of high temperature air combustion (HiTAC). HiTAC was developed for boiler and furnace applications which operate under low thermal intensity (<1MW/m^3-atm) as compared to gas turbine application (5-50MW/m^3-atm) [6]. The concept of HiTAC was developed and successfully demonstrated ultra-low NO_x and CO emissions [12]. The HiTAC principle works by preheating the inlet air stream to above the auto-ignition temperature of the fuel resulting in a flame which then no longer needs a flame stabilizer to maintain a flame.

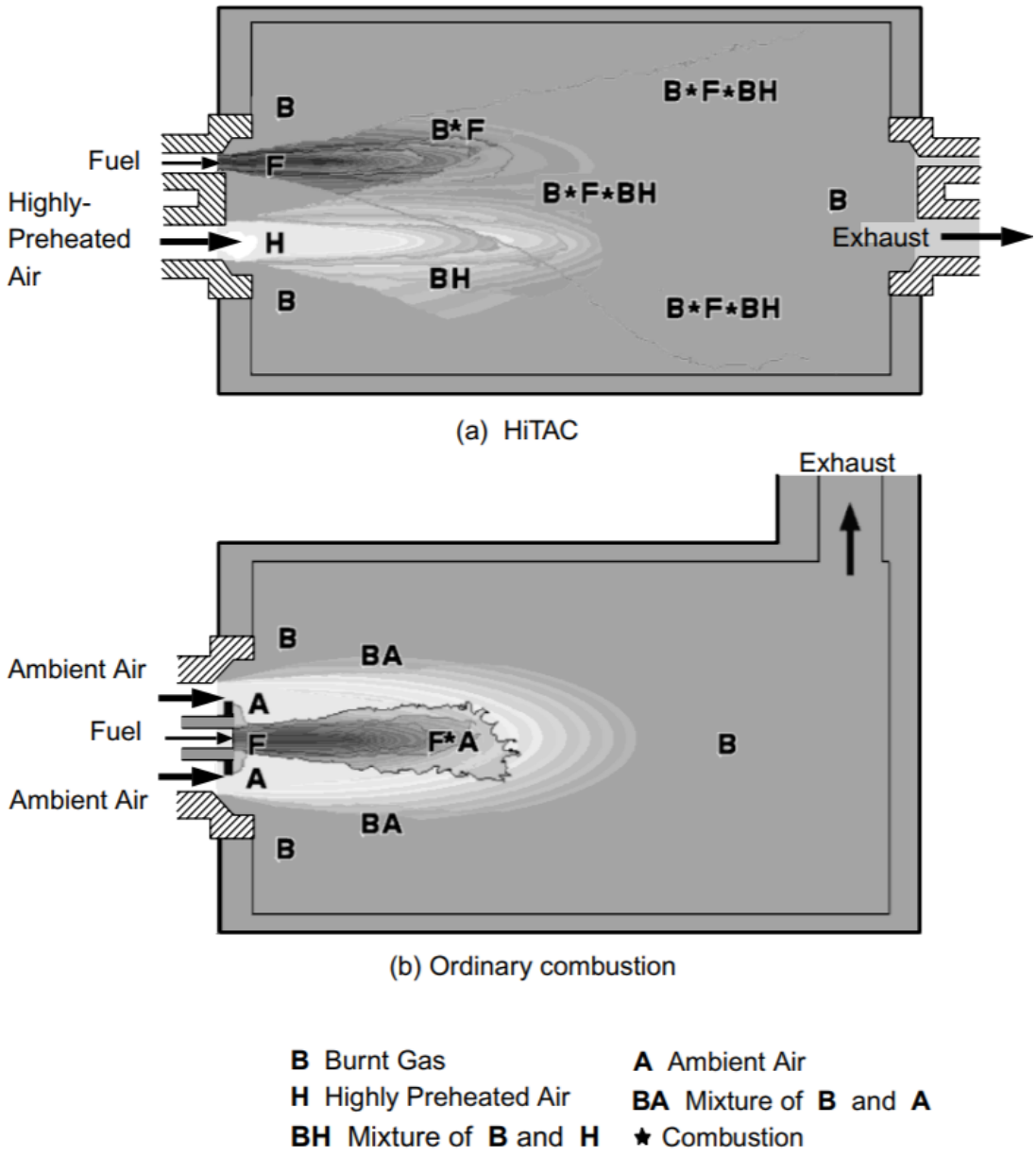

Fig. 2.1. Concept of HiTAC [12]

The concept of HiTAC is illustrated in Fig. 2.1. Under conventional combustion, fuel and air are injected close together for direct mixing, resulting in a flame front stabilized on the region of stoichiometric fuel and air (F*A). As this region is near stoichiometric there are high temperature regions (>1850K) and high levels of

NO_x are present following the Zeldovich mechanism. Entrainment of some product gases (B) are used to help stabilize the flame toward the burner outlet.

Under HiTAC mode fuel and highly preheated air (above the autoignition temperature) are injected separately, avoiding mixing of the two streams. Instead mixing between the air and entrained product gases forms a low oxygen concentration mixture (BH), while some weak reactions may occur between the fuel and the hot gaseous products as well (B*F). The primary reaction zone takes place between the entrained hot gaseous products, the fuel and the low oxygen concentration mixture (B*F*BH). A temperature rise from the inlet air to the maximum temperature is slightly greater than the self-ignition temperature, as opposed to multiple times the self-ignition temperature in a conventional flame. This results in a more distributed flame by dispersing the fuel and oxidizer throughout. In this way, hot spots are mitigated resulting in lower NO_x emissions.

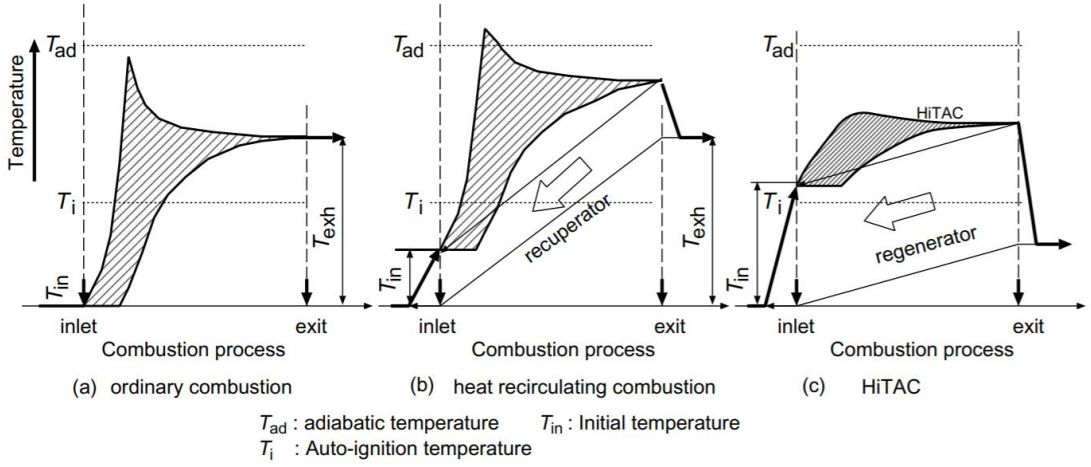

Fig. 2.2. Temporal temperature history for conventional combustion (a), convention combustion with a recuperator (b) and HiTAC (c) [12]

It is important to note that the benefits of HiTAC come from the entrainment of hot product gases and the formation of a low oxygen concentration oxidizer which is then mixed with fuel. This is not the same as recuperation wherein heat is reintroduced through the use of a traditional heat exchanger (recuperator) between the exit and inlet of the combustor. Figure 2.2 shows the differences in the temperature histories of conventional combustion, conventional combustion with the use of a recuperator, and HiTAC. Under conventional combustion, after ignition there is a large temperature spike, wherein local hot spots occur which lead to high NO_x and can lead to combustor burnout. The use of a recuperator raises the inlet temperature of the reactants but does not prevent a temperature spike after ignition of the fuel. Under HiTAC a regenerator is used, which is a special heat exchanger which is generally made up of ceramic which has a large heat capacity and thermal mass. This regenerator preheats the inlet air to above the auto ignition temperature. Due to combustion not taking place directly between the fuel and air, like in conventional combustion and instead being between a reduced oxygen concentration oxidizer, fuel, and reactive product gases, the temperature rise is limited below where thermal NO_x is dominate (below 1850K).

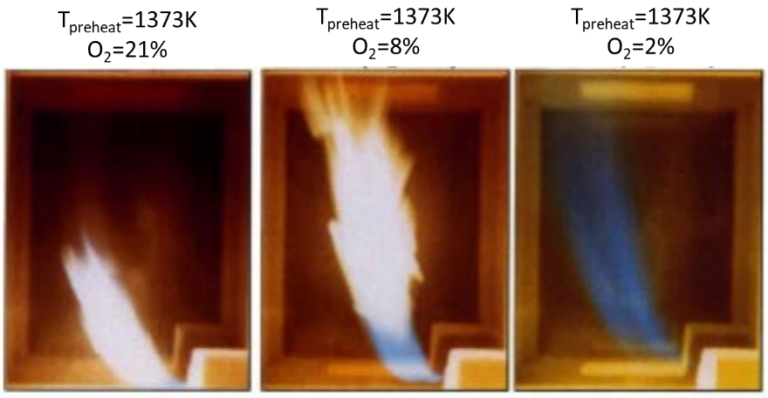

Fig. 2.3. Global photographs with combustion air preheat of 1373K and varying O_2 concentration (N_2 dilution) [13]

Diluent gases may be added to a preheated air stream in order to enhance entrainment and reduce the oxygen concentration [13]. Figure 2.3 shows the effect of added a diluent (N_2) in order to reduce the oxygen concentration and obtain HiTAC conditions. In all three cases presented in Fig. 2.3 the preheat remains constant at 1373K (above the autoignition temperature). Under the air combustion case, there is a distinctive yellow flame, suggesting sooting, additionally the flame front is very thin. As oxygen concentration is reduced the reaction zone broadens becoming more and more distributed. At 2% oxygen concentration, all yellow in the flame is gone, suggestive cleaner combustion. In addition, the visible signature has been reduced while the reaction zone becomes distributed over a larger region of the combustor.

HiTAC presents several benefits over conventional flames including energy savings, NO_x reduction, and thermal field uniformity. Energy savings of up to 30% [14] have been demonstrated through the use of HiTAC. This energy savings is possible due to the recovery of thermal energy through the use of a regenerator. This thermal energy feeds directly back into the combustor, reducing the intensive energy requirement to

initiate combustion. Additionally, due to this energy savings reduction on emissions as a whole go down as less fuel is required for the same power output. As previously mentioned, due to reaction taking place between a reduced oxygen concentration air, fuel and reactive product gases peak temperature zones are reduced and NO_x formation is mitigated. Finally, thermal field uniformity is enhanced due to a more distributed reaction zone and reduced temperature fluctuation intensity [15]. Combustion temperature is only about 50-100K higher than that of the inlet preheated air, resulting in a near uniform temperature profile.

2.2 Flameless Oxidation (FLOX)

Flameless oxidation (FLOX) is a proprietary combustion method for reduced pollutant emission which employs internal exhaust gas recirculation to create an oxidation region where no visible signature and no spike in temperature are present [16]. FLOX uses a loop reactor, where the inlet and outlet streams are on the same side of the combustor, forcing the flow to make two passes across the combustor length. Fuel is injected in the center of a concentric ring of multiple air injection nozzles. Through the use of preheat of the inlet air stream above the auto-ignition of the fuel, entrainment is promoted within the combustor. Through entrainment of gaseous products at the base of the flame, the flame root disappears and the flame appears lifted due to a non-visible, no temperature rise region directly out of the burner. Figure 2.4 shows the conventional combustion and FLOX combustion modes. A key feature of FLOX is that the temperature profile does not reach the peak temperatures thatoccur

under standard combustion, and the temperature gradient present is not as steep under FLOX.

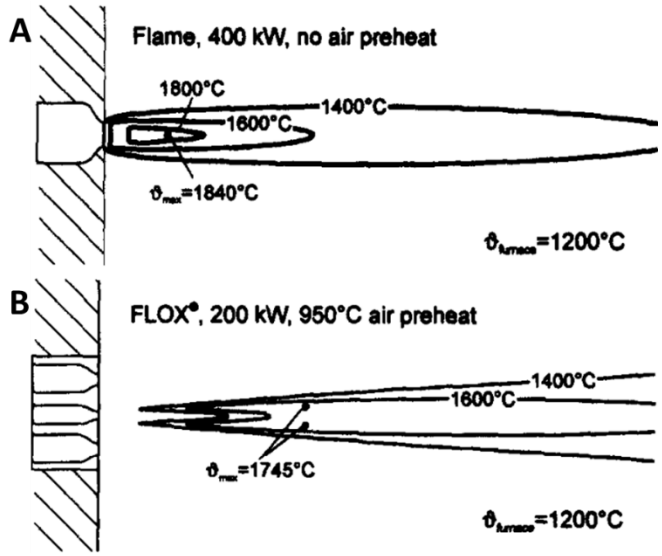

Fig. 2.4. Temperature distribution of conventional (A) and FLOX (B) combustion [16]

2.3 Moderate or Intense Low Oxygen Dilution (MILD)

Moderate or intense low oxygen dilution (MILD) is a similar method to HiTAC, wherein air is preheated to above the auto ignition point of the fuel which favors internal entrainment of product gases leading to a low visible signature combustion. The primary difference between HiTAC and MILD is the working temperature conditions. Under both HiTAC and MILD the inlet air temperature is greater than the self-ignition temperature of the fuel; however, what separates these methods is the working condition temperature inside the combustor is different. For HiTAC, the change in temperature between the inlet air temperature to the maximum temperature is greater than the self-ignition temperature, while under MILD this same temperature change is less than the self-ignition temperature [17]. Additionally as the name

suggests, MILD is not only for furnace application, but also for higher thermal intensities (>1MW/m^3iatm).

2.4 Colorless Distributed Combustion (CDC)

Colorless distributed combustion (CDC) is based on the principles of HiTAC, with the goal of obtaining a more uniform temperature reaction zone and reduced pollutant emissions utilizing internal entrainment inside the combustor. Where HiTAC is for furnace application, thermal intensity <1MW/m^3-atm, CDC is for gas turbine application, thermal intensity >5MW/m^3-atm. Research on CDC have examined the various input and operational parameters required to achieve enhanced stability, ultra-low pollutant emission, uniform temperature profile combustion at high thermal intensity.

Unlike HiTAC, FLOX and MILD, CDC does not require preheats over the autoignition temperature. CDC is defined as combustion taking place in the distributed reaction regime, see figure 2.5, which occurs due to internal entrainment of hot reactive gaseous species to aid in a more broadened and uniform reaction zone which has a low visible signature (colorless). The key to CDC is a low oxygen concentration oxidizer, which will slow the chemical length scale down enough to promote mixing and entrainment prior to combustion, resulting in ulta-low emissions and a more uniform thermal field.

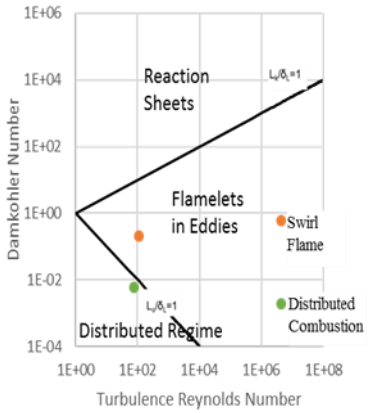

Fig. 2.5. Combustion regimes

CDC has been investigated on multiple burner designs including rectangular combustors, circular swirling combustors and swirl stabilized combustors. Global images from each of these designs are shown in figure 2.6. Investigations on the rectangular combustor design for CDC have focused on wide ranging thermal intensities, combustor geometry and fuel flexibility. Thermal intensities ranging from 5-198MW/m^3-atm have been investigated in both premixed and non-premixed modes. Ultra-low emissions have been achieved with this design with NO emissions near unity ppm and CO levels of around 100ppm for both gaseous and liquid fuels. It was determined that the most favorable combustor geometry was a reverse flow combustor wherein the inlet and outlet are on the same side to in order to increase residence time [18]. Additional studies were performed using a swirl combustor at thermal intensities up to 36MW/m^3-atm. Various injection locations and fuel types, ranging from methane, propane, ethanol, and jet fuels were investigated to determine the robustness and fuel flexibility of CDC. Under swirling CDC, NO levels of under 7.5ppm and CO levels of under 40ppm for liquid fuels and 10ppm for gaseous fuels were achieved [19]. Further studies on swirl assisted CDC have been performed at thermal intensities of 2.4-

10MW/m^3-atm. These studies had a broad range of focus for the development of a distributed combustion index (DCI). The development of the DCI is beneficial in determining the conditions required for CDC to be achieved regardless of fuel type, combustor geometry, injection velocity, diluent type, preheat temperature and other parameters. Figure 2.7 gives the DCI for fuel type and preheat temperature [20].

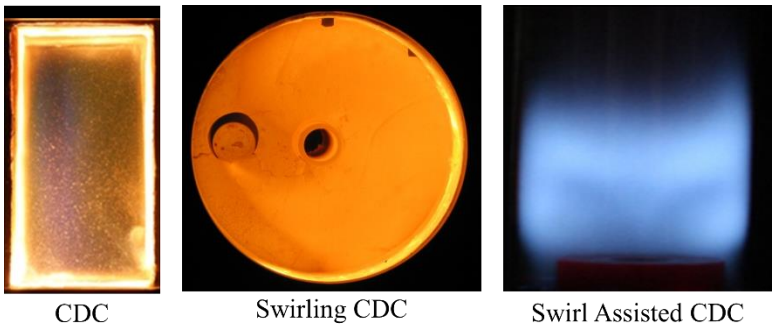

Fig. 2.6. Global images for various CDC combustors

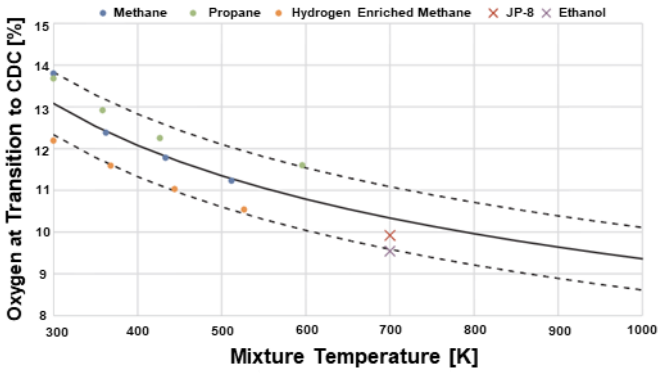

Fig. 2.7. Oxygen concentration for CDC transition for various fuel types [20]

Chapter 3: CDC Fuel Enrichment

3.1 Naphthalene Fuel Addition to Ethanol

CDC is reported to show ultra-low pollutants emissions using biofuels compared to liquid fossil fuels [21]. Therefore, focusing on CDC for biofuels would be increasingly beneficial, considering fuel additives could enhance even further effective biofuel combustion, due to the traditionally low heating value of biofuels. Fuel additives have been employed in biofuels for numerous applications, such as, ignition promoters, stability enhancers, and emissions reducers [22]. Under distributed combustion conditions, the emissions were substantially reduced by some 95% to result in NOx emissions of less than 2 ppm with minimal impact on CO emission from both JP-8 and ethanol fuels at an equivalence ratio of 0.9. Lower equivalence ratios demonstrated even lower emissions. Combining the data obtained with liquid fuels with those from gaseous fuels revealed that, regardless of the fuel used, the oxygen concentration at which CDC prevailed can be predicted based on mixture temperature within a range of 0.75% [20]. Naphthalene, well known for its use as the main ingredient in old mothballs, has been used as a fuel additive in order to reduce engine deposits [23], as well as increase fuel performance [24, 25]. However, there is currently a very limited amount of relevant literature detailing the effects of naphthalene addition in fuels, on performance or emissions. Prior to this research no studies on the use of naphthalene under distributed combustion condition had been examined. In this section, the use of naphthalene as a fuel additive in ethanol was examined with a focus

on providing data for naphthalene undergoing combustion and its subsequent effect on emissions and combustor performance. This provided useful insights on the use of naphthalene in the CDC design for stationary gas turbine combustion applications.

3.1.1 Materials and Methods

Naphthalene (99%, Acros Organics) and ethanol (200 Proof ACS/USP Grade, Pharmco-Aaper) were used as purchased without further purification. 0.1, 0.3 and 0.4 M solutions of naphthalene in ethanol were prepared at room temperature and compared to pure ethanol. The densities of these solutions were calculated using interpolation of the published data for naphthalene-ethanol mixtures [26]. The heating value of the mixture was calculated by multiplying heating values of the fuel constituent by the respective mole fraction, assuming complete combustion.

The combustion experiments were performed using a swirl burner shown in Fig. 3.1. Details of this burner can be found elsewhere [27]. A schematic diagram of the experimental setup is given in Fig. 3.2. The air and nitrogen flow rates were controlled by laminar flow controllers with accuracies of ± 0.8% of the reading and ± 0.2% of full scale. Carbon dioxide was controlled using a gravimetric flow controller with an accuracy of 1.5% of full scale. The liquid fuel was supplied using a liquid handling pump with an accuracy of ± < 0.5%. Heating tape was used to heat and vaporize the fuel into gaseous form while retaining the fuel chemical composition.

In order to support CDC condition, spatial distribution of OH* chemiluminescence signal was investigated [28]. An ICCD (intensified charged-coupled device) camera coupled with a narrow band filter for OH∗ chemiluminescence

detection was used with UV interference filter centered at 307 nm, FWHM ± 10 nm. The camera was set to a gain of 0 and an exposure time of 70 ms.

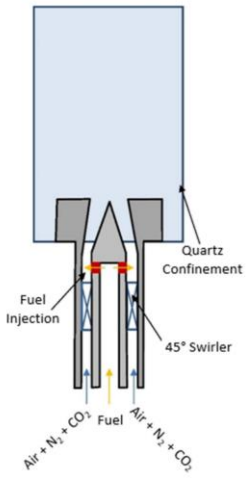

Fig. 3.1 Schematic of the experimental test combustor facility

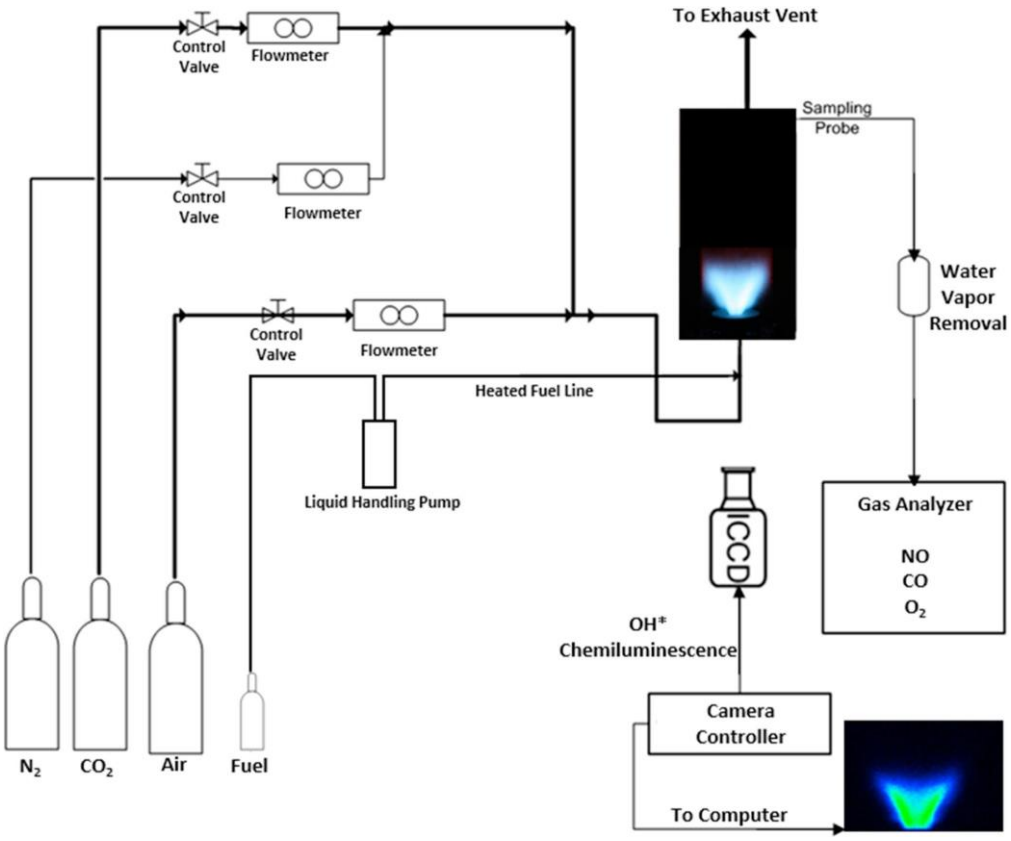

Fig. 3.2. Schematic of the experimental setup

The pollutants emission as well as the combustion products speciation were continuously sampled at the outlet of the burner and then passed through a desiccant to remove any moisture. NO was measured using an NO-NOx chemiluminescent gas analyzer while CO was measured using a non-dispersive infrared method. The O2 concentration was measured using the galvanic cell method. The O2 measurement was used for correcting the NO and CO emissions to the standard 15% oxygen concentration used for gas turbine emissions.

Table 3.1 summarizes the experimental conditions reported for naphthalene fuel addition in this section. Naphthalene content in ethanol was varied from 0.1 mol/L to 0.4 mol/L. Although the solubility limit of Naphthalene in ethanol is just over 0.6 mol/L of ethanol at 298 K [29], concentrations of naphthalene in ethanol higher than 0.4 mol/L were practicably not achievable. Due to extensive required mixing time and practically of having the fuel always stored at above 298 K, the naphthalene concentration was limited to 0.4 mol/L. For all conditions the inlet fuel temperature was maintained at 500 K (which is above the boiling points of both ethanol: 351 K and Naphthalene: 491 K) in order to ensure the fuel mixture examined in the burner was the same as prepared. The results are reported at two equivalence ratios of $\Phi = 0.9$ and 0.7. The equivalence ratio is a non-dimensional parameter, defined as the ratio of actual fuel-air ratio (FAR) to stoichiometric fuel-air ratio (FAR_{st}), i.e., $\Phi = FAR/FAR_{st}$. The particular equivalence ratios examined are higher than that used in todays' gas turbine engines. They are useful for the design of future generation CDC gas turbines that offer higher thermodynamic efficiency and increased performance. In gas turbine combustion excess air is used so that the turbine blades can handle the high temperatures and also mitigate the hot spot

zones to minimize the amount of NOx, CO, unburnt hydrocarbons formed. An equivalence ratio of 0.9 was chosen due to excessive NOx formation under normal conditions at such a high equivalence ratio. Reduction of NOx at such high equivalence rations using higher energy density fuels is of great importance for demonstrated ability of CDC for practical deployment in gas turbines. Additionally, carbon monoxide, unburnt hydrocarbons, and carbon/soot emissions are reduced under distributed combustion conditions. Combustion of aromatics and polyaromatic compounds, such as naphthalene, are of concern as they often give higher pollutants emission, including soot. Although hydrocarbon emission was not investigated here, unburnt hydrocarbon emission has been shown to be provide similar trend to CO [2]. Air, nitrogen, and carbon dioxide; however, were supplied at 300 K. Nitrogen and carbon dioxide were supplied using a 90:10 N2 to CO2 mixture in order to reduce the oxygen concentration.

Table 3.1 Experimental parameters at a fuel flow rate of 10 mL/min and fuel inlet temperature of 500 K

	Naphthalene Content	Equivalence Ratio	Oxygen Concentration [%]	Heat Release Intensity [MW/m3-atm]
1	Pure Ethanol	0.9	21-12.6	2.90
2	Pure Ethanol	0.7	21-15.75	2.90
3	0.1 mol/L	0.9	21-12.6	2.96
4	0.1 mol/L	0.7	21-15.75	2.96
5	0.3 mol/L	0.9	21-12.6	3.09
6	0.3 mol/L	0.7	21-16.8	3.09
7	0.4 mol/L	0.9	21-12.6	3.15
8	0.4 mol/L	0.7	21-17.85	3.15

3.1.2 OH* Chemiluminescence

The experiments focused on flame behavior as inlet oxygen concentration was lowered and CDC features developed. In order to observe flame structure and behavior,

OH∗ chemiluminescence signal intensity was captured, with the results presented in Figs. 3.3 and 3.4 at Φ = 0.9 and 0.7, respectively. The flame initially exhibited a characteristic swirl combustion structure with swirl lobes that supports the previously reported work on CDC [30, 31]. However, due to higher flame speed of ethanol than previously examined gaseous fuels using this burner, a propensity of flashback toward the fuel injection point was observed. Reduction in oxygen concentration provided a more uniform OH∗ distribution in the entire reaction zone. At Φ = 0.9, this transition started to occur at 14.7–15.75% oxygen concentrations and was attributed to a transition between the so called a 'V' and 'M' shaped flame. At oxygen concentrations lower than this the OH∗ signal was well distributed. Additionally, under the CDC mode there was no longer any flashback towards the burner exit, which be attributed to a reduction in flame speed under low oxygen concentrations. This behavior demonstrates the ability of CDC for use in preventing flashback in gas turbine combustors especially when using liquid fuels. At Φ = 0.7 a similar behavior was observed; however, the transition to the distributed regime occurred much faster in higher concentration naphthalene flames. In addition, the higher naphthalene content flames became unstable and blow-off occurred at inlet oxygen concentrations of 15.75% and 16.8% for the 0.3 mol/L and 0.4 mol/L solutions, respectively. At all other conditions examined the flames were extremely stable, with no indicators of flame blow-off.

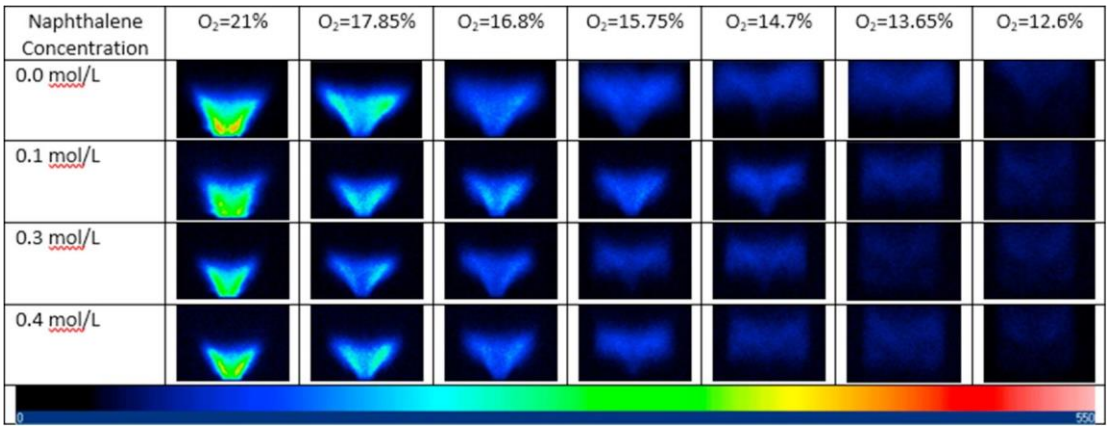

Fig. 3.3. OH* Chemiluminescence intensity signals for Φ = 0.9 at different concentrations of Naphthalene in Ethanol

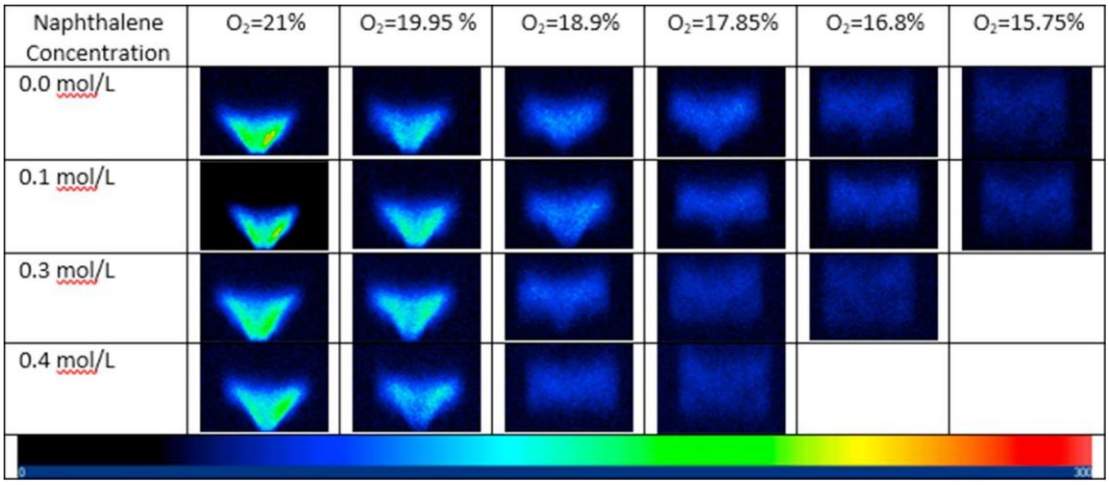

Fig. 3.4. OH* Chemiluminescence intensity signals for Φ = 0.7 at different concentrations of Naphthalene in Ethanol

3.1.3 Pollutants Emission

In addition to the OH∗ chemiluminescence intensity images, the pollutants emission was recorded and reported for all the conditions. Fig. 3.5 shows NO emission at Φ = 0.9. In general, as the inlet oxygen concentration was reduced, the NO emissions were reduced for all the conditions examined. As the oxygen concentration was reduced the reaction zone temperature also reduced to result in lower yields of thermal NOx. Moreover, as the amount of dissolved naphthalene in ethanol increased the NO yield decreased. Further support for this can be observed from the OH∗ chemiluminescence

images, wherein the intensity decreased with an increase in naphthalene content in the solution. Marchese et al. [32] have suggested that because the highest OH emission intensity is very close to the maximum flame temperature, OH∗ chemiluminescence can be used to determine the position of the flame front. Thus, the most intense regions of the flame can be identified. Furthermore, the OH∗ signal was observed to be slightly stronger in the pure ethanol flame, i.e. decreased chemiluminescence signal strength was detected with increase in naphthalene concentration, to reduce the thermal NOx formation. This behavior was consistent with the data obtained from the gas analysis that also revealed low NOx.

Table 3.2 Calculated heat content of the naphthalene-ethanol mixture at various naphthalene concentrations (Density and heat content calculated using Ref. [26])

Conc. of naphthalene [mol/L]	Wt.% of naphthalene in 1 L ethanol [%]	Mixture density [g/cm3]	Heat content (Mass basis) [kJ/kg]	Heat content (Volumetric basis) [kJ/L]
0	0	0.785	−29829.9089	−23416.4785
0.1	1.62	0.791	−30255.2193	−23931.8785
0.3	4.87	0.802	−31125.5343	−24962.6785
0.4	6.5	0.808	−31532.2754	−25478.0785

Fig. 3.6 shows the CO emission at $\Phi = 0.9$. The results show CO emissions to be under 6.5 ppm for all conditions. They were found to be under 6 ppm for most conditions. The increase in CO at the lowest oxygen inlet concentration was attributed to fuel-air mixture conditions approaching the flammability limit [31]. Overall there was a small reduction in CO with increase in naphthalene concentration; however, the difference between the highest and lowest corrected CO at any given condition was not more than 0.5 ppm.

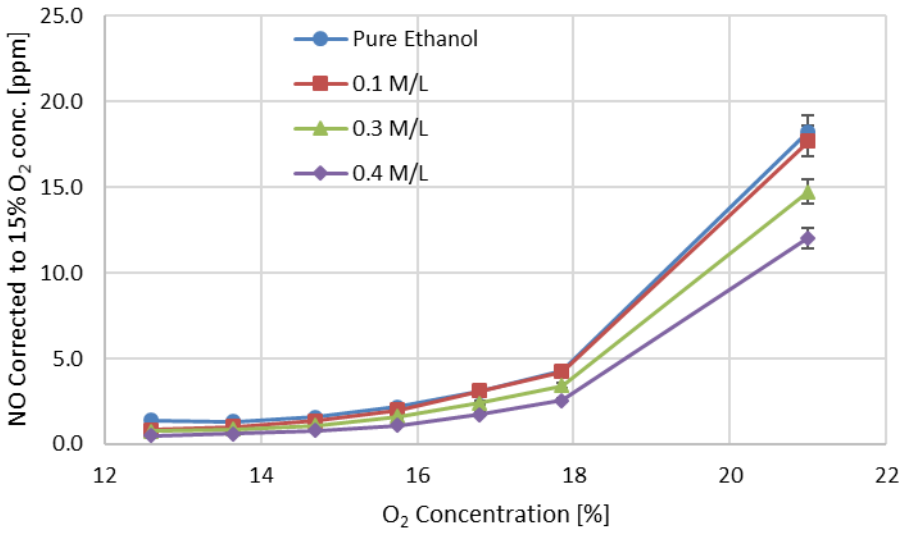

Fig. 3.5. NO emissions for Φ = 0.9 at different concentrations of Naphthalene in Ethanol

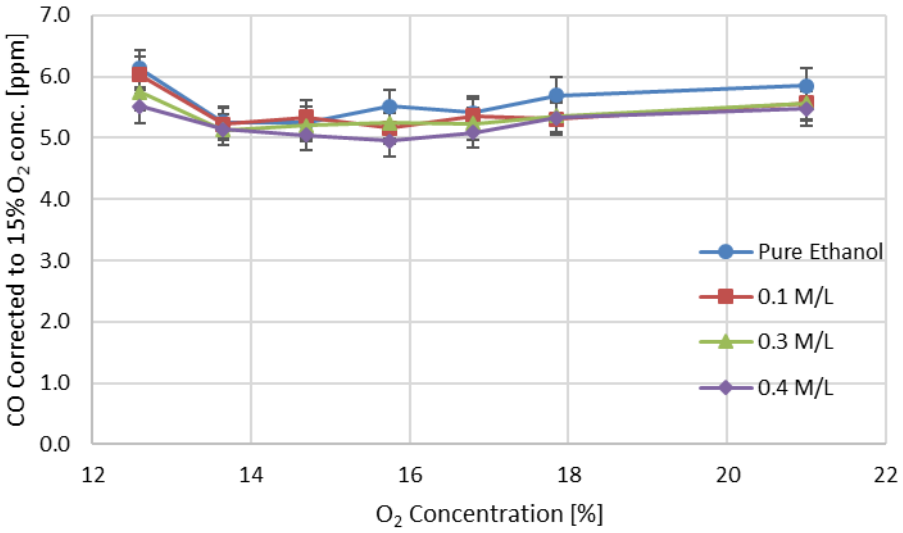

Fig. 3.6. CO emissions for Φ = 0.9 at different concentrations of Naphthalene in Ethanol

The results on NO and CO emission at Φ = 0.7 are shown in Figs. 3.7 and 3.8, respectively. Reduction in inlet oxygen concentration and increase in naphthalene concentration in the fuel also resulted in NO reduction that is consistent with the results obtained at Φ = 0.9 on NO emission. This also supports good agreement with the OH∗

chemiluminescence signal as discussed earlier for the data reported at Φ = 0.9. Although the CO levels were repeatedly low (under 6.5 ppm for all conditions) there was a slight increase in CO yield in the 0.3 mol/L and 0.4 mol/L naphthalene solutions cases as compared to the pure ethanol and 0.1 mol/L naphthalene solution cases.

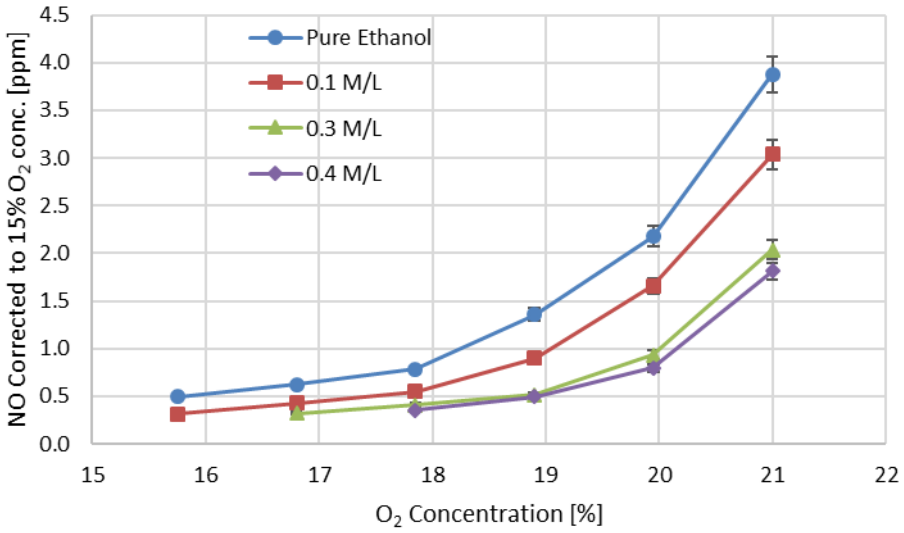

Fig. 3.7. NO emissions for Φ = 0.7 at different concentrations of Naphthalene in Ethanol

Reported flame colors with clear green shades reported in the experiments when naphthalene was included in methanol solutions were not observed with ethanol alone flames [33]. Moreover, yellow color sooting flames were not observed for any of the conditions examined. Only light blue flames were observed, which became almost invisible upon approaching CDC condition.

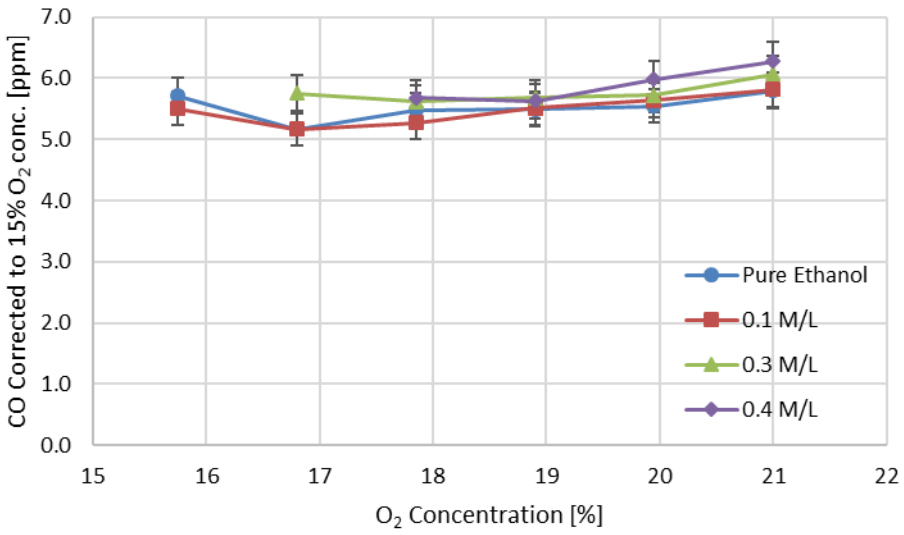

Fig. 3.8. CO emissions for $\Phi = 0.7$ at different concentrations of Naphthalene in Ethanol

The literature revealed the heat content of pure ethanol and pure naphthalene to be −1367 kJ/mol and −5154 kJ/mol, respectively [34]. Considering involved number of moles of naphthalene and assuming constant moles of ethanol in every solution, the heat contents of the mixtures could be calculated. For example, for a 0.1 mol/L solution of naphthalene in ethanol with a density of 0.791 g/cm^3, the heat content was −30255.2193 kJ/kg on a mass basis and −23931.87851 kJ/L on a volumetric basis. Furthermore, an increase in concentration of naphthalene from 0 to 0.4 mol/L provided an 8.8% increase in heating value (on volumetric basis) or 5.7% increase in heating value (on mass basis) of the resulting fuel. This is significant as one seeks for higher energy density fuels as most propulsion systems have restrictive weight and space limitations. Calculated density and heating value are given in Table 3.2.

Based on qualitative analysis of combustion products, naphthalene decomposition may be summarized as a multi-step oxidation process. Decomposition

characteristic of naphthalene at different equivalent ratios reflected in N2 and O2 emissions, as the primary products were created stoichiometrically [35]. The ring-cleavage of aromatic compounds may be further fragmented and finally mineralized into CO, CO2.

3.2 Hydrogen Enriched Fuel

Energy production requirements are constantly rising due to continuously increasing demand for electricity, heating and cooling. Most of these energy requirements are met with fossil fuels due to their high energy content. However, rapidly decreasing fossil fuel reserves have caused a major concern on their future availability in addition to concerns on carbon and pollutant emission, which are known to degrade the environment. Many scientists and engineers are actively engaged in finding alternative fuels using available resources and enhance efficiency to increase energy output while reducing emissions. Several coal-derived fuels, which can be produced either through gasification, called syngas, or gases released during the carbonization process, called coke oven gas or blast furnace gas, are more suitable alternative fuels than the direct use of coal as less harmful greenhouse gases are released, as well as negligible particulate matter emission as compared to those arising from coal combustion. In particular, coke oven gas is of interest due to its relatively high heating value for an alternative fuel (approximately one-half of that of natural gas). Coke oven gas is used in several industrial applications, such as hydrogen and syngas production, methanol synthesis for partial oxidation, dry reforming, tar utilization and methanation. Before the availability and use of natural gas, hydrogen enriched gas (such as coke oven gas) was utilized to meet the domestic energy demand

in several cities such as Sheffield and Birmingham in England [36]. At present coke oven gas is consumed directly as a gaseous mixture in different on-site processes during steel production due to ease in implementation. Approximately, 40% of the coke oven gas obtained in the US is now being utilized as an alternative fuel in blast furnaces in order to decrease dependency on natural gas. A payback period of less than one year and an annual savings of over 6 million dollars has been reported by US Steel Corp. when coke oven gas was utilized as a fuel in blast furnaces [36]. Coke oven gas can also be utilized in some turbine applications. In Japan, some industries have developed gas turbines that operate with coke oven gas. In Brazil, a company has successfully developed a 200 MW regenerative Rankine cycle power plant which utilizes coke oven gas and blast furnace gas as fuels [36].

The composition of the coke oven gas released during carbonization depends directly on the coal utilized for coking. Its production requires several processes of gas purification, NH3 removal, and desulfurization for improving the quality of gas [36]. Coke oven gas includes high amount of hydrogen (up to 60% on volumetric basis) and a moderate amount of methane (up to 40% on volumetric basis) depending on the production process. In addition, small amounts of carbon monoxide and non-combustible gases such as nitrogen and carbon dioxide are also present in the fuel. When coke oven gas is conventionally burned, the hydrogen in the coke oven gas leads to the formation of hot spots in the flame due to high adiabatic flame temperature associated with the combustion of hydrogen fuel, which leads to high levels of NOx formation [37]. Lee et al. [38] performed experimental studies on the combustion of various H2/CO mixtures and found NOX emission increased while CO emission

decreased with increase of H2 concentration in the mixture. e. For this reason, it is advantageous to use a novel combustion method such as CDC in order to mitigate emissions of NO_x and CO without reducing thermal performance with these types of hydrogen enriched fuels.

Due to high hydrogen concentration in coke oven gas, increased flame temperature and hot spot zones occur during combustion, which are primarily responsible for increased thermal NO_x formation. Increased hydrogen content in the fuel can also lead to flame instabilities such as flash back and excessive noise emission. CDC offers a good solution for the reduction of pollutants emission and enhance flame stability and alleviation of flash back, through reduction in the chemical reaction rate at high thermal intensity resulting in a more uniform and stable reaction zone. CDC allows one to use fuels having high hydrogen content, such as coke oven gas, at high efficiency and flame stability.

In this section, colorless distributed combustion using three blends of hydrogen rich fuel which may simulate alternate coke oven gas fuels was performed to further investigate fuel flexibility using alternative fuels having high hydrogen content. Focus here is on improving flame stability, particularly with the use of high hydrogen content fuels, to obtain a more uniform thermal field, and reduce NO and CO emission. The OH* chemiluminescence flame signatures were obtained along with emissions of NO and CO at the combustor exit. Either nitrogen or carbon dioxide was selected as the diluent that provided reduction of the oxygen concentration in the oxidizer stream for seeking distributed combustion condition. The experiments were conducted at various equivalence ratios to understand the effect of gas specific air dilution on flame

signatures and emissions from the combustion of hydrogen enriched fuels. The fuel composition was simulated by using selected mixture compositions of hydrogen, methane, carbon dioxide and nitrogen.

3.2.1 Materials and Methods

A swirl stabilized burner, with a (nominal) calculated swirl number of 0.77, was utilized in the experiments. A schematic diagram of the burner is shown in Fig. 3.1 with the option of either N_2 or CO_2 being used as the diluent added to the oxidizer line. In the burner, the fuel line supplying the hydrogen enriched fuel was located at the longitudinal center axis of the burner. The fuel was injected radially outwards into the oxidizer stream, which was coaxially positioned along the outside of the fuel line. The oxidizer line was used to feed in air, or the air/diluent mixtures simulating entrainment of hot reactive gases. This burner had outlet radius of approximately 0.395 in. that was fitted to a quartz tube making up the combustor test section, having an internal diameter of 2 ⅜ in. and a height of 7 ⅞ in. The quartz tube allowed for complete optical access downstream of the burner.

A schematic diagram of the combustion system used here is given in Fig. 3.9. The supply gases were fed through two sets of lines, one of which was a fuel line while the other was the oxidizer line. The fuel line was comprised of a mixture of hydrogen, methane, carbon dioxide and nitrogen, while the oxidizer line included air along with either nitrogen or carbon dioxide. Flow controllers were used to accurately meter the flow rates. The air and the oxidizer diluent flow controllers were laminar flow controllers having an accuracy of ± 0.8% of the reading and ± 0.2% of full scale, corresponding to an overall accuracy of approximately 1.5% of the reading. For gases

in the fuel line, flowrates were controlled using gravimetric flow controllers each having accuracies of 1.5% of full scale.

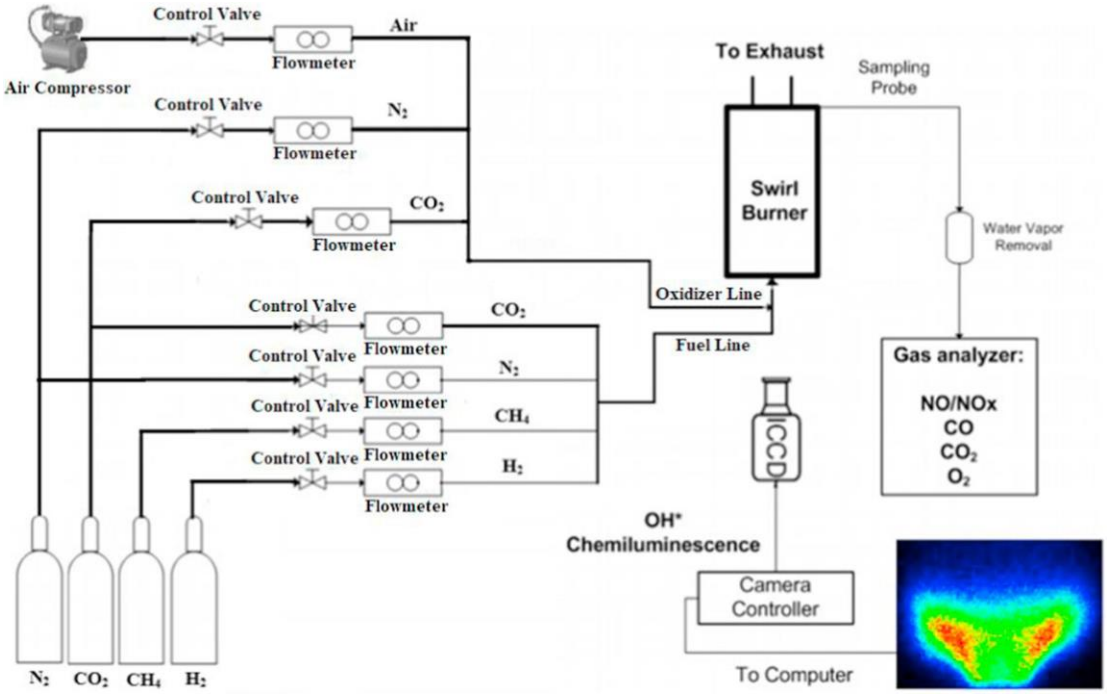

Fig. 3.9. A schematic diagram of the combustion test facility

Flame signatures were recorded using an ICCD (Intensified Charge Coupled Device) camera as depictured in Fig. 3.9. The camera was coupled with a narrow band filter to detect OH* chemiluminescence (UV interference filter centered at 307 nm with a FWHM of ± 10 nm). The camera was positioned at a distance of 40 in. from the flame. The product gases at the combustor exit were measured for NO, CO and O2 concentrations using a gas analyzer. The gas analyzer measured NO through a crossflow modulation chemiluminescence detection method, CO through the non-dispersive infrared absorption method, and O2 concentration determined by the galvanic method that allowed corrections on the NO and CO emissions for a standard

15% oxygen concentration. NO and CO concentrations were measured with estimated accuracies of 1.5% of full scale.

The hydrogen enriched fuels comprising of three different concentrations of hydrogen and methane were burned in the combustor, while keeping carbon dioxide and nitrogen concentrations constant in the fuel. Table 3.3 shows the fuel mixture which simulated the various hydrogen enriched fuel compositions examined.

Table 3.3 Composition of select hydrogen enriched gases (volume %), calorific value, and volumetric flow rate for constant heat release intensity of 5.7 MW/m^3-atm

Fuel	H2 [%]	CH4 [%]	N2 [%]	CO2 [%]	Heating Value [MJ/m3]
1	40	40	10	10	~18.6
2	50	30	10	10	~16.1
3	60	20	10	10	~13.6

For the oxidizer mixture, air was first used as a baseline. Nitrogen or carbon dioxide was then introduced into the air flow stream in order to examine the effects of reduced oxygen concentration. The introduction of diluents in the oxidizer stream, while maintaining the stoichiometry, was used to simulate hot reactive product gas entrainment for seeking distributed combustion condition. For all conditions, heat load, heat release intensity, mixture temperature, and pressure were kept constant at 3.25 kW, 5.7 MW/m^3-atm, 300 K (room temperature), and 1 atm (atmospheric pressure flame), respectively. Equivalence ratio was varied in order to examine air dilution without changing oxygen concentration in the oxidizer. Experimental conditions for each of the fuel compositions are presented in Table 3.4.

Table 3.4. Hydrogen enriched fuels experimental parameters

Fuel	Equivalence Ratio	Fuel Flowrate [L/min]	Air Flowrate [L/min]	Diluent		Oxygen Concentration [%]
				N2 [L/min]	CO2 [L/min]	
1	0.9	12	53.95	N/A	N/A	21
2	0.9	14.3	52.94	N/A	N/A	21
3	0.9	10.5	55.53	N/A	N/A	21
1	0.9	12	53.95	~9–54	N/A	18–10
2	0.9	14.3	52.94	~8.9–71	N/A	18–9
3	0.9	10.5	55.53	~9.3–50.5	N/A	18–11
1	0.9	12	53.95	N/A	~5.7–33.2	19–13
2	0.9	14.3	52.94	N/A	~5.6–48.2	19–12
3	0.9	10.5	55.53	N/A	~5.9–27.8	19–14
1	0.8 – 0.6	12	~60.7–80.9	N/A	N/A	21
2	0.8 – 0.4	14.3	~59.5–120	N/A	N/A	21
3	0.8 – 0.6	10.5	~62.5–83.3	N/A	N/A	21

3.2.2 OH* Chemiluminescence

The OH* chemiluminescence flame signatures for each of the hydrogen enriched fuels are now presented. The effect of reduced oxygen concentration on flame signature when nitrogen was entrained into the oxidizer as the diluent is shown in Fig. 3.10. The scaling used was in arbitrary units and normalized against the highest intensity obtained from fuel 2 using normal air combustion at an equivalence ratio of 0.9. The results show that the reduction in oxygen concentration resulted in considerable decrease in OH* flame signatures. In particular, the reduction in oxygen concentration to 13% resulted in broadening of the OH* flame signatures along with reduced intensity, which suggests that the flame front became stretched along with reduction in peak temperature as OH* chemiluminescence is a marker of high temperature flame regions. Transition to colorless distributed combustion was achieved at oxygen concentration of approximately 12, 11, and 10% for hydrogen enriched fuels 1, 2, and 3, respectively. The transition to CDC can be more easily seen from Fig. 3.11

which shows the OH* signal at a lower intensity scale to more clearly see the transition to CDC. The variation of CDC transition point for each of the fuel composition is due to different concentration of hydrogen and methane in the fuel. The CDC condition occurred when the reaction rate was slowed down enough for combustion to occur over a broader region of the combustor. High hydrogen content in the fuel provided higher flame speeds so that the reaction must be slowed down more for achieving distributed reaction conditions.

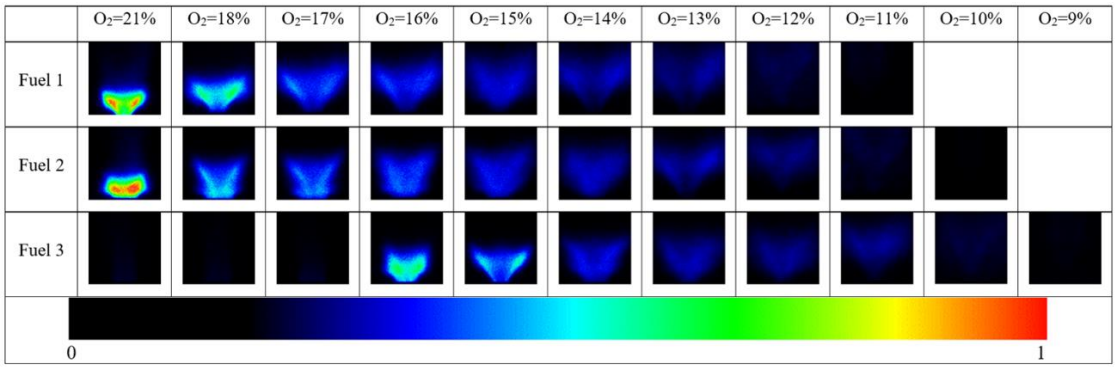

Fig. 3.10. OH* chemiluminescence signatures for $\phi = 0.9$ at different oxygen concentration using N_2 dilution (at a scale of 0–1)

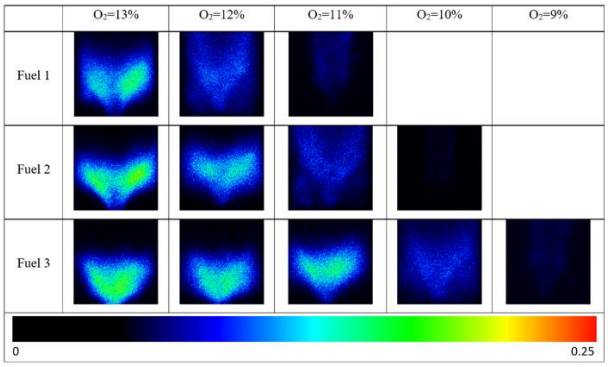

Fig. 3.11. OH* chemiluminescence signatures for $\phi = 0.9$ at different oxygen concentration using N_2 dilution (at a low intensity scale of 0–0.25)

The blowout limits for each fuel mixture at the lower flammability limits are shown in Figs. 3.10 and 3.11, which were different for each alternative fuel mixture, which included different hydrogen amounts. Hydrogen, due to its high flame speed,

increases the propensity to flashback and broadens the flame blowout limits. For fuel 3, for example, there was no substantial flame signatures until oxygen concentration of 16% due to flashback into the burner. For this fuel, reduction of oxygen concentration below the 16% threshold resulted in reduction of flashback with the flame stabilized downstream of the burner exit. Therefore, the controlled amounts of entrained nitrogen as diluent for fuel 3 helped to foster distributed combustion condition and also mitigate flame instability.

The use of CO_2 as an entrained diluent was also examined at various dilution rates in order to achieve colorless distributed combustion. The OH* chemiluminescence flame signatures under CO_2 dilution are presented in Fig. 3.12 (at high intensity scale of 0–1) and Fig. 3.13 (at low intensity scale of 0–0.25). Entrainment with CO_2 showed transition to distributed combustion condition at oxygen concentration of 15, 14, and 13% for fuels 1, 2, and 3, respectively. The results clearly show that transition to CDC using carbon dioxide dilution occurred at higher oxygen concentrations than that with nitrogen dilution. This can be attributed to higher heat capacity of CO_2 as well as carbon dioxide dissociation [39]. Peak flame temperatures decreased and as a result the flame speed reduced when the oxidizer was diluted with any diluent such as N_2, CO_2 or excess air [40]. CO_2 having a higher heat capacity than N_2 provided greater reduction of flame speed and temperature, that resulted in a reduction of the reaction rate allowing for adequate mixing to occur for volumetric distribution of the flame. For fuel 3, flashback was mitigated starting at an oxygen concentration of 19% due to the reduction in flame speed and increase in fresh gas mixture velocity. Therefore, for combustion of fuel 3, carbon dioxide as a diluent can

be utilized for reduction of flame instabilities and also to achieve distributed combustion condition at higher oxygen concentration than with nitrogen dilution.

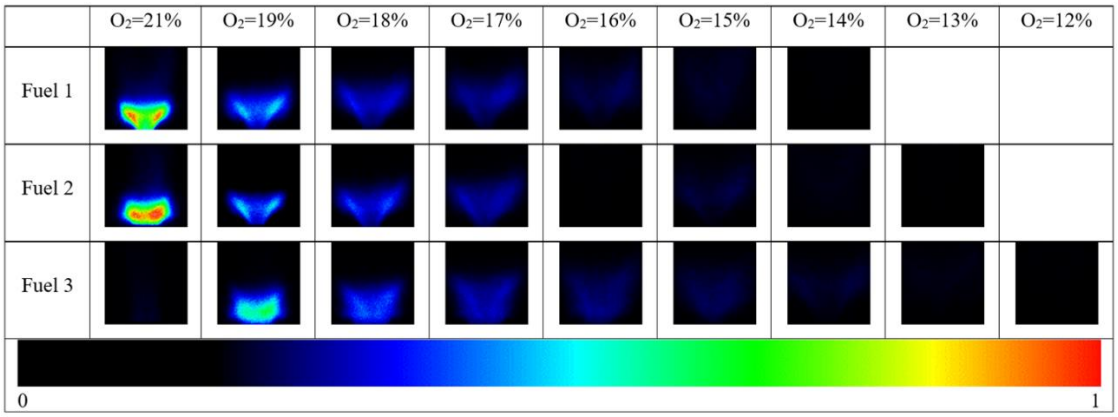

Fig. 3.12. OH* chemiluminescence for ϕ = 0.9 at different oxygen concentration using CO2 dilution (at a scale of 0–1)

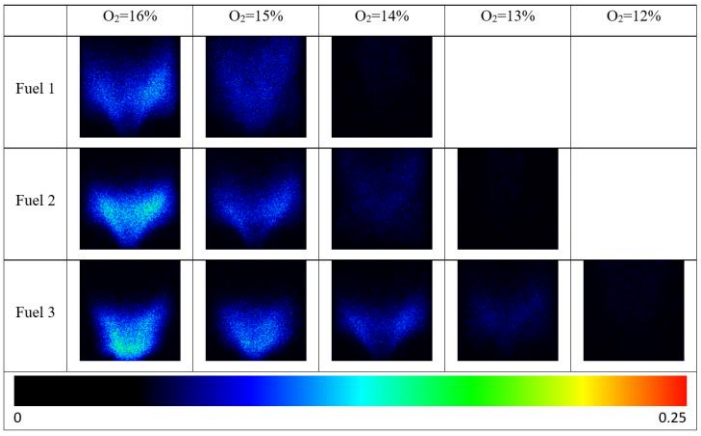

Fig. 3.13. OH* chemiluminescence for ϕ = 0.9 at different oxygen concentration under CO2 dilution (at low intensity scale of 0–0.25)

Reducing equivalence ratio is a dilution method that results in greater dilution without changing the oxygen concentration in the oxidizer. The effects of non-oxygen concentration reduction (dilution) for the three hydrogen enriched fuels examined at various equivalence ratios (see Fig. 3.14). The results showed that reduction in the OH* flame signature intensity can also be achieved using air dilution by reducing the equivalence ratio. The case for reduced equivalence ratio for fuel 3 was of particular interest here. An equivalence ratio of 0.4 was required to achieve a flame without any

flashback occurring; blowout occurred just after this equivalence ratio. This situation demonstrates the ability of mitigating flame instability using dilution with either N_2 or CO_2. It should be noted under reduction of equivalence ratio alone did not demonstrate volumetric distribution combustion as high OH* signal regions were still present indicating high temperature regions.

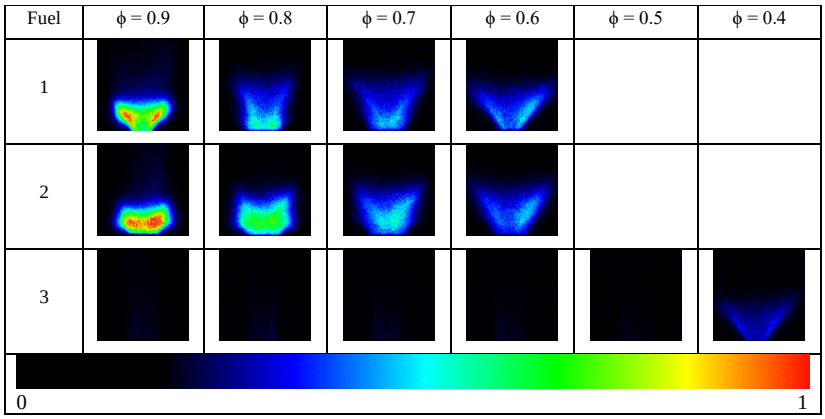

Fig. 3.14. OH* chemiluminescence at various equivalence ratios (at a scale of 0–1)

3.2.3 Pollutants Emission

In order to examine the effects of hydrogen enrichement on CDC, the resulting NO and CO emissions were measured for each fuel composition at the combustor exit under conventional and distributed combustion conditions (using the entrainment of either N_2 or CO_2). The effect of reduced oxygen concentration with N_2 on NO emission is shown in Fig. 3.15 for all hydrogen enriched fuels presented here. The maximum NO levels were observed under conventional combustion conditions. NO levels were seen to decrease significantly at an oxygen concentration of 18% for all the conditions. Subsequently, the measured NO values for each fuel decreased gradually upon approaching distributed combustion condition. At favorable CDC condition NO levels were below 1 ppm for each of the fuel compositions examined. For fuel 3, the NO

emissions exhibited higher levels at oxygen concentrations of 17 and 18% than the other compositions using nitrogen dilution, see Fig. 3.15. This was due to flashback into the burner at these concentrations, wherein the burner walls were subsequently heated, resulting in more hot spots leading to higher NO levels. The NO emissions with CO_2 dilution are presented in Fig. 3.16. The results show that CO_2 dilution can also reduce NO levels under 1 ppm. Additionally, due to reduced flashback under CO dilution, higher NO levels were not observed with fuel 3 versus the other fuel compositions with added dilution. The other positive effect of entrained CO as a diluent was that oxygen concentrations at which transition to distributed condition took place were higher than that of nitrogen. Figs. 3.15 and 3.16 reveal ultra-low NO (less than 1 ppm) can be achieved at a higher oxygen concentration using carbon dioxide as the diluent.

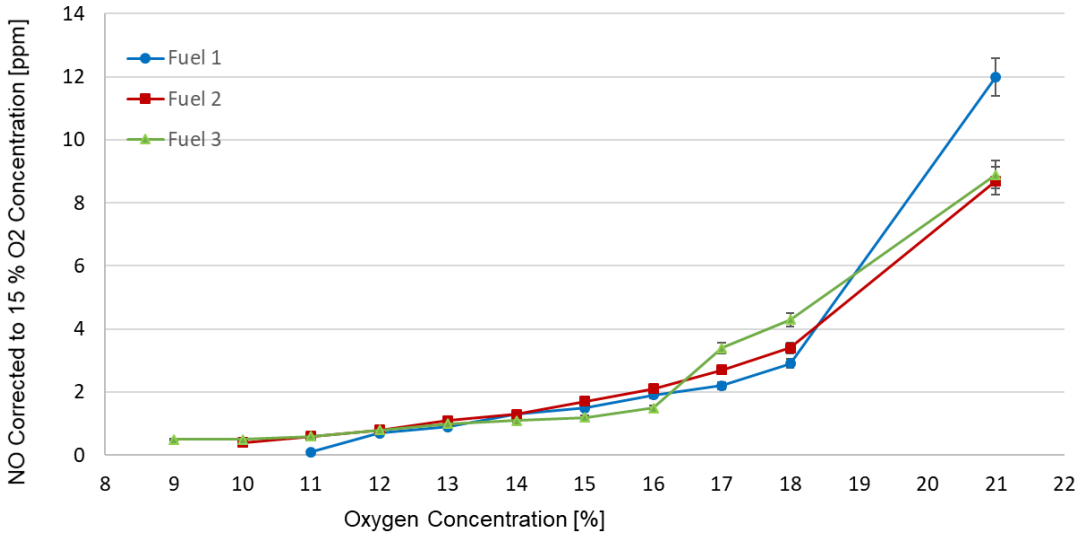

Fig. 3.15. NO emission for $\phi = 0.9$ at different oxygen concentration using N_2 dilution

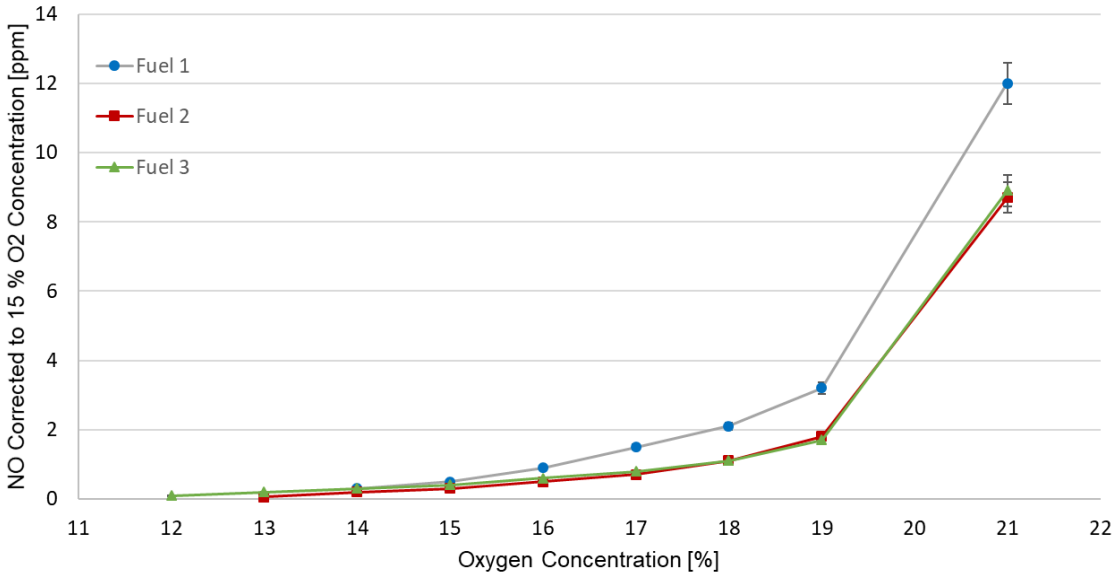

Fig. 3.16. NO emission for $\phi = 0.9$ at different oxygen concentration using CO_2 dilution

The effect of excess air on NO emission is illustrated in Fig. 3.17. For each hydrogen enriched fuel composition, NO emission was reduced with decrease in equivalence ratio. In the case of fuel 3, NO emission was much higher than the other compositions until an equivalence ratio of 0.4. This is attributed to the propensity of flashback of fuel 3 until an equivalence ratio of 0.4. After an equivalence ratio of 0.4 was achieved with fuel 3, flashback was mitigated, and the NO levels decreased further to align with the NO levels obtained using fuel 1 and 2 with the trends extended past the blow-off point.

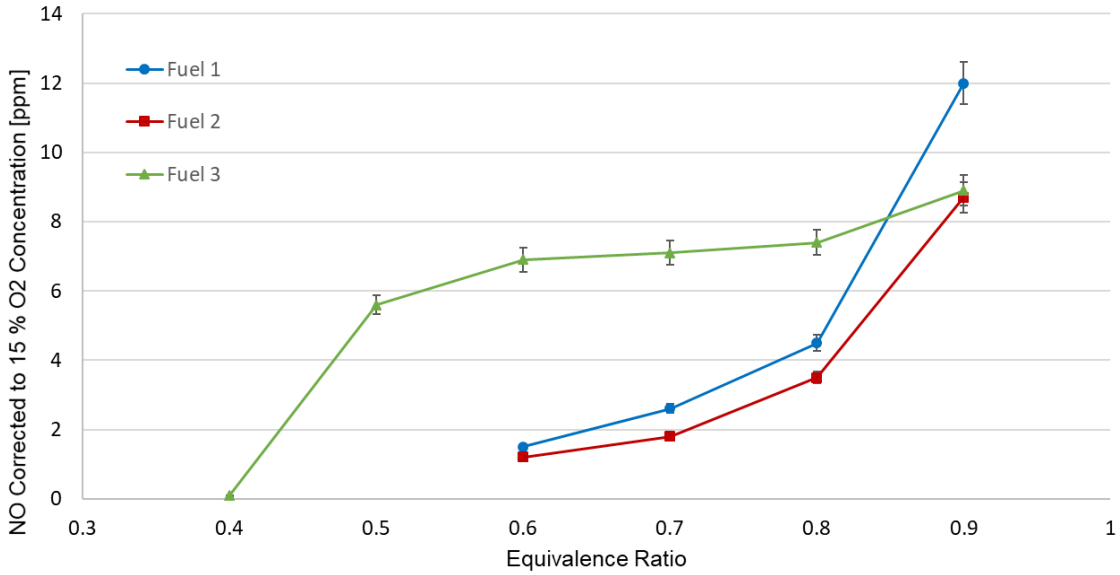

Fig. 3.17. NO emission at different equivalence ratios

The effects of oxygen concentration reduction through entrainment of N_2 or CO_2 on CO emissions are presented in Fig. 3.18 and Fig. 3.19, respectively. When the oxygen concentration was reduced to relatively high O_2 concentrations (19% for CO_2; 16–18% for N_2), CO levels increased slightly for fuel 3. This was due to flashback increasing the apparent residence time, and reaction occurring much earlier (further upstream) in the combustor, leaving more time for CO_2 to CO conversion. This was not seen from fuels 1 and 2. After flashback was mitigated for fuel 3, CO levels gradually decreased similar to that observed from fuels 1 and 2. After oxygen concentrations were reduced beyond the CDC transition point, CO levels increased. CO levels were slightly higher with CO_2 dilution as compared to N_2 dilution due to the dissociation of CO_2 to CO at higher temperatures [41, 42]. Note that fuel 1 had the highest methane and lowest hydrogen concentration among the examined fuels. Achieving CDC through nitrogen dilution is beneficial to reduce CO levels. Single digit ppm levels have been

demonstrated here for all hydrogen examined enriched fuel compositions under favorable distributed combustion condition.

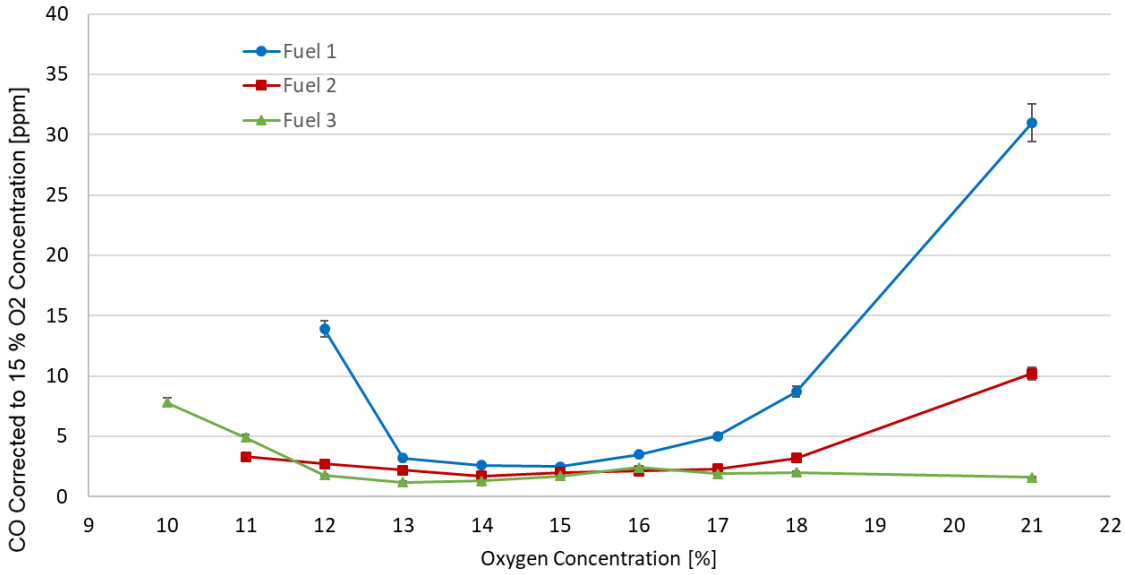

Fig. 3.18. CO emission for $\phi = 0.9$ at different oxygen concentration using N_2 dilution

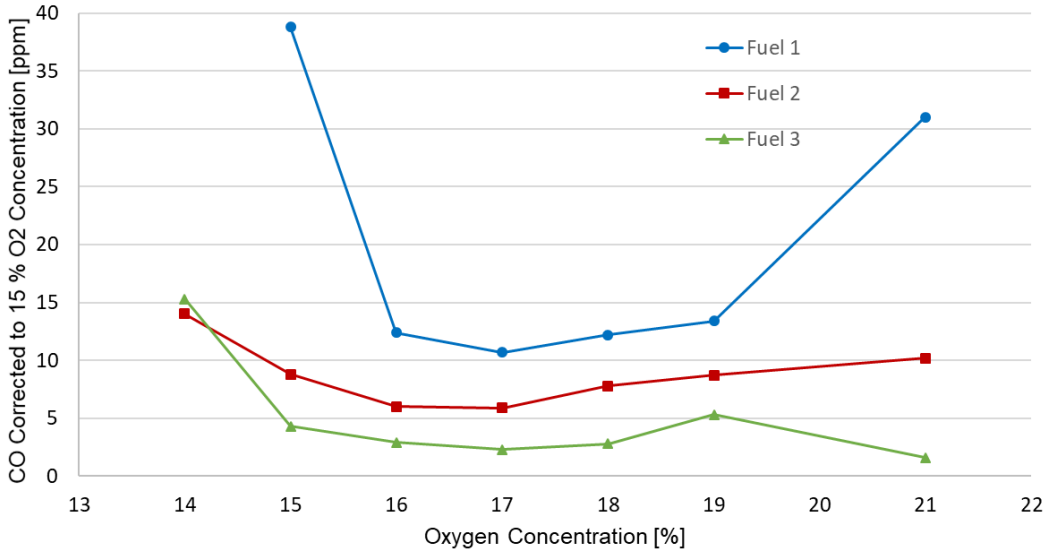

Fig. 3.19. CO emission for $\phi = 0.9$ at different oxygen concentration using CO_2 dilution

3.3 Summary

The effect of fuel enrichment has been examined, namely, naphthalene as a fuel additive and hydrogen enriched fuels. The combustion and emission characteristics of naphthalene ethanol mixtures having naphthalene concentrations of 0–0.4 mol/L, corresponding to an increase in heating value up to 8.8% (volume basis) over ethanol where first examined. The mixture fuels were evaluated at equivalence ratios of 0.9 and 0.7 under distributed combustion conditions, in order to determine the effects of higher heating value fuel and equivalence ratio on emissions. The results showed the direct role of naphthalene addition to ethanol with ultra-low emission of NO and CO at high thermal intensity, and high stability. Distributed combustion, observed with OH∗ chemiluminescence signals, was achieved using N2/CO2 addition to air. Under favorable CDC conditions, the NO and CO emissions were less than 1 and 6 ppm, respectively, at high thermal intensity and high equivalence ratios.

The results at $\Phi = 0.9$ showed that increasing naphthalene concentration reduced the NO emission. The difference in between the highest and lowest corrected CO at any given condition was within 0.5 ppm. The results at $\Phi = 0.7$ showed a reduction in NO with negligible change in CO emission at all naphthalene concentrations in ethanol. The emissions results show use of polyaromatic fuels with CDC without increasing emissions often accompanied with these fuels.

The results presented show the benefit of using naphthalene as a fuel additive in ethanol under distributed combustion conditions for seeking ultra-low emissions. In the distributed combustion conditions of the naphthalene-ethanol fuel, emissions of NO were under 1 ppm whereas CO emissions were under 6 ppm. It was also shown that as

naphthalene concentration increased, the NO emission was reduced. In addition, mitigation of flashback towards the burner with the use of liquid fuels under the CDC condition demonstrates an enhanced stability design, which supports alleviation of combustion instability, along with combustor longevity. The combustion stability enhancement and ultra-low emissions, from increased heating value fuels (higher thermal intensity) highlight the benefits of using naphthalene as a fuel additive under distributed combustion condition.

Additionally, in this section hydrogen enriched fuels were examined, of which coke oven gas, which can be up to 60% H_2 was examined. Three different fuels of varying degrees of hydrogen enrichment in a methane-based fuel was examined under conventional and distributed combustion conditions using a swirl-stabilized burner at moderate thermal intensity (5.7 MW/m^3.atm) combustion conditions for gas turbine applications. Distributed combustion condition was fostered with reducing the oxygen concentration in the oxidizer through controlled entrainment of either N_2 or CO_2. The oxygen concentration at which transition to CDC occurred were investigated using OH* chemiluminescence diagnostics. Signal intensity of OH* signals reduced gradually with decrease in the oxygen concentration to provide volumetric broadening of the reaction regime. The oxygen concentrations at which distributed combustion occurred was approximately at 12, 11, and 10% for hydrogen enriched fuels 1, 2 and 3, using N_2 as the entrained gas, or 15, 14, and 13% for hydrogen enriched fuels 1, 2 and 3, respectively using CO_2 as the entrained gas. Differences in oxygen concentration at transition to CDC for the hydrogen enriched fuel compositions examined varied with the amounts of hydrogen and methane in the fuel. Reaction rates were higher with

increase in hydrogen content that resulted in the requirement of further reducing the oxygen concentration in order to slow down the reaction for adequate mixing to occur for CDC condition. The results demonstrated that CO_2 was more effective in promoting transition to distributed combustion condition compared to N_2 due to its higher heat capacity, lowering of the flame temperature and slowing the reaction down at a much faster rate. Additionally, instabilities due to flashback were mitigated when transitioning towards CDC. Dilution with excess air did not provide flames which exhibited distributed OH* signatures. Additionally, the flashback instability observed for hydrogen enriched fuel 3 (H_2=60% by volume) was maintained until an equivalence ratio of 0.4 using air dilution.

Pollutants emission of NO and CO were also examined for each of the hydrogen enriched fuels examined here. Near-zero NO emission (<1ppm) was achieved under CDC conditions using N_2 or CO_2 as the dilution gas. Under CDC with nitrogen as the diluent, single digit CO levels were achieved, while with carbon dioxide as the diluent CO levels were slightly higher due to CO_2 dissociation.

The results show exemplary fuel flexibility using distributed combustion, as shown by the different compositions of hydrogen enriched fuels presented here. These gases can be used as alternative gaseous fuels. Flame stability was enhanced, and ultra-low emissions were achieved under CDC condition. The demonstrated CDC potential in alleviating environmental pollution and flashback issues using a range of hydrogen rich gaseous fuels is of significant importance for fuel flexibility and energy security.

Chapter 4: Distributed Combustion Index

CDC provides a beneficial means of achieving clean combustion, reducing pollutants emission, reducing noise, providing a more uniform thermal field and reducing pressure drop across the combustor. However, there are many factors that impact the ability to achieve distributed combustion condition. It is therefore necessary to develop a distributed combustion index (DCI) based on varying operational conditions for aid in prediction and implementation of colorless distributed combustion condition in gas turbine combustors. In this section, colorless distributed combustion using methane as a fuel was performed under different oxygen concentrations, varying heat release intensity, equivalence ratio, and mixture preheat temperature with either N_2 or CO_2 as the diluent. The determined distributed combustion index is expected to be useful for further investigations and design of CDC combustion systems. Focus on the OH* chemiluminescence flame signatures, to determine onset of CDC, along with emissions of NO and CO at the combustor exit under conventional and colorless distributed combustion conditions.

4.1 Materials and Methods

A swirl stabilized burner, which has a (nominal) calculated swirl number of 0.77, was used for all conditions reported here. A schematic diagram of the burner is shown in Fig. 3.1 with the oxidizer being a mixture of air, air and nitrogen or air and carbon dioxide. The fuel line was located at the longitudinal center axis of the burner. The fuel was injected radially outwards into the oxidizer stream, which was coaxially positioned along the outside of the fuel line. This allowed fuel used to be entrained by

the oxidizer and become partially premixed by time of ignition. The oxidizer line was used to feed the air, or the air/diluent mixtures simulating entrainment of hot reactive gases. This burner was fitted to a quartz tube making up the combustor test section, having an internal diameter of 2 ⅜ in. and a height of 7 ⅞ in. This quartz tube provided full optical access downstream of the burner.

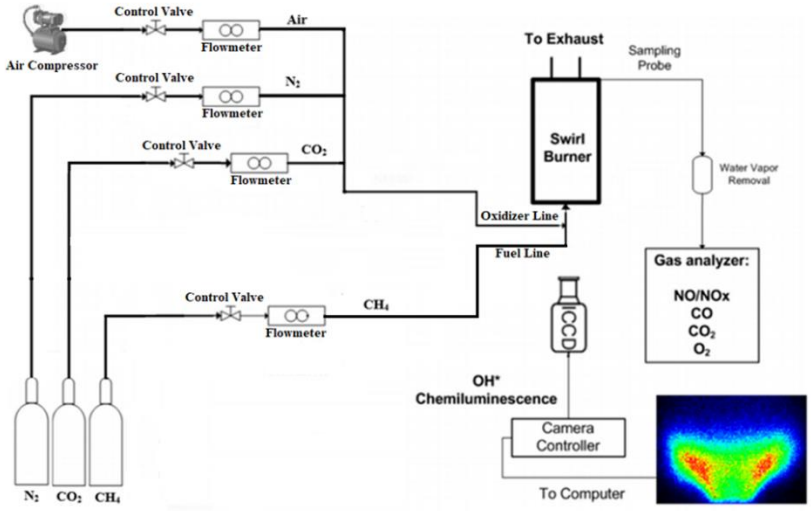

Fig. 4.1. Schematic of the combustion test facility

A schematic diagram of the combustion system used here is given in Fig. 4.1. The supply gases were fed through two sets of lines, one of which was the fuel line while the other was the oxidizer line. The fuel line carried methane, while the oxidizer line included air along with either nitrogen or carbon dioxide. Flow controllers were used to accurately meter the flow rates. The air and the oxidizer diluent flow controllers were laminar flow controllers having an accuracy of ±0.8% of the reading and ±0.2% of full scale, corresponding to an overall accuracy of approximately 1.5% of the reading. For the fuel line, methane flowrate was controlled using gravimetric flow controllers having accuracies of 1.5% of full scale.

Flame signatures were recorded using an ICCD (Intensified Charge-Couple Device) camera as depictured in Fig. 4.1. The camera was coupled with a narrow band filter to detect OH* chemiluminescence (UV interference filter centered at 307 nm with a FWHM of ±10 nm). The camera was positioned at a distance of approximately 40 in. from the flame. The product gas concentrations of NO, CO and O_2 were measured at the combustor exit using a gas analyzer. The gas analyzer measured NO through a crossflow modulation chemiluminescence detection method, CO through the non-dispersive infrared absorption method, and O_2 concentration by the zirconia cell method that allowed corrections of the NO and CO emission to a standard 15% O_2. NO and CO concentrations were measured with estimated accuracies of 1.5% of full scale.

Prior to introducing N_2 or CO_2 into the oxidizer, air was first used as a baseline oxidizer in order to examine the effect of diluent addition on CDC. Nitrogen or carbon dioxide was then introduced into the air flow stream in order to achieve colorless distributed combustion condition. The introduction of diluent into the oxidizer stream, while maintaining the stoichiometry, was used to simulate hot reactive product gas entrainment for seeking distributed combustion condition. For all conditions, pressure was kept constant at 1 atm (atmospheric pressure flame). Other relevant experimental conditions are presented in Table 4.1.

Table 4.1. Distributed combustion index experimental parameters

Case	Heat Load [kW]	Heat Release Intensity [MW/m^3-atm]	Mixture Temperature [K]	Equivalence Ratio	Oxygen Concentration [%]	
					N_2	CO_2
1	3	5.72	300	0.9	21 – 14	21 – 16
2	3.5	6.67	300	0.9	21 – 14	21 – 16.5
3	4	7.63	300	0.9	21 – 14.5	21 – 16.5
4	4.5	8.58	300	0.9	21 – 14.5	21 – 16.5
5	5	9.53	300	0.9	21 – 14.5	21 – 16.5
6	3	5.72	300	0.8	21 – 14.5	21 – 17
7	3	5.72	300	0.7	21 – 15.5	21 – 18
8	3	5.72	300	0.6	21 – 18	21 – 19
9	3	5.72	400	0.9	18 – 13	20 – 15.5
10	3	5.72	500	0.9	17 – 12	19 – 15
11	3	5.72	600	0.9	16 – 11	18 – 14.5
12	3	5.72	700	0.9	15 – 10	17 – 14

4.2 Heat Release Intensity

Heat release intensity is of great interest in the development of a CDC combustor. In order to develop high thermal intensity combustors for both land and aviation use it is critical to understand the behavior of CDC under conditions of high heat release intensity. The OH* chemiluminescence flame signatures obtained at different oxygen concentrations and heat release intensities are now presented. Figure 4.2 shows the effect of reduced oxygen concentration on flame signature using nitrogen as the entrained diluent into the oxidizer. The scale used was arbitrary units normalized against the highest intensity obtained from normal air combustion at an equivalence ratio of 0.9. It can be seen in Fig. 4.2 that the reduction in oxygen concentration resulted

in substantial decrease in the OH* flame signature intensities from 21% to its flammability limit for each heat release intensity examined. The addition of the diluent reduced the oxygen concentration and broadened the flame shape to cover the entire volume of the combustor to support in the evolution of CDC regime. According to the OH* flame signatures obtained, it can be concluded that the flame enlarged and occupied a greater region in the combustor when heat release intensity was increased. This can be attributed to an increase in the flow rate as well as fuel used, leading to a higher velocity making the flame stabilize further downstream and occupy a larger combustor region. The flame blowout was observed below 14% oxygen concentration at HRI of 5.72 and 6.67 MW/m^3-atm and below 14.5% oxygen concentration at HRI's between 7.63-9.53 MW/m^3-atm. The slight raise in oxygen concentration attributed to flame blowout is due to an increase in flow rate which reduced residence time. The oxygen concentrations at which transition to CDC occurred with N_2 dilution were at 15%, 15.5%, 15.5%, 16% and 16% for 5.72, 6.67, 7.63, 8.58 and 9.53 MW/m^3-atm, respectively. It was demonstrated that there was no considerable change on the flame structures with change in heat release intensity although transition points changed slightly and the flame broadened both horizontally and vertically due to higher flow rate and as a result lower residence time. It can also be concluded that the OH* flame signature intensities increased with increase in heat release intensity.

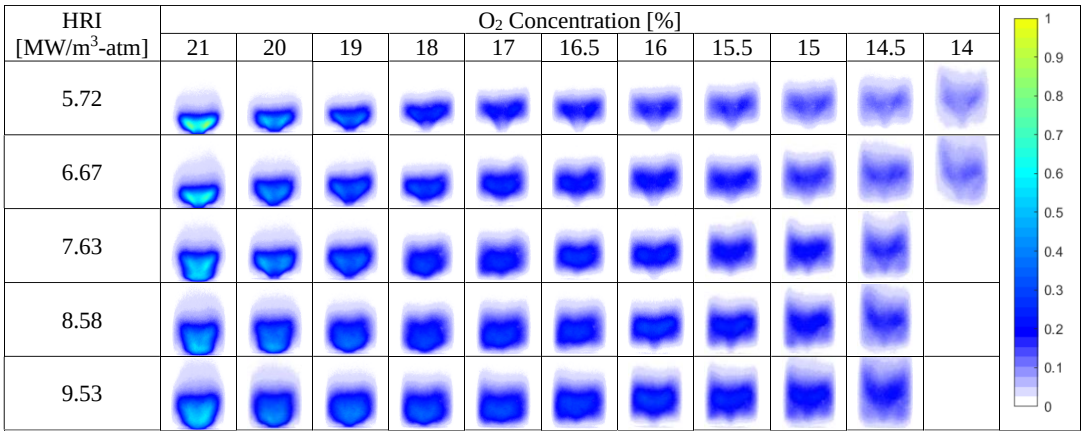

Fig. 4.2. OH* chemiluminescence signature using N_2 dilution at various heat release intensities

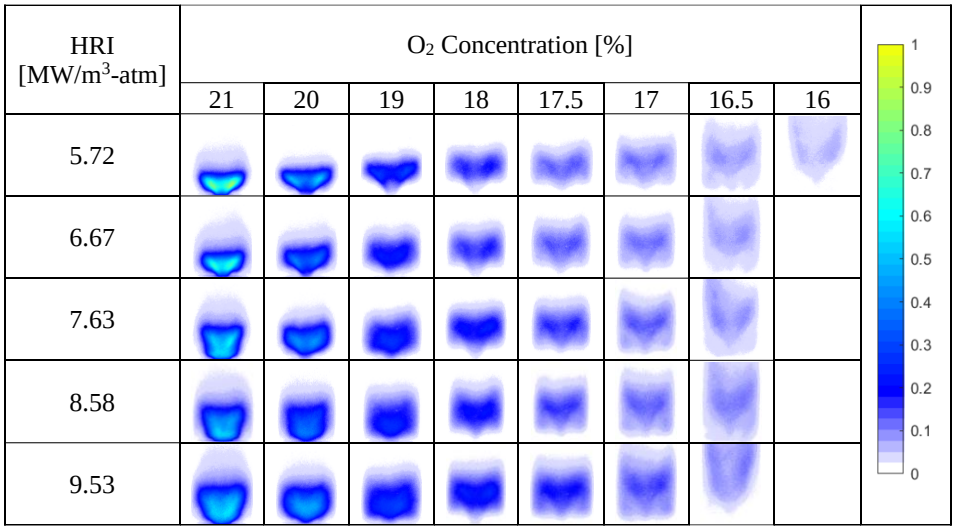

Fig. 4.3. OH* chemiluminescence using CO_2 dilution under various heat release intensities

The effect of heat release intensity on CDC using CO_2 diluent is given in Fig. 4.3. The intensities for the OH* flame signatures reduced faster, and is attributed to the effect of higher heat capacity associated with CO_2 as the diluent, as compared to N_2. This greater effect led to a transition to CDC, which occurred at higher oxygen concentration along with the blow-out condition due to the lower flammability limit. The change in heat release intensity only slightly affected the oxygen concentration at which transition to CDC occurred using CO_2 as the entrained diluent into the oxidizer.

These results are similar to when N_2 was used as the diluent. The transition to CDC with CO_2 as the diluent occurred at the oxygen concentrations of 17%, 17%, 17.5%, 17.5% and 17.5% for 5.72, 6.67, 7.63, 8.58 and 9.53 MW/m^3-atm, respectively due to lower residence time.

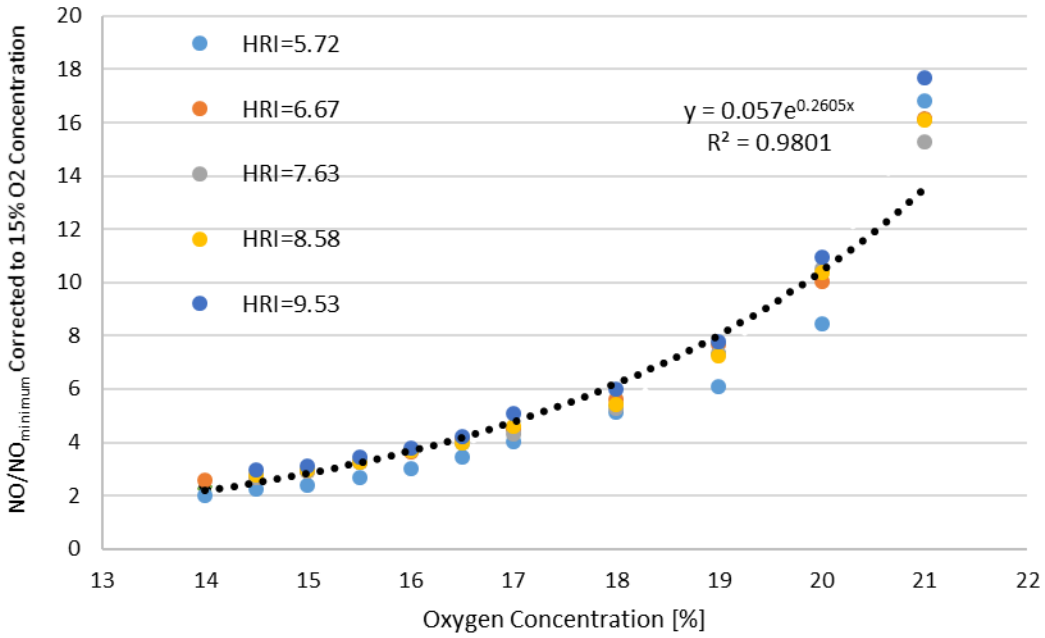

Fig. 4.4. NO emission at different HRI using N_2 dilution

The effect of heat release intensity on NO and CO emission from the combustor under conventional and distributed combustion conditions were examined to help develop distributed combustion index using either N_2 or CO_2 as the diluent. The NO value measured and corrected to 15% O_2 was only 0.92 ppm at 5.72 MW/m^3-atm at 16% O_2 using CO_2 dilution. All other NO emission levels examined using N_2 or CO_2 were normalized by this value and the resulting values are presented in Figs. 4.4 and 4.5. As expected maximum NO levels were determined to occur under conventional combustion conditions. The results showed that NO levels decreased gradually as oxygen concentration in the oxidizer decreased for each diluent entrained. At favorable

CDC condition NO levels were below 2.5 ppm with N_2 dilution and 1.5 ppm with CO_2 dilution. Figures 5 and 6 reveal that ultra-low NO can be achieved at the higher oxygen concentration using CO_2 as the diluent.

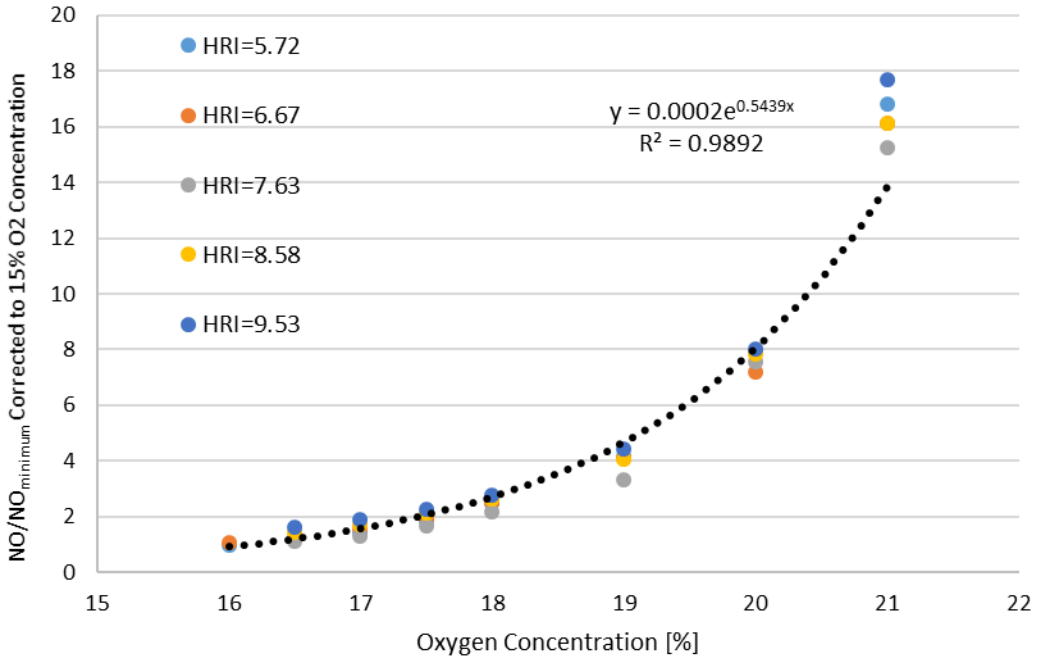

Fig. 4.5. NO emission for different HRI using CO_2 dilution

The effect of heat release intensity and oxygen concentration has the focus to develop a distributed combustion index. The NO results reveal that there is no discernable effect of heat release intensity on NO emission. Therefore, for the development of DCI for HRI one can reduce a function to only consider the effect of oxygen concentration. A relationship describing NO emission with respect to NO emission for the optimum case representing the minimum NO value case can then be obtained. The obtained data for each diluent are shown in Figs. 4.4 and 4.5. The data were curve fitted to an exponential fit with equations 4.1 and 4.2 representing N_2 and CO_2 dilution, respectively for the range of conditions examined. Note that this correlation should not be extended to extreme case of 0% O_2 concentration or greater

than 21% O_2 concentration. The curve fits were determined to have R^2 values of 0.9801 and 0.9892 for the N_2 and CO_2 dilution cases, respectively. A simple relation for each diluent is proposed here for the fraction of oxygen concentration ($f\left(O_{2_{N_2}}\right)$ and $f\left(O_{2_{CO_2}}\right)$) in DCI_{N_2} and DCI_{CO_2}, wherein the NO values measured and corrected for each diluent are normalized by the value required for optimum CDC performance, resulting in optimum distributed reaction condition to a value of 1. The portion of oxygen concentration ($f\left(O_{2_{N_2}}\right)$ and $f\left(O_{2_{CO_2}}\right)$) in DCI_{N_2} and DCI_{CO_2} can be formulated in equations 4.3 and 4.4 as follows:

$$NO_{N_2}/NO_{min} = 0.057 * e^{0.2605*O_2} \quad \text{(Eq. 4.1)}$$

$$NO_{CO_2}/NO_{min} = 0.0002 * e^{0.5439*O_2} \quad \text{(Eq. 4.2)}$$

$$f\left(O_{2_{N_2}}\right) = 1 - \frac{\left(NO_{N_2}/NO_{min}\right)_{\%\,O_2} - \left(NO_{N_2}/NO_{min}\right)_{15\%\,O_2}}{\left(NO_{N_2}/NO_{min}\right)_{21\%\,O_2} - \left(NO_{N_2}/NO_{min}\right)_{15\%\,O_2}} \quad \text{(Eq. 4.3)}$$

$$f\left(O_{2_{CO_2}}\right) = 1 - \frac{\left(NO_{CO_2}/NO_{min}\right)_{\%\,O_2} - \left(NO_{CO_2}/NO_{min}\right)_{\%17\,O_2}}{\left(NO_{CO_2}/NO_{min}\right)_{\%21\,O_2} - \left(NO_{CO_2}/NO_{min}\right)_{\%17\,O_2}} \quad \text{(Eq. 4.4)}$$

The effects of oxygen concentration and heat release intensity with N_2 or CO_2 dilution on CO emission are presented in Fig. 4.6 and Fig. 4.7, respectively. The results show a gradual decrease in CO levels with decrease in oxygen concentration in the oxidizer. However, with decrease in residence time, CO level increased as the total flow rate was increased under higher HRI.

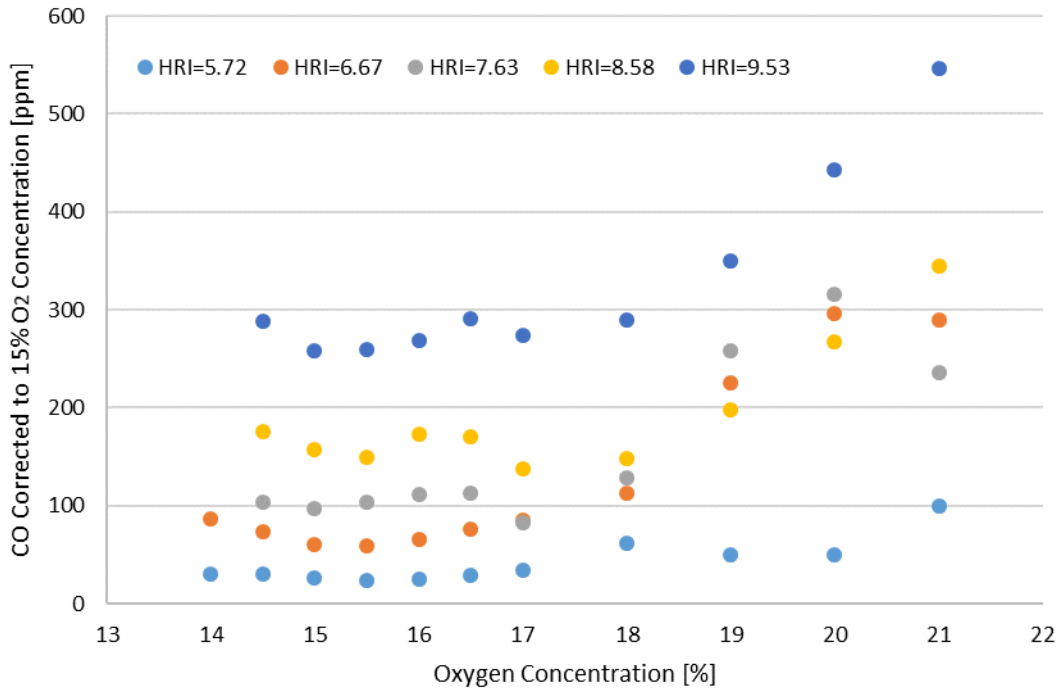

Fig. 4.6. CO emission for different HRI using N_2 dilution

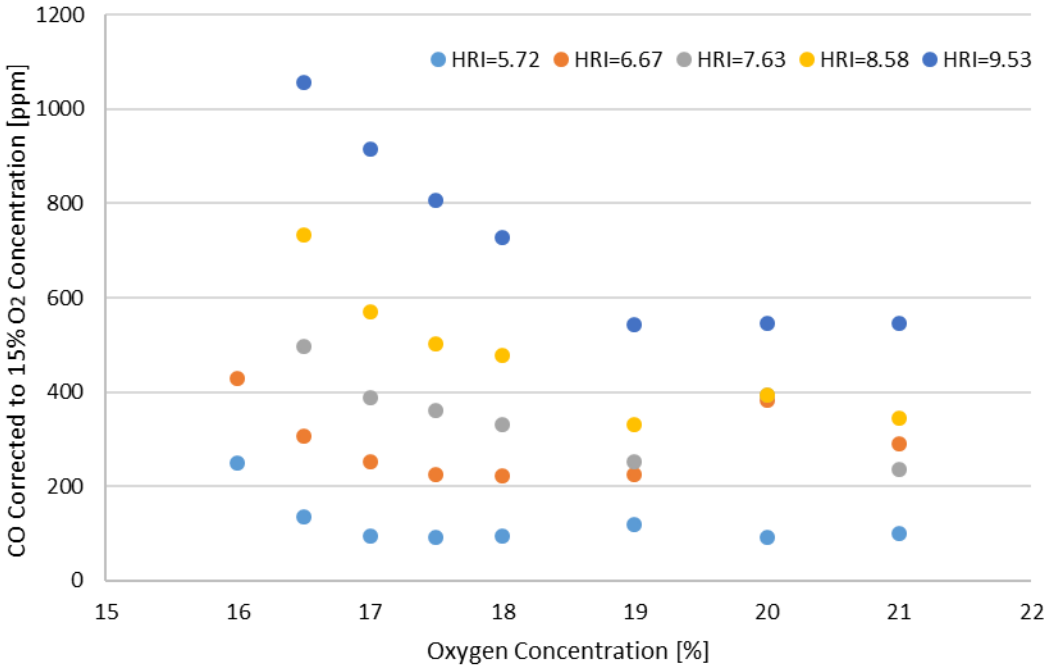

Fig. 4.7. CO emission for different HRI using CO_2 dilution

4.3 Equivalence Ratio

The role of equivalence ratio was the third examined parameter of interest to develop DCI. In order to understand the effect of the equivalence ratio, OH* flame signatures along with NO and CO pollutants emission were obtained and these are presented here. Figure 4.8 shows the effect of reduced oxygen concentration and equivalence ratio on flame signature using nitrogen as the entrained diluent into the oxidizer. Reduction in oxygen concentration resulted in considerable decrease in intensity of the OH* flame signatures. The effect of equivalence ratio on OH* flame signatures showed that transition to CDC occurred faster at higher oxygen concentration. The results reveal that the flames examined broadened faster due to the slowdown of reaction with CO_2 dilution. This resulted in blowout to occur at higher oxygen concentration and causing full flame broadening not to occur for the lowest equivalence ratio case of 0.6. This can be attributed to lower residence time. The oxygen concentrations at which transition to CDC occurred were approximately 15%, 16% and 17% for equivalence ratios of 0.9, 0.8 and 0.7, respectively. The results revealed considerable effect of equivalence ratio on the onset of CDC.

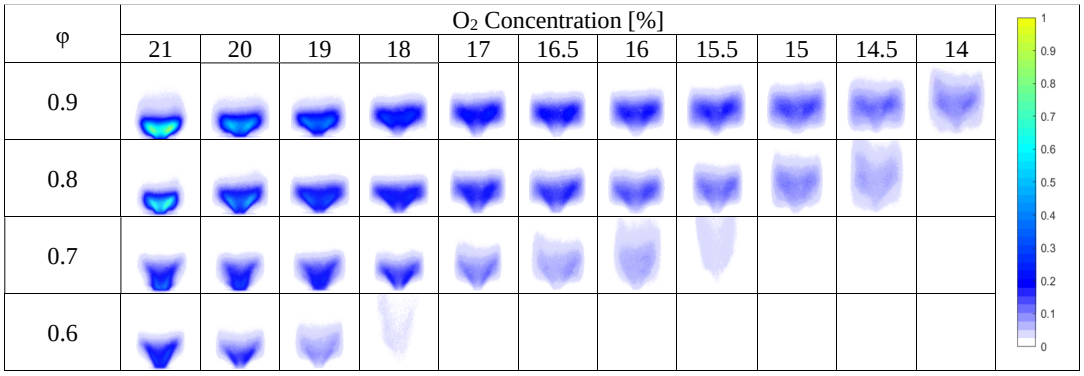

Fig. 4.8. OH* chemiluminescence using N_2 dilution at various equivalence ratios

Figure 4.9 shows the effect of reduced oxygen concentration and equivalence ratio on CDC using CO_2 as the diluent in terms of the OH* flame signatures obtained. Because of greater effect of CO_2 entrainment, the reaction rate was reduced much faster than that of the N_2 dilution case. Figure 4.9 shows transition to CDC started at about 17%, 18%, 19% and 20% at equivalence ratios of 0.9, 0.8, 0.7 and 0.6, respectively. In particular examination of the OH* flame signatures at lower equivalence ratios (such as 0.7 and 0.6) reveals that flame blowout occurred before full broadening occurred due to much lower residence time.

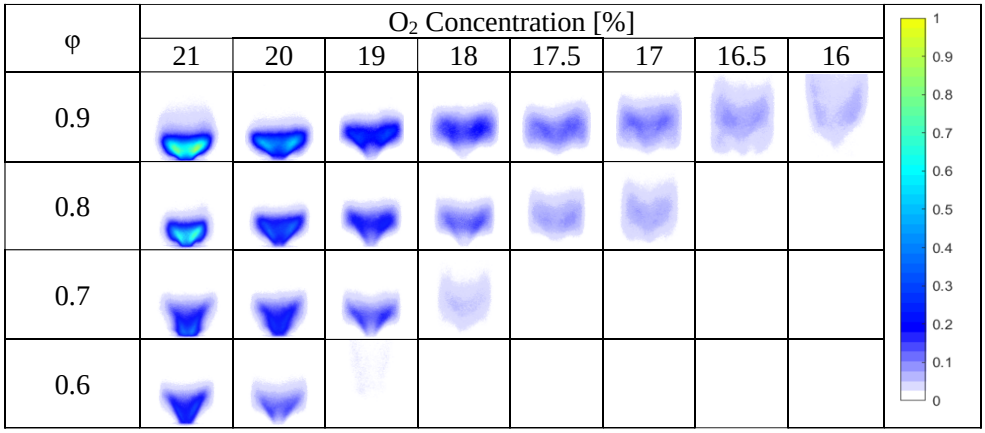

Fig. 4.9. OH* chemiluminescence using CO_2 dilution at various equivalence ratios

The effect of equivalence ratio on the resulting NO and CO pollutants emission at the combustor exit for each diluent entrained under CDC was measured under conventional and distributed combustion conditions. The NO values were normalized by the minimum NO value (about 0.19 ppm at Phi=0.6 and 18% O_2 using N_2 dilution) and the results are presented in Figs. 4.10 and Fig. 4.11. These results show that change in equivalence ratio greatly affects the NO level. At Phi=0.6 the lowest NO value was only 0.19 ppm at 18% O_2 concentration using N_2 diluent, and 0.29 ppm at 19% O_2 concentration using CO_2 as the diluent. Note that CO_2 dilution was more effective for

the reduction of NO due to its heat capacity that helped provide greater effect on NO abatement.

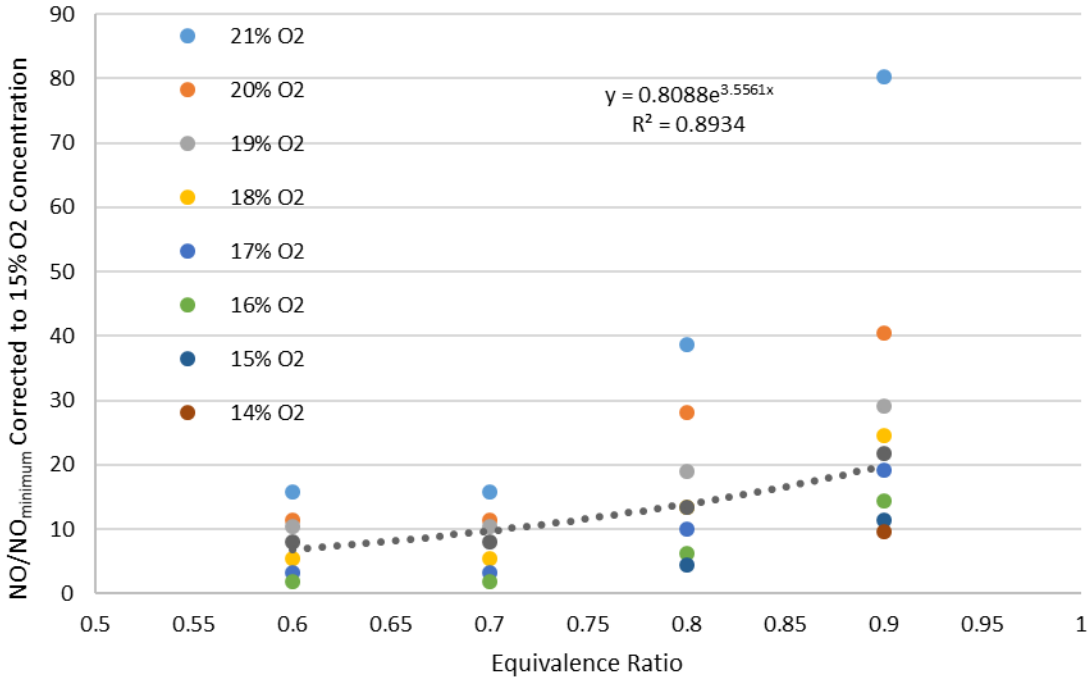

Fig. 4.10. NO emission for different equivalence ratio using N_2 dilution

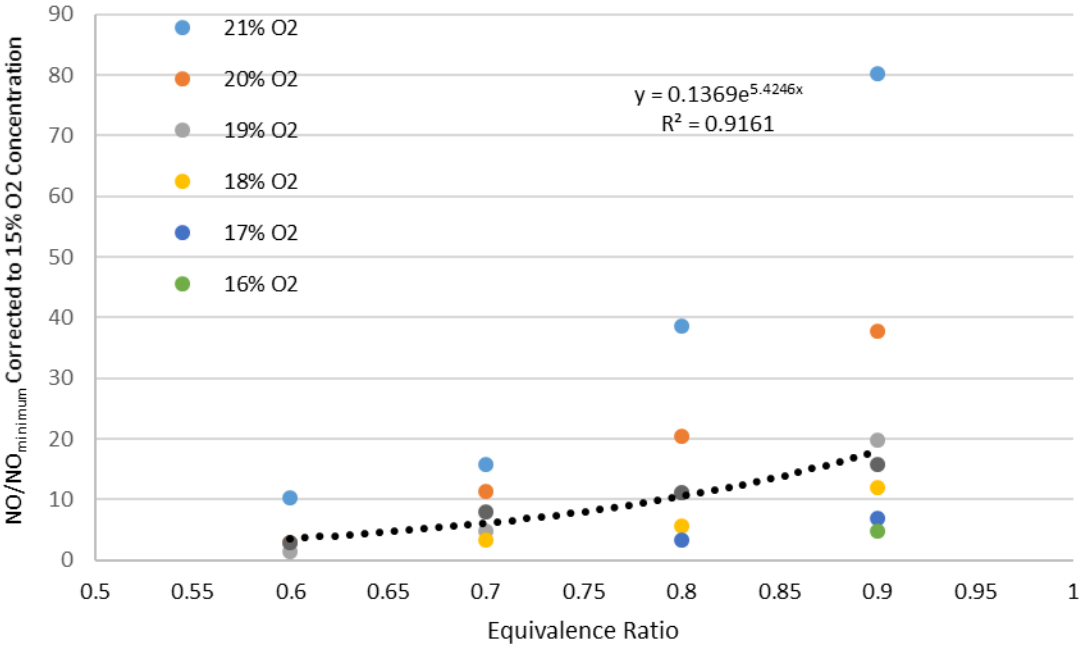

Fig. 4.11. NO emission for different equivalence ratio using CO_2 dilution

The effect of equivalence ratio on the DCI is the focus here. The results show substantial effect of equivalence ratio on NO values. Therefore, a relationship can be determined that describes NO emission with respect to NO emission for the optimum case. Figures 4.10 and 4.11 show the data obtained for each diluent case. The data was curve fitted into exponential curve fit, represented in equations 4.5 and 4.6 for N_2 and CO_2 dilution, respectively. A simple relation for each diluent is proposed here for the portion of equivalence ratio ($f(Phi_{N_2})$ and $f(Phi_{CO_2})$) in the DCI_{N_2} and DCI_{CO_2}, wherein the NO values measured and corrected for each diluent were normalized by the value required for optimum CDC performance, resulting in optimum distributed reaction condition for a value of 1. The portion of equivalence ratio ($f(Phi_{N_2})$ and $f(Phi_{CO_2})$) in DCI_{N_2} and DCI_{CO_2} is formulated in the equation 4.7 and 4.8 as follows:

$$NO_{N_2}/NO_{min} = 0.8088 * e^{3.5561*Ø} \quad \text{(Eq. 4.5)}$$

$$NO_{CO_2}/NO_{min} = 0.1369 * e^{5.4246*Ø} \quad \text{(Eq. 4.6)}$$

$$f(Phi_{N_2}) = 1 - \frac{\left(NO_{N_2}/NO_{min}\right)_{\Phi} - \left(NO_{N_2}/NO_{min}\right)_{\Phi=0.6}}{\left(NO_{N_2}/NO_{min}\right)_{\Phi=0.9} - \left(NO_{N_2}/NO_{min}\right)_{\Phi=0.6}} \quad \text{(Eq. 4.7)}$$

$$f(Phi_{CO_2}) = 1 - \frac{\left(NO_{CO_2}/NO_{min}\right)_{\Phi} - \left(NO_{CO_2}/NO_{min}\right)_{\Phi=0.6}}{\left(NO_{CO_2}/NO_{min}\right)_{\Phi=0.9} - \left(NO_{CO_2}/NO_{min}\right)_{\Phi=0.6}} \quad \text{(Eq. 4.8)}$$

The effect of reduction in oxygen concentration and equivalence ratio from the entrainment of N_2 or CO_2 on CO emissions are presented in Fig. 4.12 and Fig. 4.13,

respectively. The results show CO levels to gradually decrease with decrease in oxygen concentration in the oxidizer and equivalence ratio. At favorable CDC conditions (at lower oxygen concentration and equivalence ratio) single digit ppm levels were demonstrated here for each diluent case. The results show that CO emission was slightly higher with CO_2 dilution due to the dissociation of CO_2 to CO at higher temperatures (especially at higher equivalence ratio) [41, 42].

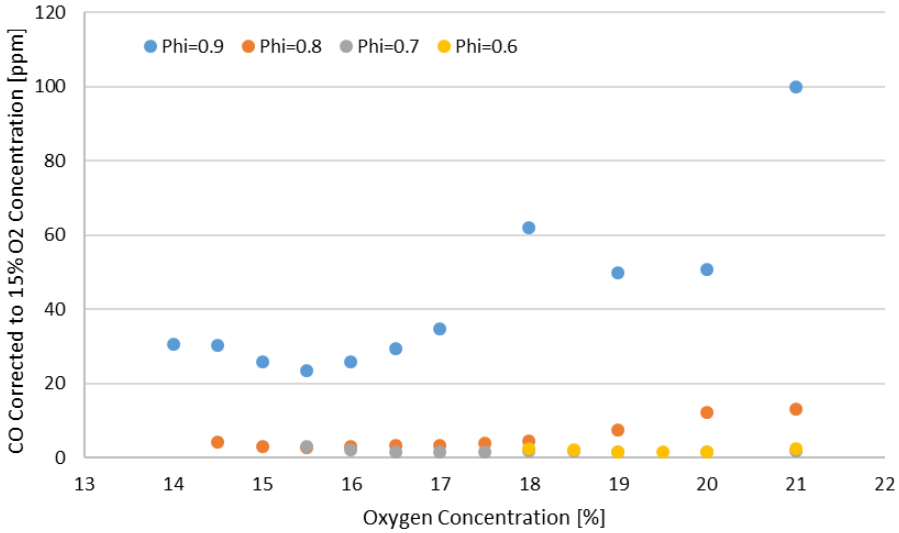

Fig. 4.12. CO emission for different equivalence ratio using N_2 dilution

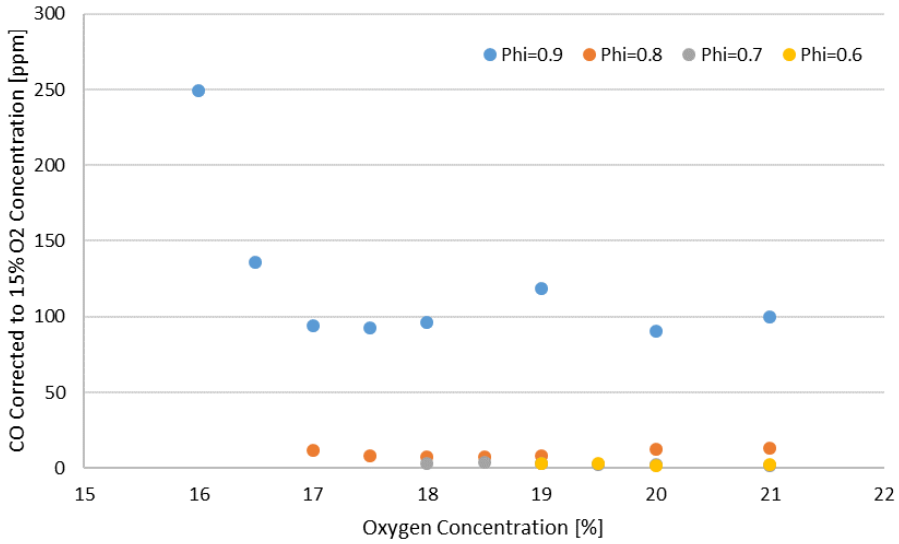

Fig. 4.13. CO emission for different equivalence ratio using CO_2 dilution

4.4 Preheat Temperature

The results on the effect of oxidizer preheat temperature and oxygen concentration on OH* chemiluminescence flame signatures are presented in Fig. 4.14 and Fig. 4.15, which help to seek out favorable combustion conditions. This data is used to help integrate CDC method into gas turbine combustors, which operate at higher inlet air temperatures. The results presented in Fig. 4.14 and Fig. 4.15, reveal that the reduction in oxygen concentration resulted in substantial decrease in the OH* flame signature intensities for each examined mixture temperature and diluent used. The shape of the flame broadened because of lower reaction rate when approaching CDC condition. The results show that the oxygen concentration at which transition to CDC occurs was lower as the mixture temperature increased with N_2 or CO_2 dilution. Flashback occurred at high oxygen concentration conditions as preheat was introduced. The flashback instability was attributed to an increase in flame speed with increase in preheat temperature. The oxygen concentrations at which transition to CDC occurred were at 15%, 14%, 13.5%, 12.5% and 12% for 300 K, 400 K, 500 K, 600 K and 700 K with N_2 dilution, and 17%, 16.5%, 16%, 15.5% and 15% for 300 K, 400 K, 500 K, 600 K and 700 K with CO_2 dilution, respectively.

The effect of mixture temperature on NO emission levels at all oxygen concentrations using N_2 or CO_2 as the entrained diluent was investigated. The NO values measured and corrected to 15% O_2 were normalized by the minimum NO value (about 0.44 ppm at T=700 K and 14% O_2 using CO_2 dilution). The results are presented in Fig. 4.16 and Fig. 4.17. The change in mixture temperature somewhat affected the NO values. The lowest NO value with N_2 or CO_2 achieved were 1.55 ppm at T=700 K

and 10% O_2 concentration and 0.44 ppm at T=700 K and 14% O_2 concentration, respectively. The CO_2 dilution was more effective in reducing NO at increased preheat mixture temperature due to its greater heat capacity as well as from the effect on reducing reaction rate and flame temperature.

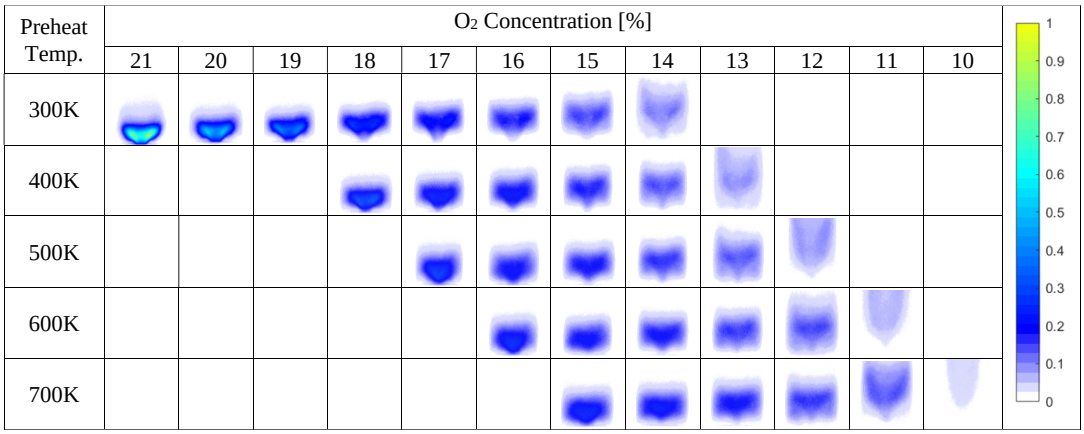

Fig. 4.14. OH* chemiluminescence using N_2 dilution under various oxidizer preheat temperatures

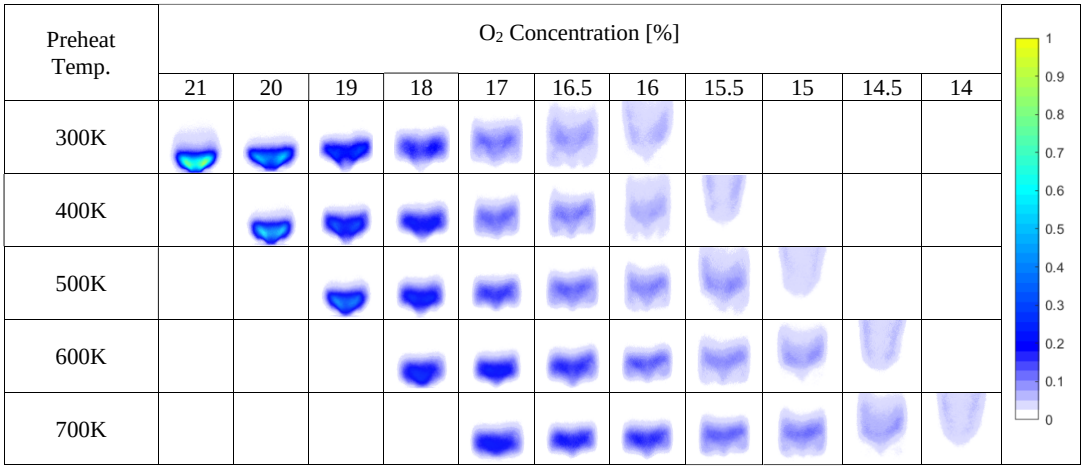

Fig. 4.15. OH* chemiluminescence using CO_2 dilution under various oxidizer preheat temperatures

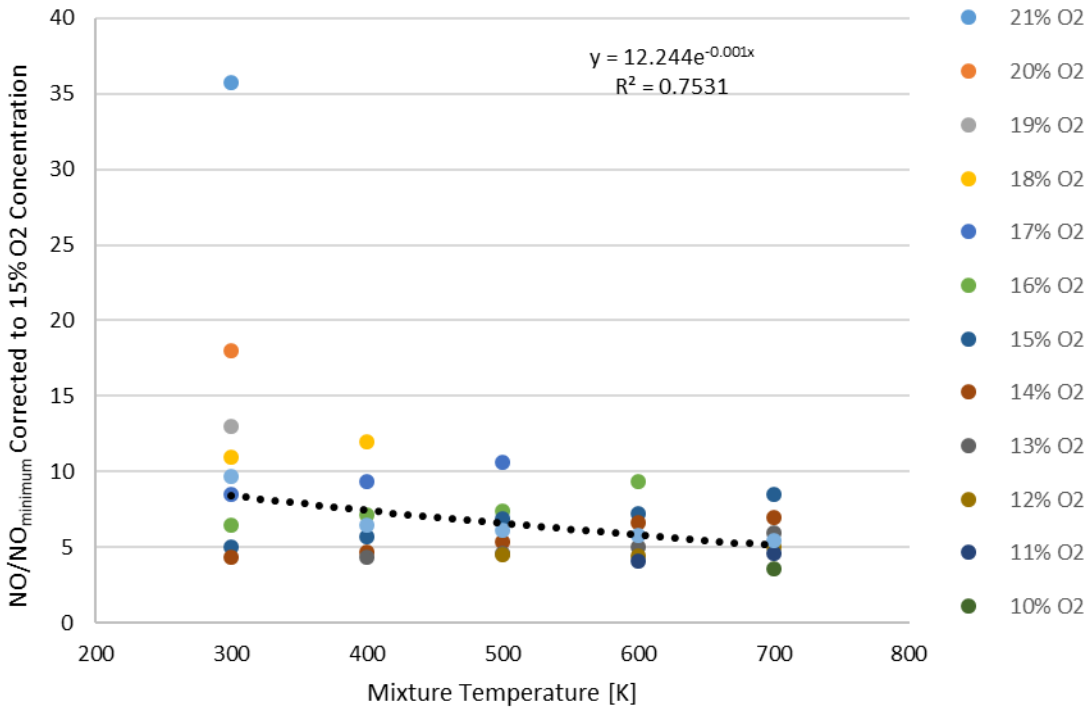

Fig. 4.16. NO emission for different oxidizer preheat temperatures using N_2 dilution

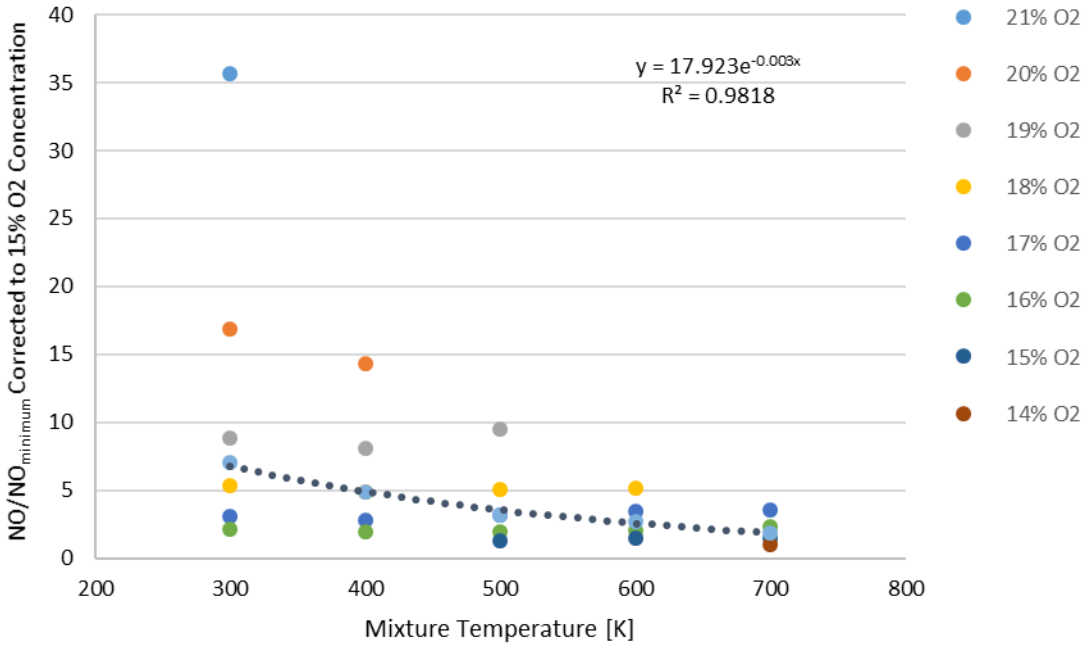

Fig. 4.17. NO emission for different oxidizer preheat temperatures using CO_2 dilution

The effect of mixture temperature on the DCI is the focus here. The NO data clearly shows the effect of oxidizer preheats temperature on NO values. Therefore, one can obtain a relationship describing NO emission with respect to optimum NO emission case. The obtained data for each diluent are plotted in Figs. 4.16 and 4.17. The data were curve fitted into an exponential fit with equations 4.9 and 4.10 representing the N_2 and CO_2 dilution cases, respectively. A simple relationship for each diluent is proposed here for the portion of mixture temperature ($f(T_{N_2})$ and (T_{CO_2})) in DCI_{N_2} and DCI_{CO_2}, wherein the NO values measured and corrected for each diluent are normalized by the value required for optimum CDC performance, resulting in an optimum distributed reaction condition that represents a value of 1. The portion of mixture temperature ($f(T_{N_2})$ and (T_{CO_2})) in the DCI_{N_2} and DCI_{CO_2} can be formulated as given in the equation 4.11 and equation 4.12, as follows:

$$NO_{N_2}/NO_{min} = 12.244e^{-0.001*T} \quad \text{(Eq. 4.9)}$$

$$NO_{CO_2}/NO_{min} = 17.923 * e^{-0.003*T} \quad \text{(Eq. 4.10)}$$

$$f(T_{N_2}) = 1 - \frac{\left(NO_{N_2}/NO_{min}\right)_T - \left(NO_{N_2}/NO_{min}\right)_{T=700K}}{\left(NO_{N_2}/NO_{min}\right)_{T=300K} - \left(NO_{N_2}/NO_{min}\right)_{T=700K}} \quad \text{(Eq. 4.11)}$$

$$f(T_{CO_2}) = 1 - \frac{\left(NO_{CO_2}/NO_{min}\right)_T - \left(NO_{CO_2}/NO_{min}\right)_{T=700K}}{\left(NO_{CO_2}/NO_{min}\right)_{T=300K} - \left(NO_{CO_2}/NO_{min}\right)_{T=700K}} \quad \text{(Eq. 4.12)}$$

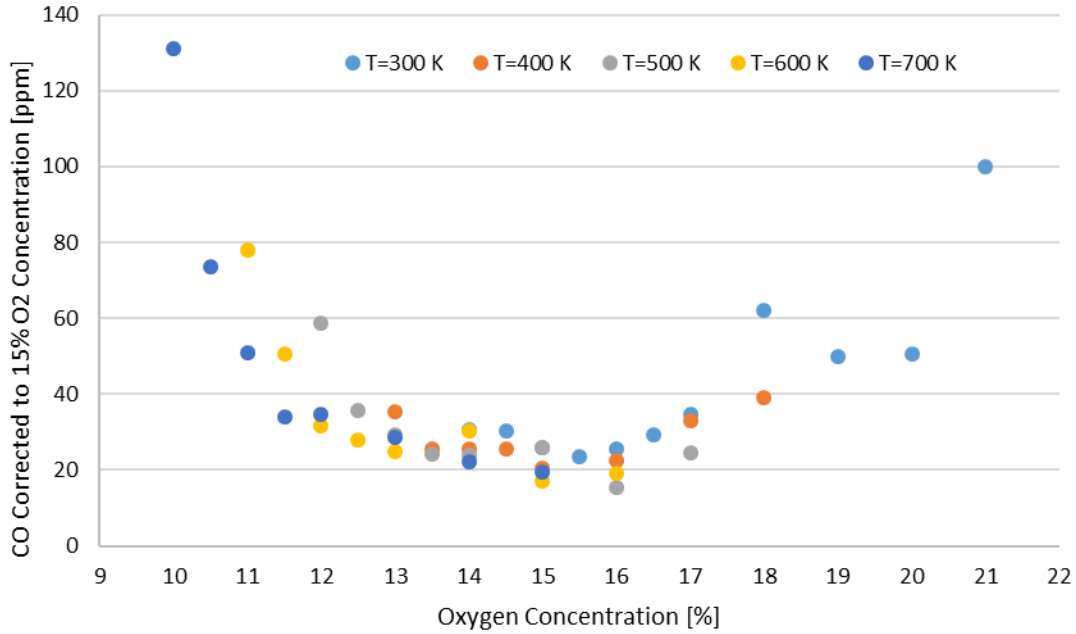

Fig. 4.18. CO emission for different mixture temperature using N_2 dilution

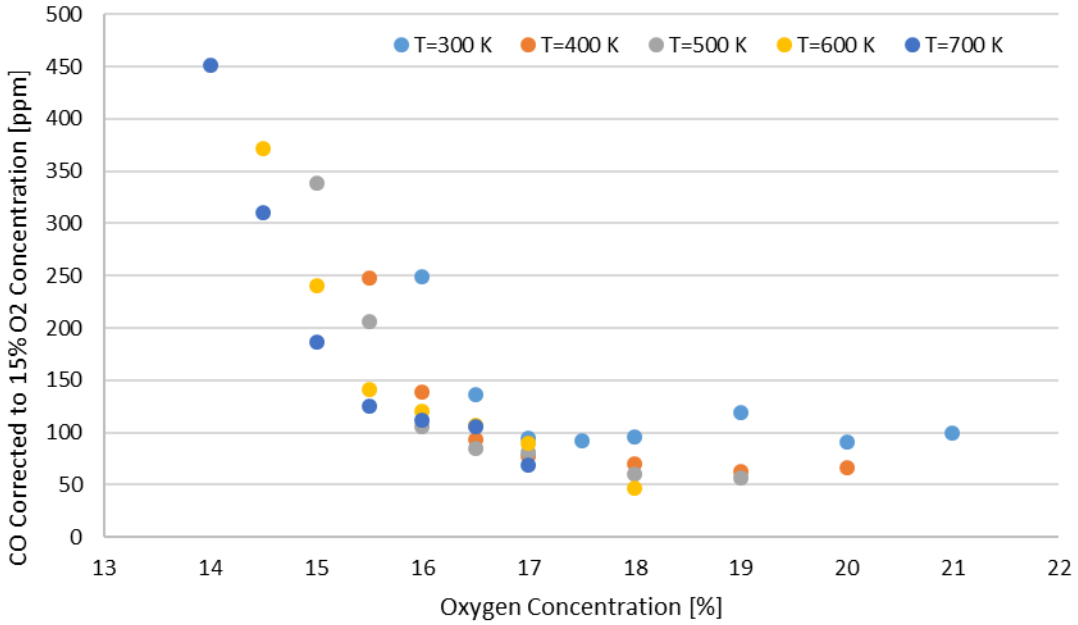

Fig. 4.19. CO emission for different mixture temperature using CO_2 dilution

The results on the effect of mixture temperature on CO emission through entrainment of N_2 or CO_2 are presented in Fig. 4.18 and Fig. 4.19, respectively. The CO levels decreased gradually with decrease in oxygen concentration in the oxidizer at

lower mixture temperatures. CO levels increased with increase in the mixture temperature, which can be attributed to the dissociation of CO_2 to CO at higher temperatures. At favorable CDC condition the CO emission level was nearly the same for each preheat temperature. Comparing the effect of diluent used on CO levels the results showed that CO emission was slightly higher with CO_2 dilution and this is attributed to the dissociation of a portion of the CO_2 in the oxidizer stream being converted to CO at higher temperatures.

4.5 Realistic Combustor Conditions and Developing a DCI

The mixture temperature examined here was varied from 300 K to 700 K in step intervals of 100 K. In real combustion applications, the temperature level of the hot reactive gases entrained from within the combustor could be around 1800 K. However, it is rather difficult to achieve this temperature level due to experimental limitations. However, an expression representing an oxygen concentration at which transition to CDC occurs at higher temperature levels than the ones performed here shall be useful. This supports the importance of developing a distributed combustion index in order to better predict CDC under non-explored conditions. This helps to determine the transition point for the realistic temperature level. Figure 4.20 shows the transition points for each diluent entrained.

The data obtained from the experiments performed was curve fitted into an exponential fit, with equations 4.13 and 4.14 representing the N_2 and CO_2 dilution cases, respectively

$$O_{2_{N_2}}[\%] = 17.67 * e^{-6*10^{-4}*[T]} \quad \text{(Eq. 4.13)}$$

$$O_{2_{CO_2}}\,[\%] = 18.691 \ * \ e^{-3 * 10^{-4} * [T]} \qquad \text{(Eq. 4.14)}$$

Using the formulated equations, an approximate oxygen concentration at which transition to CDC occurs can be determined. For example, the transition points with N_2 or CO_2 at a mixture temperature of 1800 K were found to be around 6.0% and 10.9%, respectively.

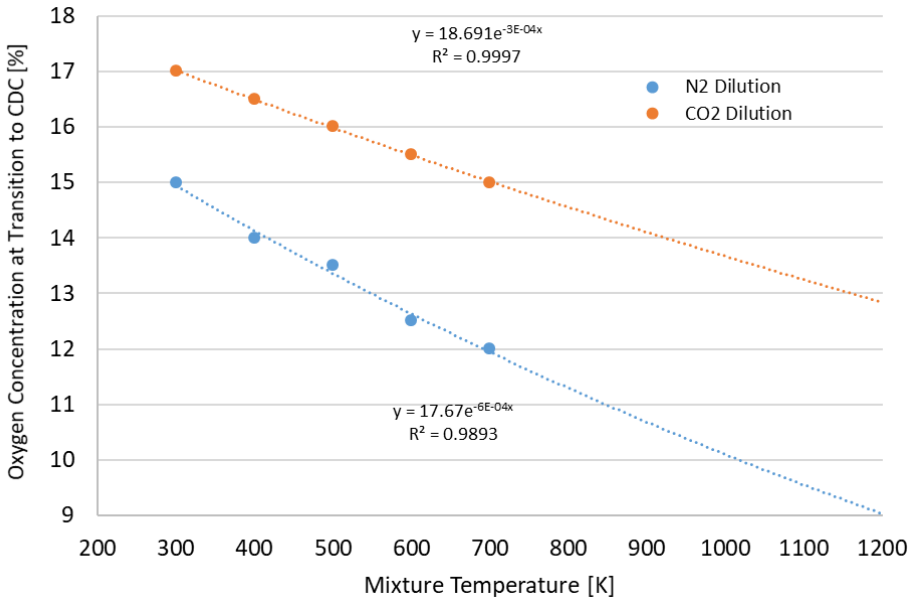

Fig. 4.20. Oxygen concentration at transition to CDC for different mixture temperatures

The previously discussed parameters were combined to formulate a distributed combustion index. The DCI describes how well the reaction is distributed in the combustor. The DCI has a maximum value of 1 meaning that distributed reaction is completely achieved. The DCI can be expressed by equations 4.15 and 4.16 for each diluent used.

$$DCI_{N_2} = \left[f\left(O_{2_{N_2}}\right)\right] * \left[f\left(Phi_{N_2}\right)\right] * \left[f\left(T_{N_2}\right)\right] \qquad \text{(Eq. 4.15)}$$

$$DCI_{CO_2} = \left[f\left(O_{2_{CO_2}}\right)\right] * \left[f\left(Phi_{CO_2}\right)\right] * \left[f\left(T_{CO_2}\right)\right] \quad \text{(Eq. 4.16)}$$

4.6 Summary

This section examined CDC conditions under various heat release intensities, equivalence ratios, and oxidizer preheat temperature in order to develop a distributed combustion index (DCI). This index will allow for a better prediction of CDC conditions in the design and development of a CDC combustor. Transition to CDC was based on the OH* chemiluminescence signatures. The CDC conditions were achieved using either N_2 or CO_2 as the diluent to the oxidizer stream that simulated entrainment of hot reactive product gases into the combustor. The oxygen concentration at transition to CDC under various HRI was shown to be relatively constant at 15 to 16% for N_2 dilution and 17 to 17.5% for CO_2 dilution. Equivalence ratio and preheat temperature, however, had considerable effect on altering the transition point to CDC. Distributed conditions were better achieved at high equivalence ratios (0.8 and 0.9). Low equivalence ratios (0.6 and 0.7) had very low residence times that hampered in full CDC stabilization before reaching the lower flammability limits. Increase in air preheats from T=300K to 700K moved the oxygen concentration transition point to CDC from 15-12% and 17-15% for the N_2 and CO_2 diluent cases, respectively.

Near unity ppm levels of NO was found for the CDC conditions. Various empirical formulas were developed to determine an approximate NO emission level for various oxygen concentrations, from conventional combustion condition to favorable CDC condition. The HRI and equivalence ratio had a greater effect on CO emission levels while the oxidizer preheats temperature had minimum effect. Change in HRI

from 5.72 to 9.53 MW/m^3-atm increased the CO level by approximately 10-fold, while change in equivalence ratio decreased the CO level considerably.

Finally, a distributed combustion index was developed based on the HRI, equivalence ratio, and preheat temperature together with the oxygen concentration. The DCI for both entrained diluents was determined in order to predict the oxygen concentration for transition to CDC. This effort is expected to help in the future design and development of next generation novel CDC gas turbine combustors.

Chapter 5: Flowfield Impact on CDC

In this section, the impact of flowfield on distributed combustion is examined. In order to examine the flowfield particle image velocimetry (PIV) is used on the non-reacting flowfield along with OH* chemiluminescence flame signatures and pollutants emission from a swirl-stabilized flame. The study was performed at near stoichiometric condition (Φ=0.9) to take advantage of the thermal efficiency provided near to stoichiometric combustion condition. Additionally, this is used to simulate gas turbine combustor conditions, wherein the fuel is burned almost stoichiometrically using approximately one-third or less of the total compressor discharge air [43]. This study also investigates lower equivalence ratio conditions in order to investigate the effect of Reynolds number and achieve distributed combustion condition. In order to obtain flowfield information, PIV, a non-intrusive flow diagnostic technique, was used to obtain information on the velocity field and eddy size under simulated conditions of traditional air combustion at higher and lower equivalence ratios and simulated CDC condition. OH* chemiluminescence was used as a marker for determining the onset of distributed combustion condition. Pollutants emission were additionally measured and analyzed to determine the effect of reduced oxygen concentration.

5.1 Materials and Methods

A swirl-stabilized burner with a swirl angle of 45° and a calculated swirl number of 0.77 was used in the present study. The fuel line was situated along the longitudinal central axis of the combustor with the surrounding coaxial oxidizer stream supplied around the fuel line. Fuel was injected radially into the oxidizer stream

immediately after the swirl vane blades. Propane was used as the fuel, while the oxidizer consisted of air, the air/diluent mixtures that simulated the entrainment of hot reactive gases for seeking distributed combustion condition.

A schematic diagram of the combustion system used here is given in Fig. 5.1. Either N_2 or CO_2 was used as the diluent gas in order to simulate entrainment of reactive combustion gases. Laminar flow controllers having an accuracy of ±0.8% of the reading and ±0.2% of full scale were used to control flow rates of air and nitrogen, leading to an overall accuracy of about 1.5% of the reading. Propane and carbon dioxide flow rates were controlled using gravimetric flow controllers having accuracies of 1.5% of full scale.

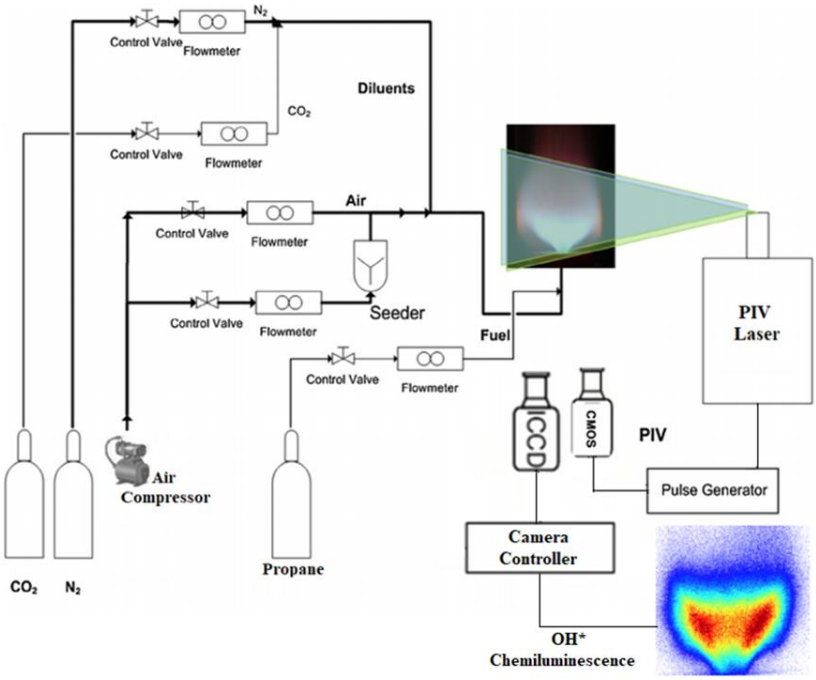

Fig. 5.1. A schematic diagram of the experimental facility including flow controllers and laser diagnostics

Chemiluminescence of OH* was recorded via an ICCD (Intensified Charge-Couple Device) camera in order to determine the oxygen concentration at transition to

CDC. The camera was coupled with a narrow band filter to detect OH* chemiluminescence (UV interference filter centered at 307 nm with a FWHM of ±10 nm). In order to measure pollutants emission, the combustion products were measured using a gas analyzer at the combustor exit. The analyzer was used to measure concentrations of NO, CO and O_2. The analyzer measured NO through a cross-flow modulation chemiluminescence detection method, CO through the non-dispersive infrared absorption method, and O_2 concentration determined by the galvanic cell method that allowed for corrections of the NO and CO emission to standard 15% oxygen concentration. NO and CO concentrations were measured with estimated accuracies of 1% of full scale.

Table 5.1. PIV Parameters

Seeding particles	Al_2O_3 (alumina oxide)
Nominal particle size	3 μm
Acquisition rate	3 kHz
No. of image pairs	3000
Laser sheet thickness	~ 1mm
Pulse separation	50 μs
Interrogation window size	24x24px
Camera resolution	416 x 688 px
Velocity field spatial resolution	0.2 mm/px
Lens focal length	50 mm
f-stop setting	1.2
Seeding air percentage	~ 15%

2-D particle image velocimetry (PIV) was used to determine the velocity field under non-reacting conditions to provide critical information on the role of flowfield

and turbulent mixing as well as resulting Kolmogorov length scales, Reynolds stresses and vorticity distribution. Particle illumination was conducted using a pulsed laser (Litron LD30-527 PIV), and the resulting signal recorded with an IDT OS9 camera. A fluidized bed seeder was used to seed particles in the test section. A portion of the main air flow was diverted to a fluidized bed which after pick up of seed particles rejoined the main air stream. The seeding particles used were alumina (Al_3O_2) with a nominal diameter of 2μm. Sheet forming optics were used on the output laser line to create a sheet beam thickness of approximately 1mm. A summary of the PIV system parameters is given in Table 5.1. Data processing was conducted using IDT Provision-XS software. The interrogation window used consisted of an adaptive grid measuring 24x24 pixels. Further processing for calculation of the mean velocity, root-mean square velocity and Kolmogorov length scale profiles were conducted using Matlab.

Table 5.2. Effect of flowfield experimental parameters

Fuel [l/min]	Equivalence ratio	Air [l/min]	Diluent		Oxygen Concentration [%]	Reynolds Number
			N_2 [l/min]	CO_2 [l/min]		
2.00	0.9	52.84	N/A	N/A	21	4087
2.00	0.9	52.84	2.64-26.42	N/A	20-14	4272 – 5943
2.00	0.9	52.84	N/A	2.64-16.51	20-16	4420 – 6192
2.00	0.8-0.6	59.44-79.26	N/A	N/A	21	4558 – 5973

The experimental investigations reported here were primarily focused on obtaining velocity fields, turbulence quantities, and Kolmogorov length scales along with OH* flame signatures and pollutants emission for the cases examined. For the oxidizer mixture, oxygen concentration in the oxidizer was gradually reduced in 1%

increments. Reduced oxygen concentration was achieved through either N_2 or CO_2 dilution, which were introduced to simulate entrainment of hot reactive species to seek colorless distributed combustion condition. Propane was used as the fuel in this section. For all conditions, heat load, heat release intensity, mixture temperature, and pressure were kept constant at 3 kW, 5.72 MW/m^3.atm, 300 K (room temperature), and 1 atm., respectively. Traditional and reduced oxygen concentration combustion conditions were investigated at an equivalence ratio of 0.9, with additional reduced equivalence ratio cases from 0.9-0.6 investigated to determine the impact of Reynolds number on achieving CDC. The experimental conditions examined for each of the compositions considered are presented in Table 5.2. In order to obtain the velocity field and turbulence quantities, PIV was used under non-reacting conditions to determine the role of flowfield and mixing on distributed combustion. During the non-reacting PIV experiments CO_2 was also used instead of propane since the density of carbon dioxide is similar to that of propane. The flowrate of simulated fuel (CO_2) was set to the same flowrate as propane fuel under combustion condition.

5.2 OH Chemiluminescence*

The OH* chemiluminescence flame signatures with various dilution amounts and diluent type are presented in Fig. 5.2. The results show the effect of reduced oxygen concentration on flame signature using differing diluents (N_2 or CO_2) entrained into the oxidizer. Reduction of oxygen concentration provided considerable decrease in peak OH* flame signatures for both the diluents examined. However, the effect of specific diluent on OH* flame signature was different in terms of oxygen concentration for

transition to CDC. The results of OH* flame signatures showed that transition to colorless distributed condition occurred at oxygen concentration of approximately 15% for N_2 and 17% for CO_2 diluents, respectively. The variation of CDC transition point for each diluent is attributed to different chemical properties of the diluents used. Higher heat capacity for CO_2 than N_2, caused considerable reduction in the reaction rate to cause in the transition to CDC at a higher oxygen concentration. Oxygen concentrations of 14 and 16% were indicative of the blow off limits of propane when N_2 or CO_2, respectively were introduced as the diluent. The flames at these conditions were not stable so that any further increase in diluents resulted in flame blow off.

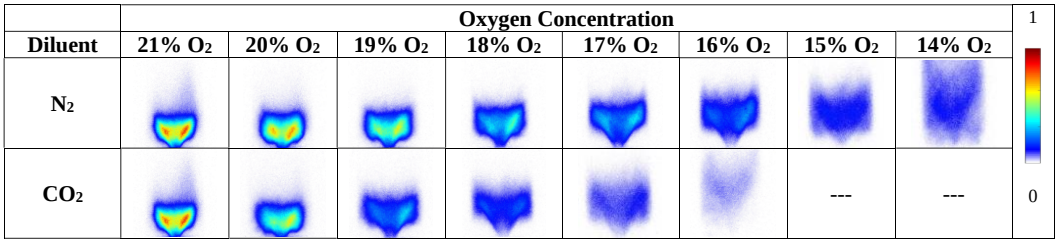

Fig. 5.2. OH* chemiluminescence signatures using either N_2 or CO_2 dilution, Φ=0.9

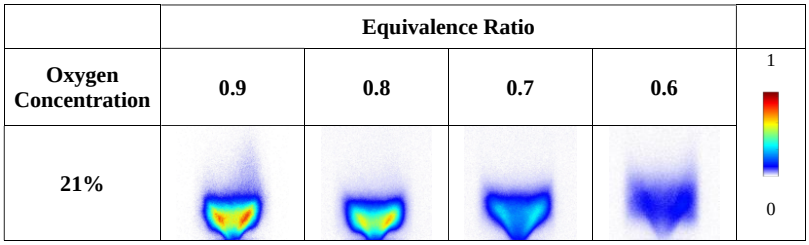

Fig. 5.3. OH* chemiluminescence signatures at various equivalence ratios

In order to determine the impact of reduced oxygen concentration on achieving CDC the role of increase in Reynolds number, and equivalence ratio on OH* chemiluminescence was examined, see Fig. 5.3. The results showed that reduction in the OH* flame signature intensity can also be achieved using air dilution by reducing

the equivalence ratio; however, this did not lead to uniform volumetric broadening of the flame.

5.3 Non-reacting Flowfield using PIV

Particle image velocimetry (PIV) is a non-intrusive laser diagnostic technique used to determine information on a flowfield including velocity, stress, strain, and turbulent quantities. For the 2-D PIV technique used in this research, the main components of the PIV system are the laser, camera, seeding particles, and timing box. The flow is seeded globally through the use of a packed bed seeder, by diverting a portion of the air through the seeder where it rejoins the main airflow upstream of the combustor. A high energy laser is double pulsed in rapid succession which illuminates the particles. The high-speed camera takes images of each illumination as is synced with the laser by use of a timing box. The camera is calibrated so that each pixel corresponds to a physical dimension. The two rapid succession images of the illuminated particles can then be correlated to determine velocity and other quantities. It is desirable to have ten particles per interrogation region and movement of no more than one-third of this region for good correlation. This differs from laser Doppler velocimetry (LDV) in which individual particles are tracked, as there are too many particles to follow. However, using statistical probability of the illumination intensity between images allows for the determination of an entire flowfield region of interest, which would be difficult in LDV which must track individual particles.

The mean and rms velocity profiles under non-reacting condition were determined using high frequency (3 kHz) particle image velocimetry (PIV). The mean

and root-mean square (rms) radial velocity profiles for the normal air and simulated CDC cases are shown in Fig. 5.4. The addition of dilution or excess air increased the mean velocity due to increase in flowrate. Additionally, the rms fluctuating velocity values increased with increase in flowrate, which enhances turbulent mixing. Figure 5.5 shows the mean and rms axial velocity profiles. Both the mean and fluctuating axial velocity increased, similar to that found for radial velocity, with increase in flowrate. The presence of an enhanced inner entrainment zone was also developed with increasing flowrate along the centerline and can be seen in Fig. 5.5. This enhanced entrainment allows for greater mixing with hot reactive gases which fostered in enabling CDC. It is important to note that enhanced turbulent mixing does not necessarily lead to CDC condition. In the reduced equivalence ratio case mixing is enhanced, however the chemical time scale is not reduced as much as the diluent cases due to a weaker impact on diminishing the probability of interaction between fuel and oxidizer before mixing is achieved,, which maintains a high reaction rate.

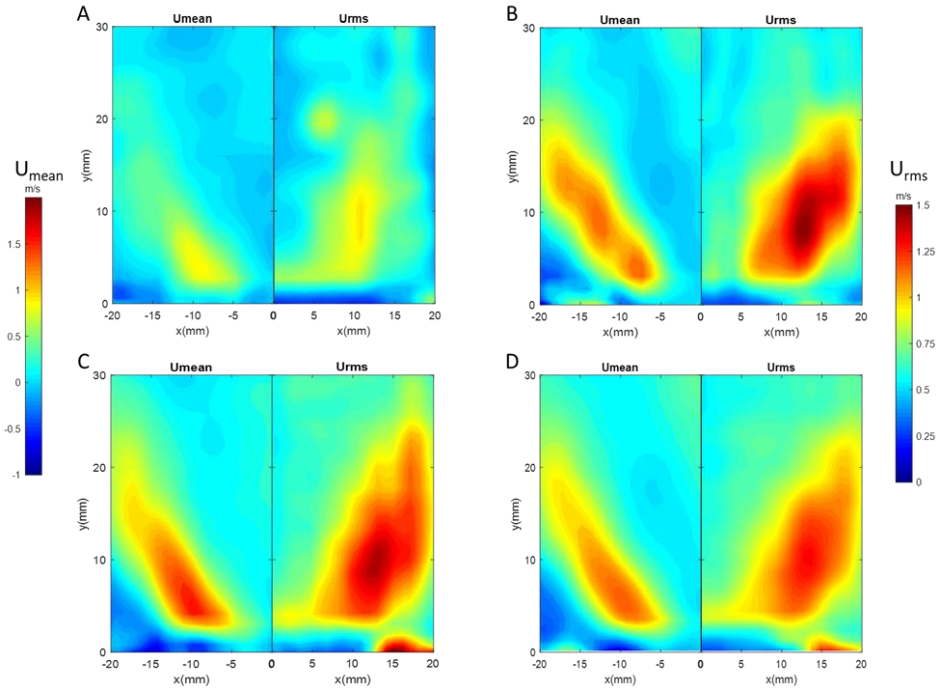

Fig. 5.4. Radial mean (left of frame) and rms (right of frame) velocity for: (A) normal air combustion, Φ=0.9; (B) normal air combustion, Φ=0.65; C) CDC with N_2 dilution, O_2 conc.=15%; and (D) CDC with CO_2 dilution, O_2 conc.=17%

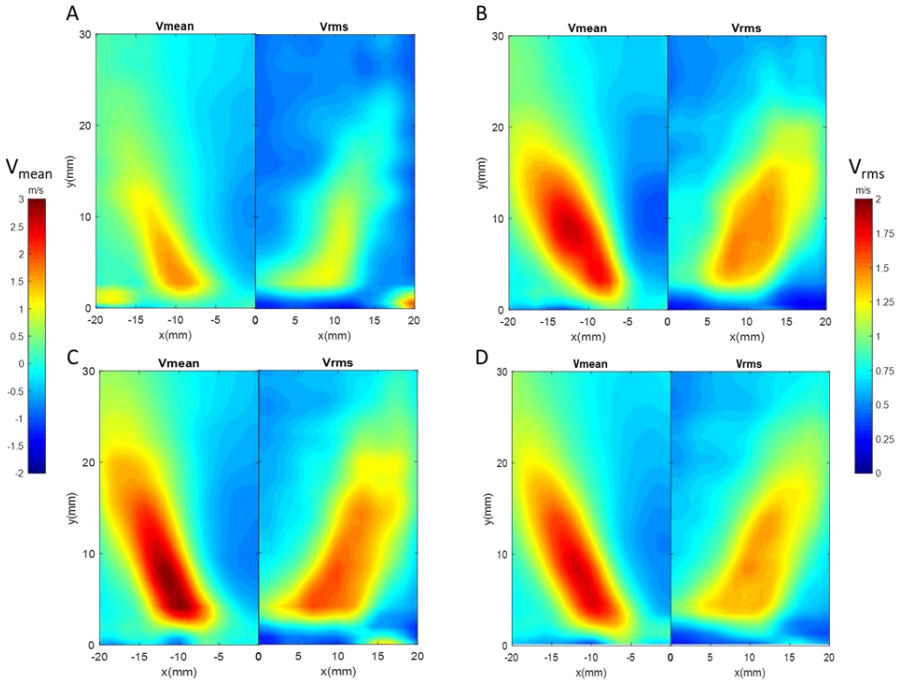

Fig. 5.5. Axial mean (left of frame) and rms (right of frame) velocity for: (A) normal air combustion, Φ=0.9; (B) normal air combustion, Φ=0.65; (C) CDC w/ N_2 dilution, O_2 conc.=15%; and (D) CDC w/ CO_2 dilution, O_2 conc.=17%

The Kolmogorov length scale and Reynolds stress are shown in Fig. 6 for the non-reacting simulated normal air and simulated CDC case using N_2 dilution under non-reacting case. The Kolmogorov length is given by:

$$\eta = \left(\frac{\upsilon^3}{\varepsilon}\right)^{1/4} \quad \text{(Eq. 5.1)}$$

Where, η is the Kolmogorov length scale, ν is the kinematic viscosity, and ε is the dissipation rate. The dissipation rate is equal to the kinetic energy production rate, which is proportional to the velocity magnitude $(V_{el})^3$ normalized by the characteristic length (L), which is the diameter of the burner outlet, and is given by:

$$\varepsilon = \frac{V_{el}^3}{L} \quad \text{(Eq. 5.2)}$$

The mixture viscosity was determined using Herning and Zipperer [44] equation for partial viscosities given by:

$$\mu_{mixture} = \frac{\Sigma(\nu_i x_i \sqrt{M_i})}{\Sigma(x_i \sqrt{M_i})} \quad \text{(Eq. 5.3)}$$

Where x is the mole fraction and M is the molecular weight of each component i. Meanwhile the Reynolds stress is determined by:

$$R_{stress} = \rho * (U' * V') \quad \text{(Eq. 5.4)}$$

Where ρ is the density and U' and V' are the fluctuating velocities in the radial and axial direction respectively.

Figure 6 shows that increased Reynolds number led to a decrease in eddy size. This suggests smaller scale mixing provides more rapid mixing and higher turbulent dissipation rates. In particular, the eddy size became significantly smaller in the swirl lobe region, which is where OH* chemiluminescence (which is indicative of higher peak temperature zones) signal is highest, to result in better dissipation in the high

temperature region and support mitigation of hot spots. Additionally, Reynolds stress, seen in Fig. 5.6, shows an increase with increase in flowrate. Due to the greater density of CO_2, the Reynolds stress associated with CO_2 dilution case was similar magnitude to the simulated N_2 dilution CDC and excess air cases even though the velocity is lower.

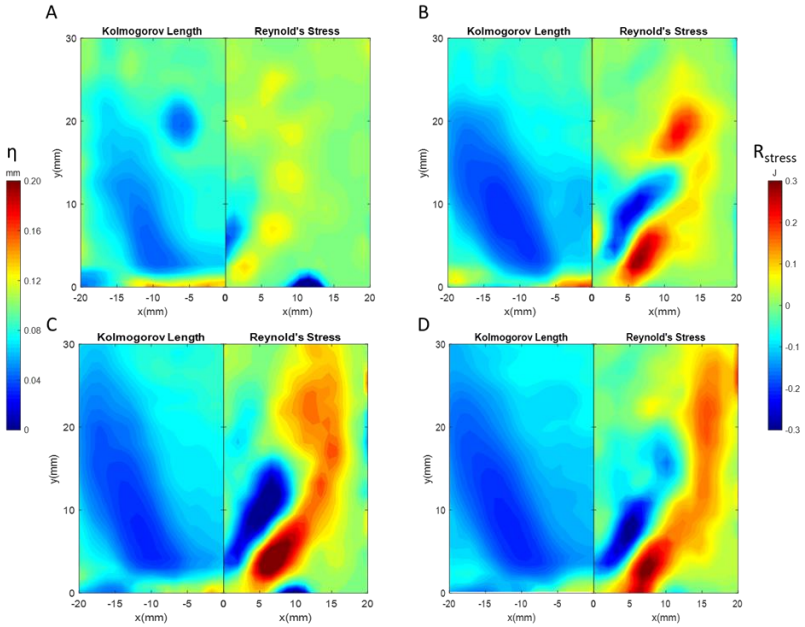

Fig. 5.6. Kolmogorov length (left of frame) and Reynold's stress (right of frame) for: (A) normal air combustion, Φ=0.9; (B) normal air combustion, Φ=0.65; (C) CDC w/ N_2 dilution, O_2 conc.=15%; and CDC w/ CO_2 dilution, O_2 conc.=17%

5.4 Pollutants Emission

In order to examine the effect of reduced oxygen concentration on pollutants emission, the NO and CO emission levels were measured for each diluent used at the combustor exit under conventional flame and near distributed combustion condition. Results on the emission of NO corrected to 15% O_2 concentration are shown in Fig. 5.7 for the specific conditions reported here. The maximum NO levels were measured at oxygen concentration of 21% representing the normal air combustion condition. The NO levels decreased significantly with decrease in oxygen concentration in the oxidizer. At the favorable CDC conditions, NO levels were below 2 ppm for N_2 as the

diluent and 1 ppm for CO_2 as the diluent. Therefore, ultra-low NO emissions were achieved under CDC. Carbon dioxide has been shown to have a greater effect on mitigating NO, which is attributed to higher heat capacity than that of nitrogen.

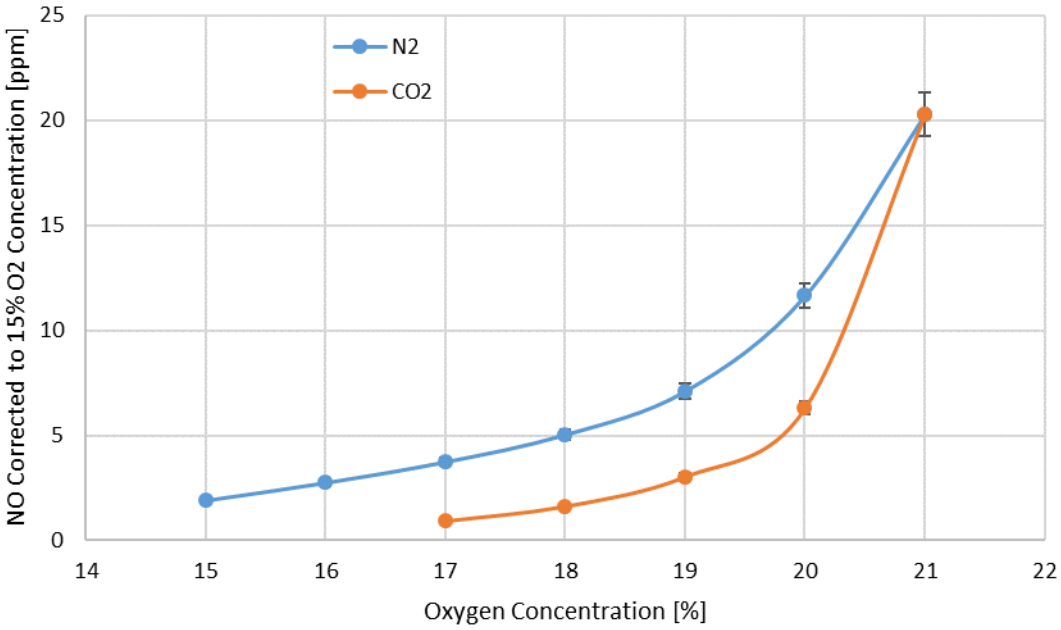

Fig. 5.7. NO emission corrected to 15% O_2 conc. at various oxygen concentrations

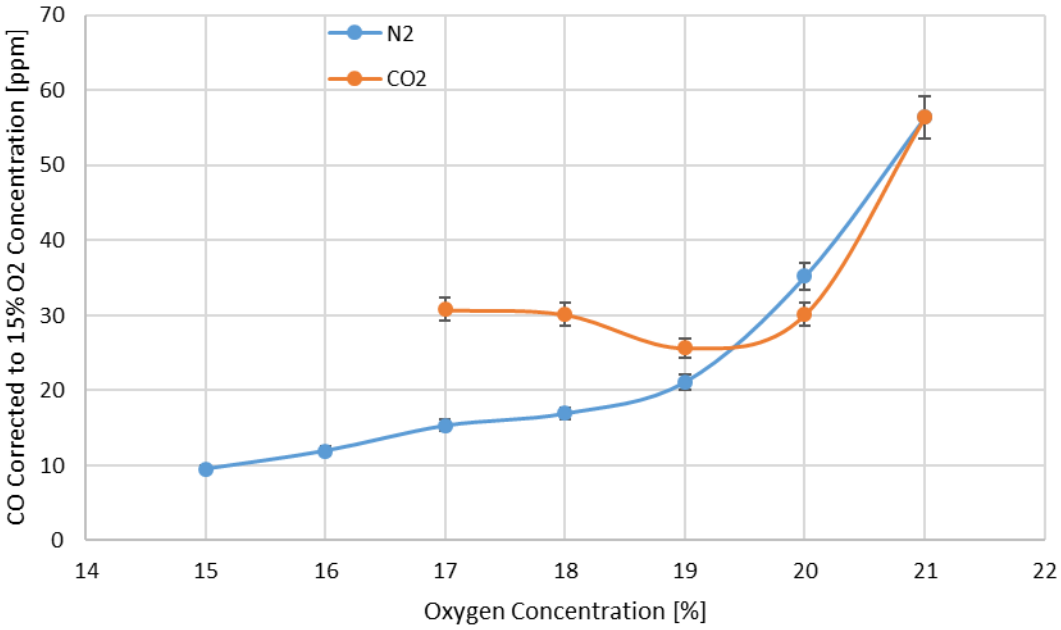

Fig. 5.8. CO emission corrected to 15% O_2 conc. at various oxygen concentrations

The effect of reduced oxygen concentration on CO emission is presented in Fig. 5.8. Carbon monoxide levels decreased considerably when N_2 was used as the diluent. At the favorable CDC condition, single digit CO levels were achieved under N_2 dilution condition. However, with CO_2 dilution, CO emission first decreased and then increased as residence time prohibited further oxidation of CO. Carbon monoxide emission was approximately 30 ppm under the CDC case. Due to CO_2 dissociation to CO, the carbon monoxide emission was somewhat higher than the N_2 dilution case. The results show both diluents provide ultra-low CO emission under CDC condition.

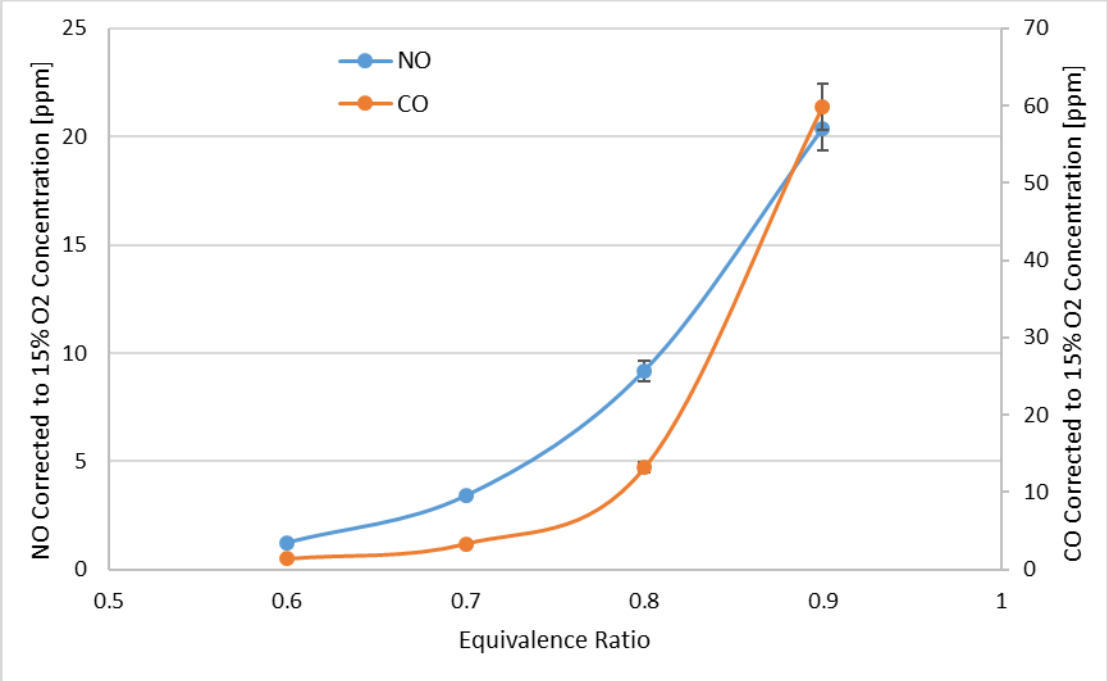

Fig. 5.9. NO and CO emissions corrected to 15% O_2 conc. at various equivalence ratios

The effect of equivalence ratio on NO and CO pollutants emission under non-oxygen reduction condition is presented in Fig. 5.9. Both NO and CO pollutants emission decreased significantly as equivalence ratio decreased. Below an equivalence ratio of 0.8, single digit pollutants emission levels were achieved.

5.5 Summary

Colorless distributed combustion conditions were examined in a swirl assisted propane-air combustor that incorporated dilution with either N_2 or CO_2 as the simulated entrained reactive gases. OH* chemiluminescence signatures were used to determine the onset of conditions for a volumetrically distributed reaction zone. CDC condition was reached at 15 and 17% O_2 concentration for N_2 and CO_2 dilution cases, respectively. Flowfield information was obtained using high speed 2-D PIV (3 kHz) under non-reacting conditions for both normal air combustion and simulated CDC cases. The results showed that dilution increased both the mean and rms velocity in both the radial and axial direction to promote faster mixing required for CDC. Additionally, the Kolmogorov length scale showed a significant reduction in eddy size towards CDC condition, particularly in the swirl lobe region. This reduction in eddy size results in faster turbulent dissipation rate that is important for enhanced mixing required for distributed flame regime along with reduction in temperature and thermal NO formation. Non-reacting flowfield information was also gathered at an equivalence ratio of Φ=0.9 and O_2%=21, to better determine the impact of dilution on achieving CDC. The Reynolds number of the N_2 and CO_2 CDC cases and the excess air case varied by less than 2.5%. The flowfield was shown to exhibit similar behavior of increased mean and fluctuating velocities under the excess air case; however, due to the reaction rate (chemical time scale) not being significantly reduced CDC condition was not achieved.

NO and CO emission data reported for the normal air and CDC cases showed ultra-low emission of NO with less than 2 ppm NO using N_2 dilution and 1 ppm NO

using CO_2 dilution. Significant reduction in CO was also found using N_2 dilution with single digit CO levels under CDC. CO_2 dilution provided slightly higher CO level, approximately 30 ppm, due to the dissociation of CO_2 to CO. Excess also resulted in low emissions with single digit ppm of both NO and CO found at $\Phi<0.8$. The average eddy size (Kolmogorov) and Reynolds stress were determined to examine the effect of Reynolds number on mixing timescales. Increase in dilution decreased the eddy size which in turn promoted mixing to distribute the reaction and reduce NO levels due to reduction in high reaction rate (high temperature) regions. CO_2 dilution provided enhanced Reynolds stress and thus reduction on NO level due to lower viscosity associated with CO_2 dilution.

Chapter 6: Conclusions and Recommendations for Future Work

6.1 Summary and Conclusions

Investigation of distributed combustion utilizing a swirl-assisted combustor was examined here. First, fuel flexibility was examined by investigating the effect of fuel enrichment. Enrichment of ethanol with naphthalene was examined in order to improve combustion performance under CDC. Through the use of naphthalene enrichment the heating value was increased by 8.8% while maintaining ultra-low emissions under favorable CDC condition with near unity NO and single digit ppm CO. This shows that naphthalene may be used as a beneficial fuel additive to low heating value fuels such as ethanol. Additionally, the influence of high hydrogen enrichment was examined, like that which may be found in many alternative fuels. Hydrogen enriched fuels are of interest because they may maintain a relatively high heating value (~1/2 of natural gas) while being abundant products of several industrial processes. Flashback instability due to increased flame speed with hydrogen enrichment was completely mitigated under CDC. Ultra-low NO and CO were achieved with hydrogen enriched fuels with a large reduction in CO due to less carbonaceous fuel. This shows the fuel flexibility of CDC through the combustion of hydrogen enriched fuels, as well as the ability to increase energy security by using alternative fuels.

In order to further examine the effect of combustion parameters on CDC experiments were performed to test the effect of heat release intensity, equivalence ratio, preheat temperature and diluent type, in order to develop a distributed combustion index, which will help in the prediction of CDC conditions. It was determined HRI was no strong influence on transition to CDC, while equivalence ratio, preheat temperature

and entrained diluent type all had major impacts. A DCI was developed which can be used to determine and predict the amount of distribution. This will be extremely beneficial in the design and implementation of novel gas turbine combustors utilizing CDC.

Lastly the effect of flowfield on distributed combustion was examined. The non-reacting flowfield provided valuable information on how CDC influences the flowfield. Using entrained dilution of either N_2 or CO_2 the mean and fluctuating velocities increased increasing the mixing favoring distribution. In addition turbulence parameters such as Reynolds stress were examined. Investigtion on Reynolds stress showed than under CDC condition the Reynold's stress field with either N_2 or CO_2 dilution was approximately the same even though different amounts (by volume) of each entrained gas were added in order to achieve CDC. This shows there that in order to achieve distributed combustion conditions the stress field is a determining factor in how proper mixing and entrainment is achieved required for favorable CDC condition.

6.3 Recommendations for Future Work

It is important to improve the understanding of the flame-flow interaction under CDC. For this means reacting PIV should be investigated in order to determine how CDC either dampens or enhances turbulence in order to promote entrainment. In addition, coupled PIV and PLIF experiments can help show local flame front extinction events due to the flowfield flame interaction. Additionally, high speed cinematography and chemiluminescence may be used to better understand the thermo-acoustic coupling, heat release fluctuations, and local extinction events.

It is recommended to investigate the temperature field to determine the uniformity of the thermal field. This will allow for better prediction of combustor lifetime, due to reduced hot spots and resulting burn out. This with help in design of CDC combustors with novel fuel injection and mixing techniques which will allow for a more uniform thermal field.

Investigation at high thermal intensities and high pressures is desired for simulating current aviation-based gas turbine combustor conditions as well ultra-high intensity future gas turbines. Thermal intensities of 200-400 MW/m^3-atm and pressures of up to 10 bar are recommended in order to better understand the effects of HRI and pressure on achieving CDC.

Finally, it is desired to develop an expansive DCI with a vast range of conditions including ultra-high HRI, high pressure, preheat temperature, equivalence ratio, diluent type, combustor geometry and fuel injection scheme to name a few. This DCI can then be fed into a machine learning algorithm in order to more rapidly predict advantageous parameters without needing to run experiments for each parameter. This with allow for more rapid research, development, design and manufacture of CDC prototypes and novel gas turbine combustors.

Appendix A: List of Papers

A1: Published Journal Papers

1. Karyeyen, S., Feser, J. S. and Gupta, A. K.: Flowfield impact on distributed combustion in a swirl assisted burner, Fuel, Accepted: November 12, 2019. https://doi.org/10.1016/j.fuel.2019.116643

2. Karyeyen, S., Feser, J. S. and Gupta, A. K.: Towards Distributed Combustion in a Swirl Combustor Using Hydrogen-Rich Gas Fuels, Applied Energy, Vol. 251, October 1, 2019. https://doi.org/10.1016/j.apenergy.2019.113354

3. Karyeyen, S., Feser, J. S. and Gupta, A.K.: Hydrogen Concentration Effects on Swirl-Stabilized Oxy-Colorless Distributed Combustion, Fuel, Vol. 253, pp. 772-780, October 1, 2019. https://doi.org/10.1016/j.fuel.2019.05.008

4. Feser, J. S., Bassioni, G. and Gupta, A. K.: Effect of Naphthalene Addition to Ethanol in Distributed Combustion, Applied Energy, Vol. 216, pp. 1-7, April 15, 2018. https://doi.org/10.1016/j.apenergy.2018.02.090

5. Feser, J. S. and Gupta, A. K.: Effect of CO2/N2 Dilution on Premixed Methane-Air Flame Stability under Strained Condition, J. Energy Resources Technology, March 29, 2018. Doi: 10.1115/1.4039326

A2: Journal Papers Under Review

1. Karyeyen, S., Feser, J. S. and Gupta, A. K.: Development of Distributed Combustion Index from a Swirl-Assisted Burner, Applied Energy, Under Review, November 29, 2019.

A3: Conference Papers

1. Karyeyen, S., Feser, J. S. and Gupta, A. K.: Effect of Fuel Dilution in a Hydrogen-Methane Blended Fuel Under Oxy-Distributed Combustion, AIAA Propulsion & Energy Forum, Indianapolis, IN, August 19-22, 2019.

2. Karyeyen, S., Feser, J. S. and Gupta, A.K.: Hydrogen Enrichment Effects in Gaseous Fuels on Distributed Combustion, ASME Power Conference, Salt Lake City, UT, July 14-18, 2019, Paper Power2019-1893.

3. Feser, J. S., Karyeyen, S. and Gupta, A.K.: Impact of Flowfield on Pollutants Emission from a Swirl Assisted Distributed Combustor, Clearwater Clean Energy Conference, Clearwater, FL, June 16-21, 2019.

4. Feser, J. S. and Gupta, A. K.: Flowfield Investigation in a Non-Reacting Reverse Flow Isothermal Combustor, AIAA Scitech 2019 Forum, San Diego, CA, January 7-11, 2019.

Bibliography

[1] U.S. Energy Information Administration, "Annual Energy Outlook 2019," DOE/EIA, 2019.

[2] A. H. Lefebvre, “Gas Turbine Combustion,” Philadelphia: Taylor & Francis, 1999.

[3] T. Lieuwen and V. Yang, "Combustion Instabilities in Gas Turbine Engines," Progress in Astrounautics and Aeronautics, vol. 210, 2005.

[4] C. L. Vandervort, "9 ppm NOx/CO Combustion System for "F" Class Industrial Gas Turbines," Journal of Engineering for Gas Turbines and Power, vol. 123, pp. 317-321, 2001.

[5] Environmental Protection Agency, Standards of Performance for Stationary Combustion Turbines, Final Rule, vol. 71, Federal Register, 2006.

[6] E. T. Vincent, “The Theory and Design of Gas Turbines and Jet Engines,” New York: McGraw-Hill, 1950.

[7] S. R. Turns, “An Introduction t Combustion: Concepts and Application,” Boston: McGraw-Hill, 2006.

[8] H. Kobayashi, A. Hayakawa, K. D. K. A. Somaranthne and E. C. Okafor, “Science and Technology of Ammonia Combustion,” Proceedings of the Combustion Institute, vol. 37, pp. 109-133, 2019.

[9] G. Leonard and J. Stegmaier, "Development of an Aeroderivative Gas Turbine Dry Low Emissions Combustion System," Journal of Engineering for Gas Turbines and Power, vol. 116, no. 3, pp. 542-546, 1994.

[10] S. M. Correa, “A review of NOx Formation Under Gas-Turbine Combustion Conditions,” Combustion Science and Technology, Vol. 87, 1992, pp. 329-362.

[11] W. A. Sirignano, T. K. Pham and D. Dunn-Rankin, "Miniature-scale LiquidFuel-Film Combustor," Proc. of the Combustion Institute, vol. 29, no. 1, pp. 925-931, 2002.

[12] H. Tsuji, A. K. Gupta, T. Hasegawa, M. Katsuki, K. Kishimoto, and M. Morita, “High Temperature Air Combustion: From Energy Conservation to Pollution Reduction”, CRC Press, 2003.

[13] A. K. Gupta, “Thermal Characteristics of Gaseous Fuel Flames using High Temperature Air,” Journal of Engineering for Gas Turbines and Power, Vol. 126, 2004, pp. 9-19.

[14] M. Katsuki and T. Hasegawa, "The Science and Technlogy of Combustion in Highly Preheated Air," Proceedings of the Twenty Seventh Symposium (Intl) on Combustion, vol. 27, pp. 3135-4146.

[15] K. Kitagawa, N. Konishi, N. Arai and A. K. Gupta, "Temporally Resolved 2-D Spectroscopic Study on the Effect of Highly Preheated and Low Oxygen Concentration Air on Combustion," Journal of Engineering for Gas Turbines and Power, vol. 125, pp. 326-331, 2003.

[16] J. A. Wunning, J. G. Wunning, "Flameless Oxidation to Reduce Thermal NO-Formation," Progress in Energy and Combustion Science, Vol. 23, pp. 81-94, 1997.

[17] M. M. Noor, A. P. Wandel and T. Yusaf, "A Review of Mild Combustion and Open Furnace Design Consideration," International Journal of Automotive and Mechanical Engineering, Vol. 6, pp. 730-754, 2012.

[18] V. K. Arghode, "Development of Colorless Distributed Combustion for Gas Turbine Application," University of Maryland, College Park, 2011.

[19] A. E. E. Khalil, "Investigation of Colorless Distributed Combustion (CDC) with Swirl for Gas Turbine Application," University of Maryland, College Park, 2013.

[20] A. E. E. Khalil, and A. K. Gupta, "Fostering Distributed Combustion in a Swirl Burner Using Prevaporized Liquid Fuels," Appl Energy 2018; 211:513–22. http://dx.doi.org/10.1016/j.apenergy.2017.11.068

[21] A. E. E. Khalil, and A. K. Gupta, "Clean Combustion in Gas Turbine Engines Using Butyl Nonanoate Biofuel," Fuel 2014; 116:522–8. http://dx.doi.org/10.1016/j.fuel.2013.08.022

[22] R. M. Nubia, A. C. Pinto, C. M. Quintella, et al., "The Role of Additives for Diesel and Diesel Blended (Ethanol or Biodiesel) Fuels: A Review," Energy Fuels 2007; 21(4):2433-45. http://dx.doi.org/10.1021/ef070060r

[23] R. E. Albright, F. L. Nelson, and L. Raymond, "Effect of Additives on Gasoline Engine Deposits," Ind Eng Chem 1949; 41(5).

[24] L. S. Palmer, "The Combustion of Naphthalene Solutions in Internal Combustion Engines," The Institution of Automobile Engineers; 1920.

[25] M. A. Mussa, "Experimental Study on the Combustion and Exhaust Emissions of Otto Engine Fuel with Naphthalene-Gasoline Blends," Diyala J Eng Sci 2017; 10(1):58–70.

[26] Dortmund Database; http://www.ddbst.com/en/EED/VLE/VLE%20Ethanol%3BNaphthalene.php

[27] A. E. E. Khalil, A. K. Gupta "Internal Entrainment Effects on High Intensity Distributed Combustion Using Non-Intrusive Diagnostics," Appl Energy 2015; 160:467–76. http://dx.doi.org/10.1016/j.apenergy.2015.09.053

[28] A. E. E. Khalil, and A. K. Gupta, "Thermal Field Investigation under Distributed Combustion Conditions," Appl Energy 2015; 160:477–88. http://dx.doi.org/10.1016/j.apenergy. 2015.09.058

[29] A. Seidell, and W. F. Linke, "Solubility of Inorganic and Organic Compounds," 2nd ed. New York: D. Van Nostrand Company; 1919. p. 443–6.

[30] A. E. E. Khalil, and A. K. Gupta. Impact of Internal Entrainment on High Intensity Distributed Combustion. Appl Energy 2015; 156:241–50. http://dx.doi.org/10.1016/j.apenergy. 2015.07.044

[31] A. E. E. Khalil, and A. K. Gupta. Fuel Property Effects on Distributed Combustion. Fuel 2016; 171:116–24. http://dx.doi.org/10.1016/j.fuel.2015.12.068

[32] A. J. Marchese, F. L. Dryer, V. Nayagam, R. O. Colantonio., Hydroxyl radical chemiluminescence imaging and the structure of microgravity droplet flames. Symp (Int) Combust 1996; 26(1):1219–26. http://dx.doi.org/10.1016/S0082-0784(96)80338-9

[33] A. Ostapczuk, A. G. Chmielewski, V. Honkonen, et al., Preliminary Test in Decomposition of Styrene by Electron Beam Treatment. Radiat Phys Chem 1999;56(3):369–71 http://dx.doi.org/10.1016/S0969-806X(99)00182-6

[34] P. J. Linstrom, W. G. Mallard, editors, NIST Chemistry WebBook, NIST Standard Reference Database Number 69, National Institute of Standards and Technology, Gaithersburg MD, 20899, 10.18434/T4D303

[35] S. Hosokai, K. Kumabe, M. Ohshita, et al., "Mechanism of Decomposition of Aromatics Over Charcoal and Necessary Condition for Maintaining its Activity," Fuel 2008; 87(13–14):2914–22. http://dx.doi.org/10.1016/j.fuel.2008.04.019

[36] R. Razzaq, C. Li, and S. Zhang, "Coke Oven Gas: Availability, Properties, Purification, and Utilization in China," Fuel 2013; 113:287–99. https://doi.org/10.1016/j.fuel.2013.05.070

[37] M. Ilbas, and S. Karyeyen, "An Experimental and Numerical Study on Turbulent Combustion of Hydrogen-Rich Coal Gases in a Generated Non-Premixed Burner," Fuel 2017; 194:274–90. https://doi.org/10.1016/j.fuel.2017.01.016

[38] M. C. Lee, S. B. Seo, J. H. Chung, S. M. Kim, Y. J. Joo, and D. H. Ahn, "Gas Turbine Combustion Performance Test of Hydrogen and Carbon Monoxide Synthetic Gas," Fuel 2010; 89:1485–91. https://doi.org/10.1016/j.fuel.2009.10.004

[39] F. Halter, F. Foucher, L. Landry, and C. Mounaïm-Rousselle, "Effect of Dilution by Nitrogen and/or Carbon Dioxide on Methane and Iso-Octane Air Flames," Combust Sci Tech 2009; 181(6):813–27. https://doi.org/10.1080/00102200902864662

[40] J. Natarajan, T. Lieuwen, and J. Seitzman, "Laminar Flame Speeds of H2/CO Mixtures: Effect of CO2 dilution, Preheat Temperature, and Pressure," Combust Flame 2007; 151(1–2):104–19. https://doi.org/10.1016/j.combustflame.2007.05.003

[41] A. E. E. Khalil, and A. K. Gupta, "Hydrogen Addition Effects on High Intensity Distributed Combustion," Appl Energy 2013; 104:71–8. https://doi.org/10.1016/j.apenergy. 2012.11.004

[42] A. E. E. Khalil, V. K. Arghode, A. K. Gupta, and S. C. Lee, "Low Calorific Value Fueled Distributed Combustion with Swirl for Gas Turbine Applications," Appl Energy 2012;98:69–78. https://doi.org/10.1016/j.apenergy.2012.02.074

[43] A. D. Rao, "Combined cycle systems for near-zero emission power generation," Cambridge: Woodhead Publishing Series in Energy; 2012.

[44] F. Herning, and L. Zipperer, "Calculation of the viscosity of technical gas mixtures from the viscosity of individual gases," Gas-und Wasserfach 1936; 79:69-73.